Construction of a Digitally Controlled Scanning Tunneling Microscope

by Peter Geoffrey Alexander Madden

A Thesis submitted to the Faculty of Graduate Studies and Research in partial fulfillment of the requirements of the degree of Master of Engineering

Biorobotics Laboratory
Department of Biomedical Engineering
McGill University
Montreal, Quebec, Canada
June, 1996

Copyright Peter Geoffrey Alexander Madden, 1996

COPY 1



Acquisitions and Bibliographic Services Branch

395 Wellington Street Ottawa, Ontano K1A 0N4 Bibliothèque nationale du Canada

Direction des acquisitions et des services bibliographiques

395, rue Wellington Ottawa (Ontano) K1A 0N4

Your file Votre référence

Our file Notre reference

The author has granted an irrevocable non-exclusive licence allowing the National Library of Canada to reproduce, loan, distribute or sell copies of his/her thesis by any means and in any form or format, making this thesis available to interested persons.

L'auteur a accordé une licence irrévocable et non exclusive à la Bibliothèque permettant Canada nationale du reproduire, prêter, distribuer ou vendre des copies de sa thèse de quelque manière et sous quelque forme que ce soit pour mettre des exemplaires de cette thèse à la disposition des personnes intéressées.

The author retains ownership of the copyright in his/her thesis. Neither the thesis nor substantial extracts from it may be printed or otherwise reproduced without his/her permission. L'auteur conserve la propriété du droit d'auteur qui protège sa thèse. Ni la thèse ni des extraits substantiels de celle-ci ne doivent être imprimés ou autrement reproduits sans son autorisation.

ISBN 0-612-19876-6



Abstract

The development of micro- and nano-scale robots for medical applications will require an understanding and intuition for nanoscale phenomena as well as a suite of new miniaturized technologies. The scanning tunneling microscope (STM), invented in 1980 by Gerd Binnig and Heinrich Rohrer at IBM, and related scanning probe microscopes such as the atomic force microscope are among the most advanced instruments yet built to explore our world at the nanometer and even subnanometer level. This thesis describes the construction of a computer controlled scanning tunneling microscope, the characterization of its performance, and some results that have been obtained using the microscope including atomic resolution images of highly oriented pyrolytic graphite. What is believed to be the first polymer to polymer tunneling junction is also described as the first step towards an all polymer STM. The lessons learned from the construction of the STM will be applied in the design of future nanoscale structures.

Resumé

Le développement de robots de dimensions qui approchent quelques micromètres ou même quelques nanomètres requiert une comprehension des phénomènes et de la physique qui dominent les évènements à ces échelles et d'une pluralité de nouvelles technologies miniatures. Le microscope tunnel éléctronique (STM), inventé en 1980 par Gerd Binnig et Heinrich Rohrer de IBM, et autres microscopes de la même famille tel que le microscope de force atomique, sont parmi les outils les plus avancés pour l'exploration à l'échelle nanométrique. Cette thése présente la construction d'un STM contrôlé par ordinateur, la caractérisation de sa performance, et quelques résultats qui ont été obtenus utilisant le nouveau microscope. Inclus parmi les résultats sont quelques images à résolution atomique de graphite. Des mesures qui sont possiblement les premiers de l'effet tunnel de polymère à polymère sont aussi presentés. Ces mesures furent la première étape vers la construction d'un microscope tunnel électronique fabriqué complètement de polymères. Les leçons apprises durant la construction du nouveau STM seront appliqués pendant le développement de nouveaux outils pour la manipulation et l'exploration du monde nanoscopique.

Acknowledgments

Many people have helped and taught me throughout this thesis. First, I would like to thank Professor Ian Hunter, my supervisor, who's wide range of interests and knowledge have made his laboratory a diverse and exciting environment to work in. He has provided ideas and guidance that were invaluable.

Colin Brenan, with his tremendous rigour in research, pushed me to better understand issues in the design and characterization of the STM. Colin also provided useful criticism during the writing of this thesis.

To my brother John Madden, I owe a special thanks. John offered continual encouragement and advice, even when I was less than patient with him.

Thanks go to Serge Lafontaine, who has spent countless hours answering my many questions and keeping the lab running smoothly. Serge's good natured patience is always appreciated. I would also like to thank Sylvain Martel who has helped me with the electronics for the STM.

Finally, I would like to thank my parents, who have always encouraged and supported me.

I am grateful for the support of the National Sciences and Engineering Research Council during the course of this thesis.

Table of Contents

ABSTRACT	i
RESUMÉ	ii
ACKNOWLEDGMENTS	iii
TABLE OF CONTENTS.	iv
LIST OF FIGURES	vi
CHAPTER 1: INTRODUCTION	1
1.1 MEDICAL MICROROBOTS	2
1.2 NANOSCALE SENSORS	
1.3 THESIS OUTLINE	4
CHAPTER 2: DEVELOPMENT OF THE SCANNING TUNNELING MICROSCOPE	6
2.1 THE SCANNING TUNNELING MICROSCOPE.	6
2.2 QUANTUM MECHANICS OF TUNNELING	7
2.3 APPLICATIONS OF STM	11
CHAPTER 3: SPECIAL CONSIDERATIONS FOR DESIGN	16
3.1 REQUIREMENTS	16
3.2 VIBRATION ISOLATION	
3.3 Precision Motion Control	20
3.4 Temperature Considerations	30
3.5 MICROSCOPE TIP	32
3.6 Conclusions	34
CHAPTER 4: COARSE APPROACH - THE NANOSTEPPER	36
4.1 DESIGN	36
4.2 CURRENT DESIGN	
4.2 Interferometer for Calibration	41
4.3 CALIBRATION	44
CHAPTER 5: ELECTRONICS	52
5.1 CURRENT TO VOLTAGE AMPLIFIER	53
5.2 Analog to Digital and Digital to Analog	60
5.3 ADD AND SUBTRACT ELECTRONICS	
5.4 High-Voltage Amplifiers	64
CHAPTER 6: COMPUTER FEEDBACK CONTROL	67
6.1 COARSE ATTROACE	
6.2 LINEARIZATION	
6.3 PID CONTROL	
6.4 DACTED SOAN	79

CHAPTER 7: PIEZO TUBE CALIBRATION	76
7.1 PIEZOELECTRIC CALIBRATION AND OBSERVED NON-LINEARITIES	76
7.2 MODELS OF CREEP	
7.3 X AND Y CALIBRATION	84
7.4 SUMMARY	85
CHAPTER 8: SYSTEM CHARACTERIZATION	86
S.1 FREQUENCY RESPONSE	86
8.2 SIMULATION	93
8.3 SCAN RATES	
8.4 MICROSCOPE RESOLUTION	98
CHAPTER 9: IMAGING RESULTS	101
9.1 CURRENT DISTANCE CURVE	101
9.2 HOLOGRAPHIC GRATING	103
9.3 GRAPHITE	
9.4 POLYMER TUNNELING JUNCTION	106
CHAPTER 10: CONCLUSIONS AND FUTURE WORK	108
10.1 SCANNING TUNNELING MICROSCOPE	108
10.2 FUTURE WORK	108
10.2 TUNNELING SENSORS	110
10.3 CONCLUSIONS	111
BIBLIOGRAPHY	112
APPENDIX A: CONSTRUCTION DRAWINGS FOR STM	117
APPENDIX B: C CODE FOR COMPUTER CONTROL	120
APPENDIX C: MATLAB CODE FOR STM SIMULATION	140

List of Figures

Figure 3.1: STM vibration isolation system	19
Figure 3.2: Piezoelectric material shape change	23
Figure 3.3: Measured creep of piezo tube position	25
Figure 3.4: Measured piezo hysteresis.	26
Figure 3.5: Piezoelectric tripod configuration for STM scanner.	
Figure 3.6: Piezoelectric tube with four outer electrodes	29
Figure 3-7: Photograph of the STM as built	34
Figure 4-1: Stepper design used by Niedermann et al. (1988)	38
Figure 4-2: Stage for one-dimensional translation.	39
Figure 4-3: Plot of a triangular waveform and a cycloidal waveform	40
Figure 4-4: Interferometer layout	41
Figure 4-5: Computer control for the nanostepper	44
Figure 4-6: Position vs. step number of the micro-positioner	46
Figure 4-7: Histogram of step size in the positive direction (60V, 0.5ms waveform)	48
Figure 4-8: Histogram of step size in the negative direction (60V, 0.5ms waveform)	49
Figure 4-9: Step Size vs. Pulse Duration.	50
Figure 4-10: Step Size vs. Waveform Voltage	50
Figure 5-1: Electronics for the STM	51
Figure 5-2: Current Amplifier Circuit	53
Figure 5-3: Sources of Noise and Offsets in the Current Amplifier	54
Figure 5-4: Measured frequency response of the current to voltage amplifier	58
Figure 5-5: Compensation circuit for current amplifier.	58
Figure 5-6: Measured transfer function of the compensated current amplifier	59
Figure 5-7: Addition and subtraction circuits	63
Figure 5-8: High Voltage Amplifier Circuit	64
Figure 6-1: System for computer based control of the STM	
Figure 6-2: Graphical user interface for the STM.	69
Figure 6-3: Block diagram of feedback for STM	
Figure 6-4: Flow diagram of the control loop and scanning algorithm	75
Figure 7-1: Hysteresis of the Piezo Tube	77
Figure 7-2: Creep measured with an interferometer for 30 and 60 nm steps	78
Figure 7-3: Measurement of Piezoelectric Creep	
Figure 7-4: Expanded view of creep	82
Figure 7-5: Expanded view of creep	
Figure 7-6: Simple model for creep in a material	

Figure 8-1: Position impulse response of the STM	87
Figure 8-2: Experimental setup for measuring frequency response of the STM	89
Figure 8-3: Disturbance rejection frequency response.	91
Figure 8-4: Simulated closed loop frequency response	94
Figure 8-5: Simulated open loop frequency response	96
Figure 8-6: Tip to sample stability for a polymer to polymer junction (polypyrrole)	99
Figure 8-7: Tip to sample stability for Pt/Ir to HOPG tunneling junction.	99
Figure 9-1: Measured current vs. position curve and log(current) vs. position curve	. 102
Figure 9-2: STM image of a gold plated holographic grating	. 103
Figure 9-3: Constant current image of HOPG.	. 104
Figure 9-4: Two cross-sections from Figure 9-3	. 104
Figure 9-5: Constant height image of HOPG.	. 105
Figure 9-6: Gap width stability measured between a polypyrrole tip and a polypyrrole	
sample	. 106

Chapter 1: Introduction

People have aiways sought to better understand and to better control the environment that they live in. As science has progressed, the realms which we have been able to observe and manipulate has expanded continually. And the tools and concepts that we use to explore and explain our world have evolved from simple to complex.

The ancient Greeks developed the concept of atoms, indivisible building blocks for all matter. But the Greek concept of atoms was mostly philosophical and was not based on any experimental observations of the real world. In the 17th century, the Dutch scientist Antonie van Leuwenhoek used a simple one lens microscope to systematically observe the microscopic world of insects, bacteria, and cells.

Leuwenhoek's microscope was the first in a series of tools that help us visualize the miniature world. Further refinements in the optical microscope brought significant improvements in resolution and image quality. But in 1834, George Biddell Airy showed that the resolution of microscope was limited by the wavelength of light to several hundred nanometers. The discovery by Louis de Broglie in 1924 that electrons also have a wavelength dependent on their energy led to the idea of the electron microscope. With wavelengths far shorter than light, electron microscopes can have resolutions below a nanometer. In 1980, Gerd Binnig and Heinrich Rohrer developed the scanning tunneling microscope, which uses a small extremely localized electron current to resolve individual atoms on a surface.

In parallel with the development of better and better microscopes, techniques have been discovered to allow us to manipulate materials on a smaller and smaller scale. While van Leuwenhoek's microscope lenses were ground smooth to a few hundred nanometers, technology today can build complex integrated circuits with two dimensional features sizes of several hundred nanometers. Smooth atomic layers can be deposited with thicknesses of about one tenth of a nanometer. Binnig and Rohrer's scanning tunneling microscope can

be used not only to image atoms but also to manipulate and move individual atoms, opening the possibility of atom by atom assembly.

As our understanding and our control of the microscopic realm have increased, so too has our appreciation of the potential applications of microscopic machines. In 1959, Nobel laureate Richard Feynmann noted that "There is Plenty of Room at the Bottom" [Feynmann, 1959]. Feynmann was referring to the potential of manufacturing on the submillimeter (or even sub-micrometer) scale. When Feynmann gave his talk, the state of the art in electronics was a diode only a few millimeters square. Today, millions of transistors are packed into a space a few millimeters square, but even today's technology is far from the physical limits imposed by the atomic structure of materials.

1.1 Medical Microrobots

For many applications, the potential of atomic scale manufacturing is immediately evident. For data storage, Feynmann calculated that all the information in all the books in the world (in 1959) could easily be stored in the volume of a credit card (approximately 1.5 mm by 50 mm by 80 mm). Once this happens, everybody will be able to carry around with them all of the literature, history, science, engineering, and medical knowledge that humanity has developed.

In medicine, atomic scale or even microscopic scale manufacturing will have an enormous effect. Millimeter size robots (ultimately micrometer size) will be built that will be able to move through the body to monitor and maintain our health. Surgical operations which today require weeks of in hospital recovery because of infection or healing of damage to surrounding tissue will become one day procedures. The micrometer size robots will be swallowed or injected, reducing the risk of infection and lowering healing times, and will clean arteries to improve blood flow, remove cancerous or other harmful tissue, or monitor blood chemistry to ensure the patient is healthy. Robots may even enter into cells to repair defective DNA.

Robots on the millimeter and micrometer scale have the same basic requirements as do larger scale robots: they need a power supply, motors, intelligence to control their

motion, and sensors to monitor and interact with the environment. All of these different elements need to be miniaturized as much as possible.

Eventually, in the process of miniaturization the limits of classical mechanics will be reached. Beyond this limit, behaviour is governed by quantum mechanics. Quantum mechanics, unlike the deterministic laws of classical mechanics, describes probabilities or likelihood's of events, such as an electron moving from one atom to another along a wire, on a very small scale.

1.2 Nanoscale Sensors

Sensors that are sub-micrometer in dimension will likely be based on quantum mechanics because of their small scale. The scanning tunneling microscope is a sensor that relies on quantum tunneling of electrons (electrons jump or 'tunnel' across a barrier that is classically impenetrable¹) to measure the distance between a conductive tip and atoms on a surface. As the tip is scanned across the surface (somewhat like the needle on a record player) the height of the surface at different points is measured to build up a surface map. The tunneling of the electrons occurs only between the atom on the tip that is nearest to the surface and the atom on the surface that is nearest to the tip. The sensor itself is comprised of only two atoms.

Of course, connections need to be made to the sensor so that current can be supplied and information from the measurement can be transmitted elsewhere. In STMs that are used today, the connections are much larger than the 'position sensor' itself (two wires are needed to connect to the sensor atoms). However, there is no reason that the connecting wires can not be tens of nanometers instead of millimeters. Because the STM fundamentally operates on the atomic scale and can be miniaturized, it may prove ideal as a microrobot position sensor. STM position sensors, for example, could be used to provide position feedback for microscopic robot limbs and hands.

¹ The operating principles of the STM are discussed in more detail in Chapter 2.

But the STM can measure much more than just position. The STM is used as a chemical sensor, to measure the band structure of semiconductors, to measure local electric and magnetic fields, and as an accelerometer (by measuring the deflection of a small beam). In the future, microrobots and nanorobots might make extensive use of tunneling multi-mode sensors based on STM technology.

The best way to learn about STM technology and the issues involved in designing sensors based on quantum tunneling is to design and build a tunneling microscope. By constructing an STM, practical engineering knowledge is developed. The knowledge learned is needed to address issues that arise in applying STM technology to micro-robots.

1.3 Thesis Outline

This thesis describes the construction of an STM with an emphasis on issues that were specific to scanning tunneling microscopy and nanoscale engineering. Having built the microscope within the laboratory, experience has been gaired that will allow quick implementation and testing of new ideas and concepts at the nanometer scale.

A second aspect of this thesis is a very brief investigation of a conductive polymer using scanning tunneling microscopy. Results for tunneling from a polymer coated tip to a polymer sample are presented in Chapter 9. The motivation for the polymer to polymer tunneling arises in part from manufacturing issues that could be problematic for microrobots. Assembling parts with many different types of materials (metals, semiconductors, ceramics, polymers, glasses) on such a small scale will be one of the biggest challenges in nano-engineering. Polymers as a class of materials can satisfy all the different subsystem requirements for microrobots, namely energy storage (supercapacitors), actuators (contractile polymers), intelligence (polymer transistors), and sensors (light, force, electric or magnetic field etc.). Problems of assembly and of material incompatibility can be avoided by building an entire nano-scale machine from a single class of materials. Thus polymers are likely to be the material of choice for constructing robots on the micro-scale. STM sensors used in the microrobots will also need to be made from

polymer materials. A second motivation for the polymer tunneling experiments is a more basic interest in the mechanisms and properties of polymer conduction.

Some of the measurements that have been made with the new STM, including some polymer tunneling results, are presented towards the end of the thesis. Chapter 2 of this thesis provides some background on the development of the STM and the physics of quantum tunneling. Chapter 3 describes the issues that arise when engineering is being done at the nanometer scale. Vibration isolation and thermal expansion, for example, are critically important for achieving atomic resolution with an STM. Chapters 4 through 6 discuss other parts of the microscope design, including sample positioning, required electronics, and the algorithms for computer controlled feedback. In Chapters 7, 8, and 9, calibration procedures, system performance, and results (microscope images) are presented. Finally, in Chapter 10, some conclusions are presented and future work is discussed.

Chapter 2: Development of the Scanning Tunneling Microscope

2.1 The Scanning Tunneling Microscope

In 1980, Gerd Binnig and Heinrich Rohrer at IBM Zurich invented a completely new imaging instrument, the scanning tunneling microscope (STM) [Binnig et al., 1982]. The new microscope has allowed scientists to explore material surfaces at a scale that directly shows, for the first time, the individual atoms.

The STM uses a sharp tip which is scanned across a surface to measure its height. Unlike the tip of a stylus profilometer, the STM tip never touches the surface. When a voltage is applied between the tip and the surface being imaged, a small current flows across the tip-sample gap. In classical physics, no current should flow until contact occurs (the tip touches the sample). However, in quantum mechanics, electrons can "tunnel" through gaps (or potential energy barriers) that are classically impenetrable. The likelihood of an electron tunneling across a gap decreases exponentially as the gap width increases. A current of electrons flowing across the gap also decreases exponentially with gap width.

The STM tip scans across the surface with a gap of only a few tenths of a nanometer. The gap is kept constant by raising or lowering the tip if the current flow increases or decreases. Typical currents are on the order of nanoamps.

Almost all STMs use piezoelectric materials to move the microscope tip. Piezoelectrics change their dimensions linearly when a voltage is applied across them and can easily be made to have dimensional changes of nanometers per volt. Using such small length changes per volt, the position of the STM tip can be controlled to a precision of picometers.

Picometer precision is well below the size of an atom (carbon atoms for example have radii of about 200 to 250 pm). If the scanning tip is sharp enough (with only one atom at its end), the STM can resolve individual atoms on surfaces.

2.2 Quantum Mechanics of Tunneling

While a complete mathematical description of the tunneling phenomena as it occurs in three dimensions for the scanning tunneling microscope is very complicated and cannot be analytically solved, it is easy to develop a simple model that describes the basic operating principles of the STM.

In quantum mechanics, the positions of electrons and other particles are described by probabilities. An electron in the lowest energy orbit of a hydrogen atom, for example, is most likely to be 53 pm (one Bohr radius) away from the nucleus. However, the electron could be much closer or much further away. As the distance from the nucleus increases, the chance of finding an electron drops rapidly, but never quite reaches zero.

The probability of finding an electron in a given position is given by solutions to Schroedinger's equation. Schroedinger's equation relates the probability of being in a

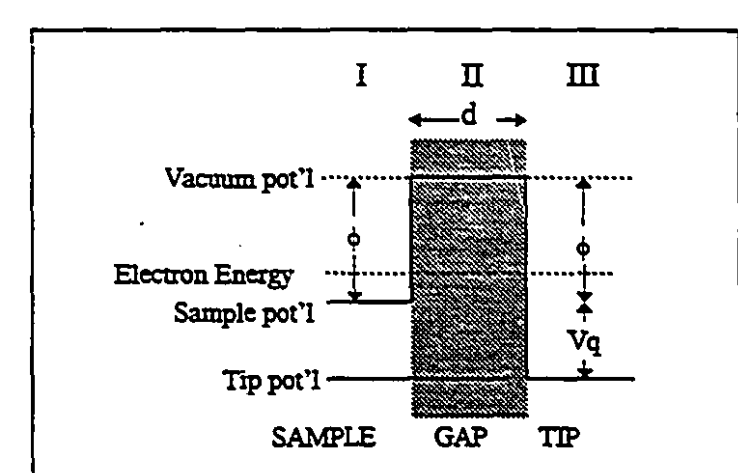


Figure 2.1: One dimensional potential barrier model. The potential energy of the sample is Vq Joules above the potential of the tip (V is a bias voltage and q is the charge on an electron). The potential barrier exists because of the energy needed to remove an electron from the sample into vacuum. V is the voltage applied to the tip and q is the charge on an electron.

certain state or position to the potential energy distribution. For the tunneling current in an STM, we will model the current using a simple one dimensional potential shown in Figure 2.1. Both the sample and tip are conductive and have uniform potentials (regions I and III). There is an energy potential difference Vq (q is the charge on an electron) between the sample and tip that is caused by a tip to sample bias

voltage. Between the two conductive regions there is a vacuum gap of thickness d (region II). The potential energy difference between the sample region I and the gap region II is given by the work function ϕ , which is the energy needed to remove an electron from the sample into the vacuum. For simplicity, we will assume that the work function of the tip is

the same as that of the sample. The potential of the tip is then the work function potential plus the potential energy due to the bias.

We can substitute the potential from Figure 2.1 into Schroedinger's equation,

$$-\frac{\hbar^2}{2m}\frac{d^2}{dx^2}\psi(x)+U(z)\psi(z)=E\psi(z),$$

where \hbar is Planck's constant, m is the mass of an electron, E is the energy of the electron, U(z) is the potential energy function, and $\psi(z)$, called the wave function, is a complex function related to the probability density at the position z^{-1} . The probability P(z)dz that the electron be found in an infinitesimal space dz around z is given by $P(z)dz = \psi(z)\psi^*(z)dz$.

In region I, to the left of the potential barrier, and in region III, to the right of the potential barrier, the solutions are of the form:

$$\psi_I(z) = \psi(0)e^{\pm ikz},$$

$$\psi_{II}(z) = \psi(d)e^{\pm ik(z-d)},$$

where $k = \sqrt{\frac{2m(E-U(z))}{\hbar^2}}$ and E > U(z). Since E > U(z), in regions I and III the possible wave functions are sinusoids of constant amplitude. The product $\psi(z)\psi^*(z)$ is a constant and so the probability of finding an electron either region I or region III does not

change with z. In region II (the barrier), E < U(z) and the possible wave functions are:

$$\psi_I(z) = \psi(0)e^{zz},$$

where $\kappa = \sqrt{\frac{2m(U(z)-E)}{\hbar^2}}$. For the case of a bias potential Vq that is much smaller than

the work function ϕ , the difference $U(z)-E\approx\phi$, and $\kappa=\frac{\sqrt{2m\phi}}{\hbar}$. The probability of finding an electron in the barrier is $\psi_{II}(z)\psi_{II}^{\bullet}(z)=|\psi(0)|^2e^{2\pi c}$, where the positive exponent gives the likelihood of finding an electron that originated on the positive z side

 $[\]hbar = 6.64 \times 10^{-34} \text{ Js, m} = 9.11 \times 10^{-31} \text{kg.}$

and the negative exponent gives the likelihood of finding an electron that originated on the negative z side of the barrier. If there is no bias voltage, electrons are equally likely to tunnel in one direction as in the other and the net tunneling current is zero. However, in the presence of a bias voltage, tunneling in one direction becomes preferred and a tunneling current flows.

The current that tunnels from the tip to the sample is proportional to the number of tip electron energy levels between the tip potential and the sample potential. Electrons in these energy levels will lower their energy when they travel across the barrier. The number of energy levels is approximately the product of the local density of energy states ρ_s and the voltage bias V_b and so

$$I_{c} \propto V_{b} \rho_{s} |\psi(0)|^{2} e^{-rd}$$

where, as before, $\kappa = \frac{\sqrt{2m\phi}}{\hbar}$, and d is the gap width.

Notice that the tunneling current decreases exponentially with the gap width d. For every increase or decrease in the gap width by a factor of $\frac{1}{\kappa}$, the magnitude of the current changes by 2.718 times (e¹ times). The current changes by an order of magnitude for an increase or decrease in the gap width by a factor of $\frac{2.303}{\kappa}$. It is the exponential dependence of current on gap width that gives the STM its very high sensitivity to surface height changes.

For common metals, the work function varies between 4 and 6 electron volts (eV) or between about 6×10^{-19} and 9×10^{-19} Joules (J). Using $\phi = 5.5$ eV= 8.8×10^{-19} J², we find that the current changes by one order of magnitude when the gap width changes by:

Some typical work functions for metals often used as either sample of tip are: gold, 5.4 eV; platinum, 5.7eV, iridium, 5.6eV. The work function used in the calculation of the value of K is usually the average of the tip and sample value. Work functions for other materials can be found in [Handbook for Chemistry and Physics, 1992-93]

$$\Delta d = 2.303 \frac{\hbar}{\sqrt{2m\phi}}$$
$$= 0.19nm.$$

Different work functions will result in different changes in current per change in distance.

By deliberately varying the tunnel gap width so that the exponential coefficient κ can be measured, scanning tunneling microscopes can differentiate between materials with different work functions, making possible a chemical analysis of a surface. Local chemical information is important for understanding alloy structure or conducting polymer morphology. Ultimately, it may be possible to determine the composition of conducting materials atom by atom across a surface. However, the concept of a work function is defined for a large uniform surface where surface electronic states interact over many atoms. For example, a single atom of gold isolated on carbon surface will exhibit a very different 'work function' than a gold atom that is part of a gold surface. Because of the complex interaction of wavefunctions from neighbouring atoms, the determination of the species of individual atoms will be very challenging.

Another characteristic of the tunneling current equation is that it depends on the local density of states of the surface being imaged. By altering the bias voltage, the local density of states can be probed at different energies. For metals (conductors) the local density of states does not change significantly even for large bias voltage changes (on the order of volts). However, semiconductors exhibit significant changes in the local density of states as the energy moves from the valence band to the conduction band. Information about the electronic structure of semiconductor bandgaps (the energy gap between the valence band and the conduction band) can be probed by taking STM images at different bias voltages³. It may also be possible to learn about the bond structure and the conduction mechanisms in conducting polymers by measuring the local density of states as a function of electron energy.

³ Examples of this type of imaging are given in [Chen, 1993] (e.g. plates 8 and 9).

2.3 Applications of STM

STMs are primarily used to investigate the structure of surfaces. Applications of STM to surface structure determination range from simply measuring grain size of sputtered gold to determining the electronic structure of semiconductor surfaces.

Some of the first atomic resolution results were obtained on graphite surfaces. The regular hexagonal pattern of the carbon atoms can be observed even in air because of the inertness of the graphite surface. Atomic resolution on many metals has been achieved but usually only for clean surfaces in a vacuum. Many metals develop a thin insulating oxide layer in air that makes imaging the surface atomic structure difficult. Gold, aluminium, copper, platinum, ruthenium, and nickel are among the metals whose atomic surface structure has been observed. The atomic structure of metals that are relatively inert such as gold and platinum have also been observed in air.

The surface structure of graphite and of many metals is periodic and can often be determined using other methods such as LEED (low-energy electron diffraction) or atom beam scattering which measure bulk crystal properties. Atomic resolution has been achieved with TEM (transmission electron microscopy) and high energy SEM (scanning electron microscopy) but samples must be very thin to image only a single layer of atoms. To obtain an SEM image of uranium atoms, individual uranium atoms are stuck on a thin carbon film [Ohanian, 1989, p. 14]. The uranium atoms appear as very bright spots on a dark background. However, for aperiodic structures or surface measurements on thick samples, LEED, TEM, SEM and other methods are unable to give complete information about structural details. In some cases even periodic surfaces are too complex for LEED to give an unambiguous surface structure.

In these cases, STM is required to give a detailed atomic level understanding of the surface. For example, the surface of gold along the (111) orientation exhibits symmetric axes that are 120 degrees apart. The points where the axes of symmetry change are randomly distributed across the surface and so the structure was not well understood until scanning tunneling microscope images were obtained [Chen, 1993, Ch. 16]. Smaller structures such as dislocations and missing atoms are also easily observed with STM. The

ability to image such surface features is what distinguishes STM from other imaging modes that have atomic resolution.

The first major discovery using an STM was the Si(111)-7x7 structure. In LEED experiments in 1959, it was found that the Si(111) surface was made up of units cells with forty-nine silicon atoms. However the exact arrangement of the atoms continued to be debated until 1985, when a group led by Takayanagi used STM images to resolve the problem [Chen, 1993]. The first image of the Si(111)-7x7 surface was in fact obtained by Binnig and Rohrer [Binnig et al., 1983a].

There is a huge range of other applications of scanning tunneling microscopy.

Large ordered structures such as liquid crystals have been imaged [Smith et al., 1989]. When the liquid crystals (n-alkylcyanobiphenyl in Smith's paper) are adsorbed onto graphite, they form two dimensional crystalline domains which can be seen by STM.

Other studies have used STM to measure the surface roughness of materials and relate roughness to observed properties such as chemical reaction rate or magnetic behaviour. For example, the magnetic properties of cobalt alloys (in magnetostriction) can be related to the alloys' surface roughness as measured by STM [Aguilar et al., 1992].

Walls et al. used the STM to examine very low load Vickers pyramid indentations (loads of 0.15-0.50 Newton) on a silicon surface [Walls et al., 1992]. The surface profile, the depth, and the angle of indentation were measured to improve the understanding of the mass displaced by the pyramid at very small scales.

Many different organic molecules have been imaged. Among the most exciting applications is the imaging of DNA. Garcia et al., for example, have imaged DNA adsorbed onto mica [Garcia et al., 1992]. In order to fix the DNA so that the tip doesn't push it across the surface and to make the surface conductive, the DNA and mica are coated with a thin metallic (usually gold) film. The resolution of the images is limited by the size of the metal grains (typically 5-10 nm) and therefore cannot yet resolve individual base pairs (separated by 0.34 nm). The stretched out DNA molecules appear as long winding protrusions in the images.

Some other organic molecules have been imaged without metallic coatings. Ohtani et al. obtained images of benzene rings (adsorbed on graphite) [Ohtani et al., 1988]. Masai et al. observed H-ATPase, a molecule important in the energy processes of all cells [Masai et al., 1992].

The major difficulties when imaging biological or organic molecules with the STM are that the molecules tend to have low conductivity and that many of the molecules are soft and flexible and so are easily moved or distorted by the STM tip. Because of these problems, the resolution obtained is not as good as for harder crystalline structures such as metals or semi-conductors. So far, atomic resolution has not been achieved.

The ability of the STM to image electronic states (e.g. local density of states) has been used to observe different dangling bonds from a silicon surface. Boland passivated a Si(100) surface with hydrogen and, by carefully heating the surface, was able to remove a small number of the adsorbed hydrogen atoms. When the hydrogen atoms leave, two adjacent silicon atoms pair their p_z dangling bonds to form a π bond which can be seen in the STM images [Boland, 1991], [Chen, 1993, Ch. 16].

STM images have been taken of surfaces in water and even in electrochemical solutions. The tunneling current in an electrolyte is mixed with a faradaic current, reducing the signal to noise ratio, but by insulating the STM tip almost to the very end, the effect of the faradaic current is minimized. Magnussen et al. observed the position of individual copper atoms as they were electrodeposited onto Au(111) and Au(100) surfaces [Chen, 1993, Ch. 16]. Robinson et al. obtained spectroscopic chemical images (which measure the change in current for a small change in tip-sample distance) in an electrolytic solution [Robinson et al., 1992].

An interesting effect that can occur with STM is light emmission from the tunneling junction. Electrons injected from the STM tip with an energy higher than the conduction band energy of the sample fall to the lower band and emit light. The emitted light can give information about the local electronic structure of the material [Renaud and Alvarado, 1992] [Uehara et al., 1992], [Ushioda, 1992].

The STM has also been used to nanofabricate surfaces. Scientists at IBM have written words using single atoms of Xenon on a surface in vacuum [Eigler and Schweizer, 1990]. Moving single atoms requires very low temperatures to avoid diffusion effects but nanometer size (10-100 atoms) fabrication has been done at room temperature. Small holes or indentations in an HOPG surface have been repeatedly made with diameters as small as 4 nm [McCarley et al., 1992] by applying a voltage pulse to tip. Small deposits of material have been made on surfaces by using high electric fields to remove small amounts of material from gold tips [Abraham et al., 1986]. Wires only 3 nanometers wide have been fashioned by selectively oxidizing a thin layer of Titanium on Silicon (using an STM/atomic force microscope combination) [Snow and Campbell, 1995]. A local oxidation reaction can be started by setting the tip voltage to the correct potential which replaces the titanium with insulating titanium oxide. By carefully controlling the time and the amplitude of the voltage that is applied, the thickness and width of the oxide layer can be controlled to leave conducting traces.

Other novel uses of the STM include non-destructive testing by measuring surface displacement waves [Strozewski et al., 1992] and possible use as a gravitational wave detector [Bocko, 1990], [Bocko et al., 1988], [Niksch and Binnig, 1988].

After the invention of the scanning tunneling microscope, many other types of scanning probe microscopes were developed. The atomic force microscope (AFM) measures the deflection of a very small beam caused by forces between a tip at the end of the beam and a sample. By scanning the tip back and forth, surface contours of insulating materials can be mapped. Other scanning probe microscopes include scanning capacitive microscopes, scanning optical microscopes, and scanning magnetic probe microscopes. Each of these microscopes gives localized information about different types of surface properties.

The STM has opened up whole new areas of scientific exploration. The microscope combines the ability to both image and manipulate surfaces at the atomic scale and so offers exciting new opportunities in nanoscale observation and fabrication. Since the microscope relies on quantum mechanics, it can be miniaturized for integration as a sensor in micro- or nanorobots. In this chapter, an overview of the STM and its applications was given. The next chapter will look at special considerations that need to be taken into account when designing a scanning tunneling microscope.

Chapter 3: Special Considerations for Design

3.1 Requirements

The successful construction of a scanning tunneling microscope requires careful attention in several areas that are not always important in mechanical design. Measurements are made on the atomic scale, and many physical effects that are normally negligible can affect STM operation. Floor and acoustic vibrations or thermal expansion can cause motions thousands of times larger than a single atom. STM tips that under a light microscope might appear to be sharp, may have radii of curvature of hundreds of nanometers or may have many small tips that cannot be resolved with visible wavelengths and which can cause multiple tunneling paths to the sample.

3.2 Vibration Isolation

The tip to sample distance in an STM needs to be maintained to within better than a tenth of a nanometer to achieve atomic resolution. But in a typical laboratory environment, vibrations of the floor can be many orders of magnitude larger. For example, measurements of the floor vibrations on the third floor of the Lyman Duff building at McGill showed a displacement amplitude of about 110 nm rms [Brenan et al., 1992]. Most of the displacement is concentrated in frequencies below about 200 Hz. Measurements of vibrations reported from other laboratories have similar frequency ranges and similar or higher amplitudes [Pohl, 1986], [Schmid and Varga, 1992]. Measurements were not made of the floor vibrations in the laboratory where the STM was used. The vibration levels are however high since it is possible to feel the floor move even if someone is walking on the other side of the room.

In the first experiments demonstrating tunneling through a controllable vacuum gap, Binnig, Rohrer, Gerber, and Weibel [Binnig et al., 1982] mounted their tunneling apparatus onto a base which had strong permanent magnets attached to it and was

¹ The microscope is currently set up at the Massachusetts Institute of Technology, Cambridge, MA.

magnetically levitated above a bowl of superconducting lead. A normally conducting metal attached to the bowl damped out vibrations using eddy currents. The tunneling apparatus was thus isolated both thermally and mechanically from the table on which it sat. The table itself was a heavy stone bench mounted on rubber inner tubes to further isolate the setup. In the tunneling experiments, the gap was stable to within 20 picometers.

The second design by Binnig and Rohrer [Binnig and Rohrer, 1983] used a two stage coil spring system² with eddy current damping provided by permanent magnets and copper rods. Again, the apparatus gave stability to better than 20 picometers. Binnig and Rohrer used this apparatus to obtain images of atomic steps on gold (the Au(110) surface) and on silicon (the Si(111) surface).

Isolation systems used in STMs now follow one of two basic designs. The first is to use a mass/coil spring/damper system much like that of Binnig and Rohrer. The other design uses stacked metal plates with an elastomer (usually Viton O-rings) between the plates [Gerber et al., 1986]. Typically, four or five metal plates are stacked one above the other, separated by short vertical pieces cut from Viton O-ring (in Gerber et al., the Viton pieces are 5 mm long and 2 mm in diameter). The elastomer provides both spring and damper. While the vibration attenuation for one metal plate is not as good as for a single spring system, by stacking plates the attenuation of higher frequencies can be good enough to provide atomic resolution. Because they are compact and easy to build, the stacked metal plates with elastomer springs are more commonly used in newer designs. Both the mass-spring-damper designs and the stacked metal plate with elastomer designs attenuate high frequencies but allow low-frequencies to pass through.

If the mechanical structure of the STM itself is very rigid (has a high resonant frequency), the low frequencies that are not attenuated by the vibration isolation are not transferred to the tip-sample junction. For vibrations that are below the structure's resonant frequency, the entire structure moves without deforming. Vibrations at and above the resonant frequency can act to deform the STM structure and change the tip-

² See also [Binnig and Rohrer, 1986] for a comparison of the different vibration isolation systems used by Binnig and Rohrer in their laboratory.

sample distance. Thus, the vibration isolation must attenuate vibrations at and above the mechanical resonant frequency to below the desired noise level. For atomic resolution, the vibrations passed by the isolation at the resonant frequency must be less than about 0.1 nm.

A number of papers have been written which analyse vibration isolation for STMs [Binnig and Rohrer, 1986], [Pohl, 1986], [Park and Quate, 1987], [Okano et al., 1987], [Kuk and Silverman, 1989], [Schmid and Varga, 1992], see also Chapter 10 in [Chen, 1993]. Park and Quate describe a two stage spring-mass-damper system and theoretically determine what the optimum parameters should be. Okano et al. compare stacked elastomer isolation to a two stage coil spring system and find that the two stage spring system actually offers better performance.

Stacked elastomer systems typically have cut-off frequencies in the tens of Hertz whereas suspended coil spring systems can have cut-off frequencies below one Hertz. For equal order systems, a lower cut-off frequency gives better attenuation at a given higher frequency. In a well designed STM, the mechanical structure is rigid enough to prevent low frequency vibrations from affecting the tip-sample separation. Since the ratio of displacements of the isolated platform to the displacements in the lab gets smaller for each decade of frequency above the cut-off, reducing the cut-off improves high-frequency attenuation.

The isolation system for the STM described in this thesis uses a three stage isolation system (see Figure 3.1). The STM sits on a single stage mass-spring-damper system that is in turn mounted on a 20 mm thick 400 mm square aluminium (T6 6061) plate. The second stage spring and damping are both provided by an inflated rubber bicycle inner tube beneath the aluminium plate. The inner tube sits on a commercial vibration isolation table, which provides the third stage of isolation (Technical Manufacturing Corporation Model 63-754, Peabody, MA). A stacked elastomer system was used initially because it was easier to construct but was not found to give adequate isolation for atomic resolution images. The three stage vibration isolation resulted in

much better tunneling gap stability (atomic resolution was achieved on HOPG (highly oriented pyrolytic graphite)).

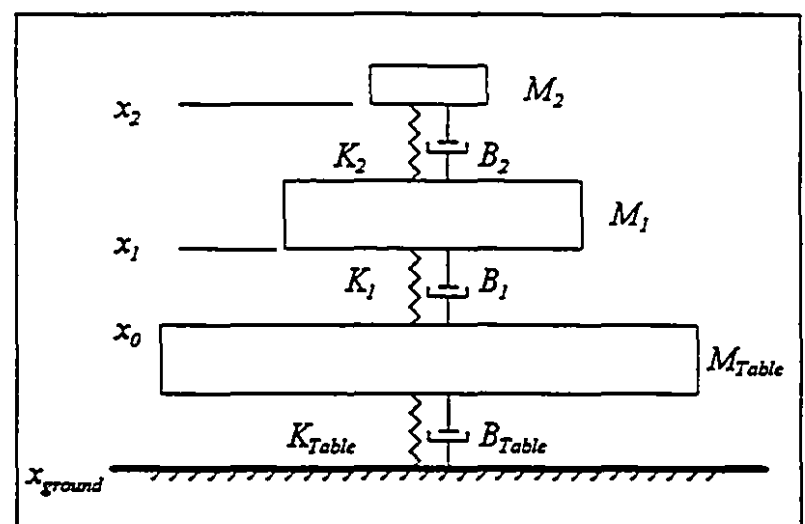


Figure 3.1: STM vibration isolation system. M_1 , B_1 , and K_1 are the effective mass, damping, and spring constant of the rubber inner tube. M_2 , B_2 , and K_2 are the mass, damping, and spring constants of the mass-spring-damper system and M_{Table} , K_{Table} , B_{Table} are the constants for the vibration isolation table. The x variables are the positions of the different stages.

The mass-spring-damper and the inner tube act as low-pass filters that are coupled and cannot be treated independently. The isolation table, however, is much more massive than the other isolation stages and can be treated on its own. The equations of motion for the rubber inner tube and the mass spring damper stages are

$$M_1\ddot{x}_1 = -K_1(x_1 - x_0) - B_1(\dot{x}_1 - \dot{x}_0) - K_2(x_1 - x_2) - B_2(\dot{x}_1 - \dot{x}_2),$$

$$M_2\ddot{x}_2 = -K_2(x_2 - x_1) - B_2(\dot{x}_2 - \dot{x}_1),$$

where the M, K and B parameters are the masses, spring constants, and damping constants of the two stages. x_0, x_1 , and x_2 are the positions of the isolation table, the 400 mm by 400 mm aluminium plate (M_I) , and the STM on the mass-spring-damper (M_2) respectively.

By taking the Laplace transform of both equations, we can solve for the transfer function between the isolation table and the STM,

$$\frac{X_2}{X_0} = \frac{(B_1 s + K_1)(B_2 s + K_2)}{\left(M_1 s^2 + (B_1 + B_2)s + K_1 + K_2\right)\left(M_2 s^2 + B_2 s + K_2\right) - (B_2 s + K_2)^2},$$

where X_0, X_1 , and X_2 are functions of the frequency variable $s = j\omega$.

Since the isolation table is effectively independent from the other two stages, the cross-coupling effects between the isolation table and the upper two stages can be neglected. The combined transfer function is given by the isolation table in series with the two other stages:

$$\frac{X_{2}}{X_{0}} = \frac{(B_{1}s + K_{1})(B_{2}s + K_{2})}{(M_{1}s^{2} + (B_{1} + B_{2})s + K_{1} + K_{2})(M_{2}s^{2} + B_{2}s + K_{2}) - (B_{2}s + K_{2})^{2}} \times \frac{B_{Table}s + K_{Table}}{M_{Table}s^{2} + B_{Table}s + K_{Table}}.$$

The transfer function is sixth order but only has a high-frequency roll-off of three orders of magnitude for every decade increase in frequency. Changing the value of the parameters will change the frequencies at which the different stages will begin to attenuate vibrations and the shape of the transfer function around those points.

While the above equation accurately describes the system if all the parameters are known, in the development of the isolation system, the parameters were not well known and the masses and damping were adjusted using somewhat qualitative measures of performance. The transfer function does however serve as a guide for predicting the performance of the system. For the mass-spring damper stage, the mass and spring constant were chosen to give a natural resonant frequency close to 1 Hz. The resonant frequency of the inner tube stage was measured to be on the order of a few Hertz and the stage is underdamped, taking about seven or eight cycles to stop oscillating. Finally, the vibration isolation table has a natural frequency of close to 1 Hz.

From the transfer function, the system behaviour is sixth order system with high-frequency attenuation of three orders of magnitude per decade. Since the natural frequencies of all the stages are on the order of a few Hertz, floor vibrations of as much as several micrometers with frequencies higher than several tens of Hertz should be attenuated at least a thousand times and frequencies of several hundred Hertz should be attenuated a million times. If the vibration amplitudes are less than micrometer, the amplitude of vibrations of the STM will be less than one nanometer above a few hundred Hertz.

3.3 Precision Motion Control

When the microscope tip is close to the sample and the tip is being scanned back and forth, very precise motion control is needed to keep the tip to sample distance constant. Since the tip to sample distance is usually on the order of tenths of a nanometer, the tip actuator needs to be controllable to within at least the picometer range. The response time of the actuator should be fast so that images of surfaces can be taken quickly. If the response time is too slow, the tip will not be able to move quickly enough to keep the gap constant and may crash into the surface³. Finally, the actuator must have a range of motion large enough that it is easy to position the sample within its reach.

There are many different materials that respond to an applied voltage by changing their shape. These fall into two broad categories, piezoelectric materials and electrostrictive materials. Both of these materials exhibit continuous changes in dimension as the voltage is changed. The actual shape change that occurs is a function of material composition and geometry. The minimum "step size" of an actuator made from either type of material is limited by the type of material, the shape of the actuator, and the noise level of the applied voltage⁴. Both piezoelectric and electrostrictive materials can be made into actuators a few centimeters long with better than picometer resolution. The maximum dimension change is determined by the material composition, geometry, and by the maximum electric field that can be applied.

Other types of materials or actuators that could be used include photostrictive or magneto-strictive materials, or electromagnetic actuators. Photostrictive and magneto-strictive materials exhibit a dimensional change when irradiated with light (see for example [Uchino, 1990]) or are subjected to a magnetic field. Electromagnetic actuators are not used for STM because commercially available actuators generate heat in the current coils that causes thermal expansion that would distort images, have low resonant frequency (because of a large mechanical structure) which limits their performance, and do not have the required picometer resolution.

³ The control algorithm used must also be fast enough to prevent the tip from crashing into the surface.

⁴ For extremely small displacements, motions due to statistical fluctuations will actually be the limit to the step size.

Almost all STM designs use piezoelectric ceramics for precision motion control. Piezoelectric ceramics are relatively inexpensive (\$100-\$200 for a typical part used in STM) and are widely available from a variety of commercial sources (e.g. EBL Crystal Products, East Hartford, CT; Siemens, Erlangen, Germany; Morgan Matroc, Vernitron Division, Bedford, OH; Phillips, Eindhoven, Netherlands).

The piezoelectric effect was first discovered in single crystals of quartz by the Curie brothers in 1880 [Chen, 1993]. In piezoelectric materials, two or more atoms form an electric dipole that creates a permanent electric field. When an external field is applied, the equilibrium distance between the atoms changes. It is the change in spacing between the atoms that causes the observed change in size of the material.

The most commonly used piezoelectric material in scanning tunneling microscopes is Lead Zirconate Titanate (or PZT). In its commercial form, PZT is a ceramic made up of small grains of crystalline PbZrO₃ and PbTiO₃. The piezoelectric effect reaches a maximum when the composition is about 45% PbZrO₃ and 55% PbTiO₃. Commercial PZT usually includes a small percentage of impurities to optimize the properties for different applications.

When the ceramics are made, the dipoles of the crystalline grains are oriented randomly. For the microscopic changes in grain size to be observed on a macroscopic level, the dipoles must be aligned with each other. The "poling" process, usually done during manufacture, requires that the material be placed in a very high electric field (for Lead Zirconate Titanate, the recommended poling field is $6x10^5$ V/m for at least an hour [Chen, 1993, Ch. 9]).

If two electrodes are put on opposite sides of a rectangular piece of (poled) PZT, the dimensions x, y, and z of the PZT change linearly with applied electric field E (see Figure 3.2):

$$\frac{\Delta z}{z} = d_{33}E_3,$$

$$\frac{\Delta x}{x} = d_{31}E_3,$$

$$\frac{\Delta y}{y} = d_{32}E_3,$$

where by convention, the z direction is the direction of polarization and is denoted by the subscript 3. d_{33} , d_{31} , and d_{32} are called the piezoelectric coefficients and, for PZT, have typical magnitudes between about 0.05 nm/V and 0.6 nm/V⁵.

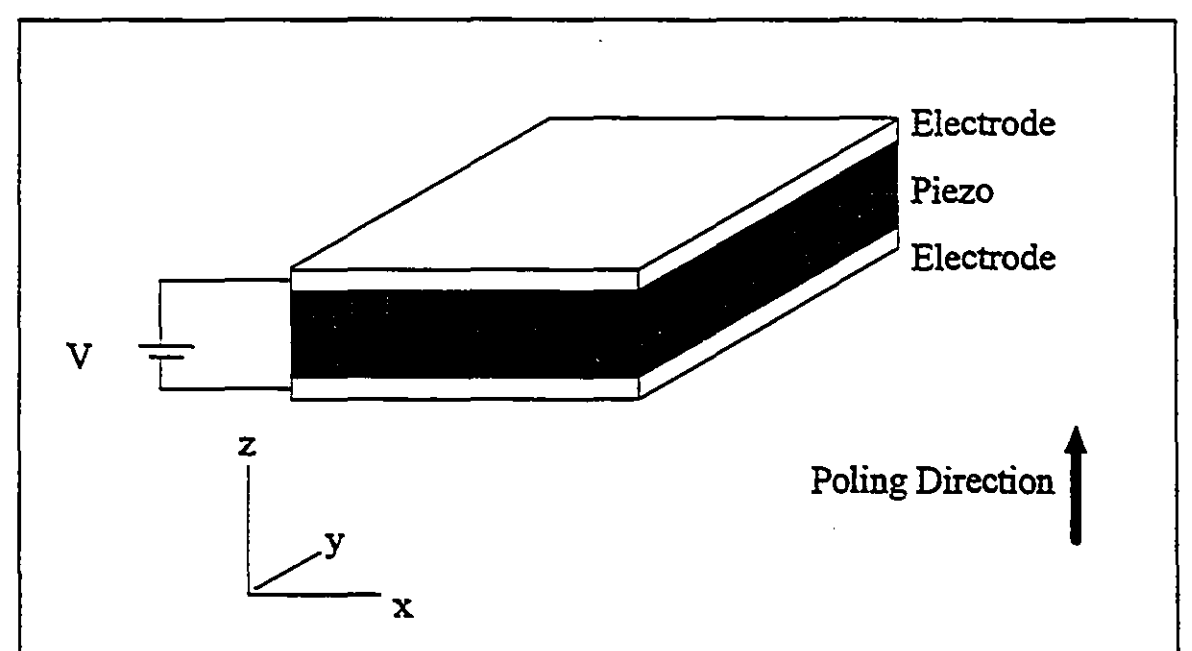


Figure 3.2: When voltage is applied to the electrodes on the piezoelectric material, the shape of the material changes.

Several properties of the PZT materials need to be kept in mind during use. There is a maximum field that can be sustained by the materials. If the piezo is subjected to a field beyond its maximum, the material can be damaged or, if the field is in the opposite direction of the poling field, the dipoles can lose their alignment and the piezoelectric effect is weakened.

⁵ For example, Morgan Matroc PZT-7A, $d_{31} = -0.060$ nm/V and for PZT-5H, $d_{33} = 593$ nm/V.

The dipole alignment can also be lost if the ceramic is raised beyond its Curie temperature (typically 200 to 300 degrees Celsius). Above the Curie temperature, the individual grains have enough thermal energy to reorient themselves randomly and the piezoelectric effect is partially or completely destroyed. At temperatures below but close to the Curie point, the piezo material will gradually lose its dipole alignment, since some of the dipoles will still have enough energy to reorient themselves.

Even well below the Curie temperature, temperature changes can cause significant variations in the piezoelectric properties. A temperature rise from 0°C to 100°C, for example, can change the d_{31} coefficient by between 10% and 40% depending on the specific PZT ceramic used. If large temperature variations are expected during operation of the STM, changes in properties need be taken into account when choosing the specific PZT material used for fine position control. Special design precautions may need to be taken to compensate for length changes of the PZT due to thermal effects.

There are also time effects in PZT. First, there is a long term change in the piezoelectric coefficients as some of the ceramic dipoles continue to change their alignment (relaxation) after the initial poling process. The changes are logarithmic with respect to time and so the materials gradually become more stable. The change over time of the piezoelectric properties varies from less than 0.1% change per time decade to almost 7% per time decade (again depending primarily on the specific composition of the chosen PZT ceramic).

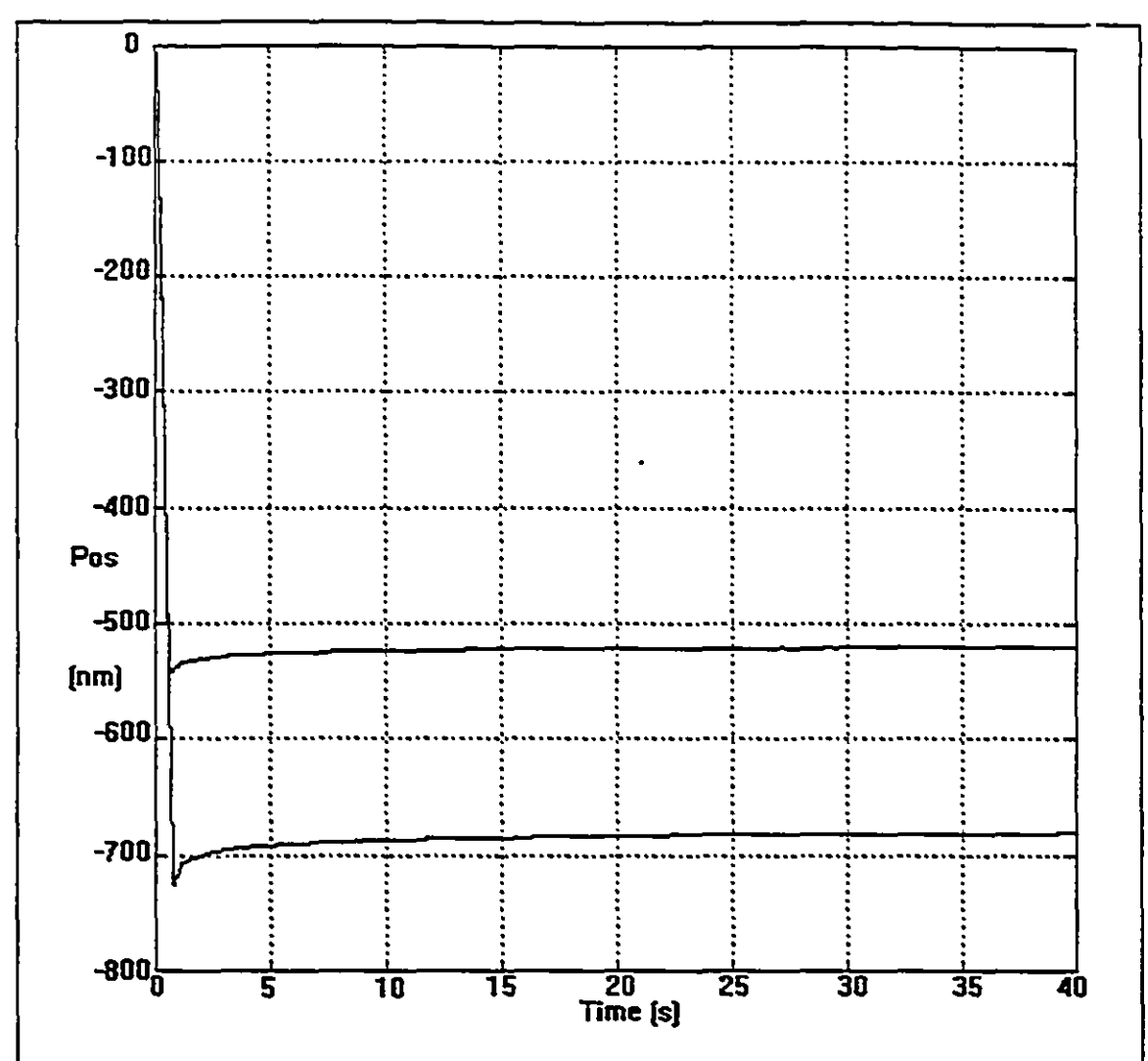
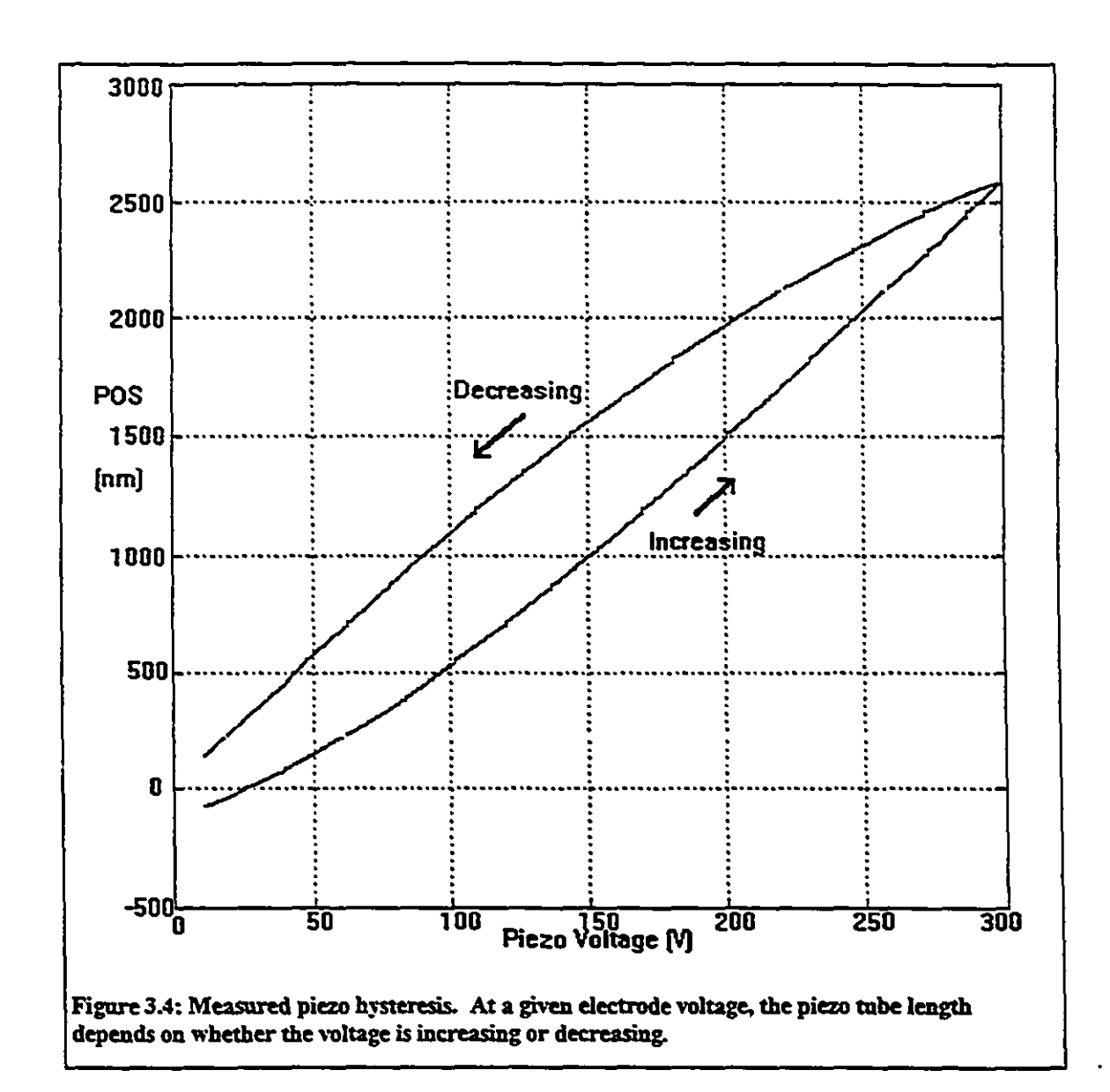


Figure 3.3: Measured creep of piezo tube position after step changes in the applied voltage. The zero position corresponds to zero volts applied to the tube.

The second time effect in PZT is a creep when the PZT is subjected to a voltage change. After an initial step change in position, the ceramic continues to move slowly in the same direction for some time. If many steps are taken in rapid succession and in different directions, the creep direction can be difficult to predict because of the combined effect of creep from all the steps. PZT creep can be as high as 20% of the step size (see Figure 3.3, which is also discussed in Chapter 7) and lasts over a time period of minutes. Creep can cause significant image artifacts, particularly if a large piezo voltages are used.

Another property of PZT ceramics that can distort images with large height variations is piezo hysteresis (measured hysteresis is shown in Figure 3.4). Hysteresis is caused by energy loss through internal friction in the piezo material itself. The piezo length follows a different path when the voltage is increasing than when the voltage is



decreasing. When the piezo material is subjected to large position changes, the difference in the path can become quite large⁶. The composition of the PZT ceramic material can be

⁶ For example, Hues et al [Hues et al., 1994] measured a hysteresis curve whose maximum path difference was over 200 nm for a total length change in their piezo tube of just over 1400 nm.

adjusted to reduce hysteresis. However, materials with less hysteresis generally have lower piezoelectric coefficients which reduces the position range over which the actuators can be used.

Other non-linearities also cause image defects for large piezo displacements. The piezo coefficients are not actually constant with applied field. As the magnitude of the field increases, the displacement per volt increases ([Viera, 1986], [Hues et al., 1994]).

In almost all STM imaging, non-linearities are ignored. They are ignored in part because they tend to be fairly small (less than five or ten percent of the total image range) but mostly because hysteresis and creep have not been well modeled for STM and so it is difficult to compensate for them.

When piezoelectrics are used as the tip actuator for STM, the tip needs to move in three dimensions — two dimensions parallel to the surface to scan back and forth and one

Z Piezo
Y Piezo
Y Piezo
Figure 3.5: Piezoelectric tripod configuration for STM scanner.

perpendicular to the surface to maintain a constant distance from the surface.

For the first few years of STM development, the scanning mechanism consisted of three orthogonal piezoelectric elements in a tripod configuration shown in Figure 3.5 (see for example [Binnig and Rohrer, 1983]). Movement in any direction x, y, or z occurred when the corresponding piezo element was extended or contracted. The other two

elements of the tripod flex slightly to accommodate the length change. For the tripod system, it is assumed that the displacement along any of the three axes is simply given by the length change of the corresponding piezo:

$$\Delta x_{i} = K \Delta V_{i}$$

where Δx is the change in length of the ith axis, K is the change in length per volt applied $(K = d_{31} \frac{L}{\ell}, L = \text{length of piezo element}, t = \text{thickness of element})$, and ΔV_i is the change in applied voltage. When one piezo element is extended, the other two bend slightly to accommodate the change in position. For the very small deflections used in STM scans, the strains are small enough that the coupling between axes is negligible. As STM designs improved and higher performance was sought, the tripod system fell out of favour because of the low mechanical resonance frequencies (typically about 3 kHz) that arise from having to move the masses of all three piezo elements.

In 1986, Binnig and Smith introduced the tube scanner [Binnig and Smith, 1986] with an inner ground electrode and four outer quadrant electrodes (see Figure 3.6). A tube scanner can be made smaller (and therefore has a higher resonant frequency) than a tripod scanner with the same range of motion. A voltage applied to all four external quadrants at the same time extends or contracts the tube. For motion in the x or y direction (perpendicular to the axis of the tube), a positive voltage is applied to one quadrant and an equal magnitude but negative voltage is applied to the opposite quadrant. One quadrant extends while the other contracts, creating a torque that bends the tube and moves the STM tip. Even at maximum bending radii, the length change in z is very slight because the motions are very small (typically less than 1µm x and y motion for a tube about 10 mm long, which causes about a 0.1 nm change in z).

The magnitudes of the x and y deflection of the piezo tube due to an applied voltage has been analytically solved by Chen [Chen, 1992]. Chen finds the tube deflection in both the case where a bipolar voltage is applied (the inside electrode is grounded and opposite outside electrodes are at potentials $\pm V$ and $\pm V$) and the case where a voltage is only applied to a single quadrant and all other quadrants are grounded. The piezo tube

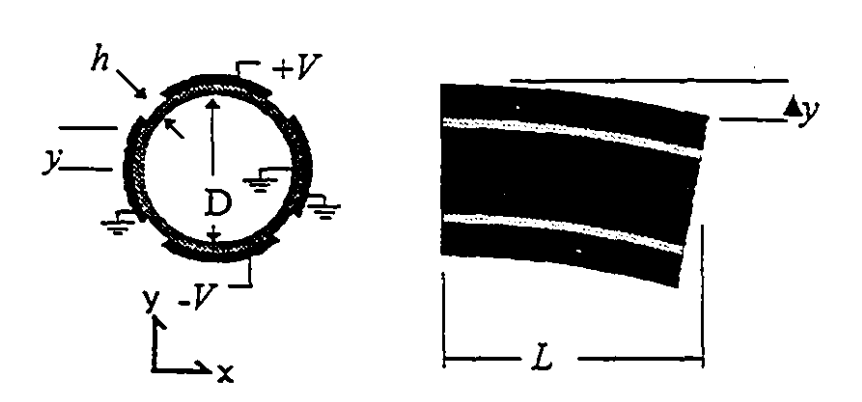


Figure 3.6: Piezoelectric tube with four outer electrodes. When a voltage is applied between outer electrodes (dark gray) and the inner electrode (on the inner surface of the tube), the piezoelectric tube deflects.

actuator used in this thesis used a bipolar voltage configuration. For a bipolar voltage V, a piezo tube of inner diameter D, thickness h, and length L with one inner electrode and four (quartered) outer electrodes (Figure 3.6), the deflection Δy is:

$$\Delta y = \frac{2\sqrt{2}d_{31}L^2}{hD\pi}V.$$

The term $\frac{2\sqrt{2}d_{31}L^2}{hD\pi}$ is called the piezo constant and determines the sensitivity and range of the piezo tube in the y direction. Since the piezo tube is symmetric, the piezo constant for the x direction is identical:

$$\Delta x = \frac{2\sqrt{2}d_{31}L^2}{hD\pi}V',$$

where V' is the bipolar voltage applied to the x-direction electrodes. The piezo constant for the 12.5 mm diameter, 12.5 mm long, 0.51 mm thick piezo tube used for this thesis is 3.8 nm/V.

If the same voltage is applied to the four outer electrodes, the tube undergoes a strain in the z direction $s_3 = V \frac{d_{31}}{h}$ or

$$\Delta z = \frac{\ddot{a_{31}}L}{h}V,$$

where V is the voltage applied to all four electrodes. The z direction piezo constant for the piezo tube used in this thesis is 4.2 nm/V.

By applying a voltage to all four outer electrodes to extend the piezotube in the z direction or adding bipolar voltages to the two x and the two y electrodes, the end of the piezotube can be moved in all three directions. The piezotube provides a very compact solution for precise motion.

The range of motion of the piezotube actuator is limited by the maximum electric field that can be applied to the piezo ceramic. For a piezo tube that has a thickness of 0.51 mm, the maximum applied voltage is 240 V. The total displacement in the x, y, and z directions are ± 845 nm, ± 845 nm, and ± 1000 nm.

The resonant frequencies of the piezo tube can be calculated using standard equations. In the longitudinal and bending directions, the resonant frequencies are:

$$\begin{split} f_{long} &= \frac{1}{4L} \sqrt{\frac{Y}{\rho}}, \\ f_{bend} &= \frac{0.56\kappa}{L^2} \sqrt{\frac{Y}{\rho}} \quad , \; \kappa = \frac{\sqrt{D^2 + d^2}}{8}, \end{split}$$

where Y is the Young's modulus and ρ is the density of the piezo material. D is the outer diameter of the tube and d is the inner diameter [Chen, 1993]. For the tube used, the resonant frequencies are $f_{long} = 58$ kHz and $f_{bend} = 22$ Hz.

3.4 Temperature Considerations

While dimensional changes that occur as the temperature rises or falls are often considered insignificant, they become very important when looking at features on the nanometer and subnanometer scale. The change in length caused by a change in temperature is given by:

 $\Delta I = I_0 \alpha \Delta T$,

where Δl is the change in length, l_0 is the length of the object, ΔT is the change in temperature, and α is the coefficient of thermal expansion (which in general is a function of the temperature).

For many solids (including most metals and many ceramics), the coefficient of thermal expansion at room temperature is between 1×10^{-6} /° C and 40×10^{-6} /° C. The piezo material PZT has a coefficient of about 4×10^{-6} /° C. For the standard piezo tube length used in most STM designs (including the STM described in this thesis) of 12.5 mm, a one degree Celsius change results in a length change of almost 50 nm. To keep the length change below one nanometer, the temperature should be kept stable to within one fiftieth of a degree over the time period of the image acquisition (which can be several hours).

There are three approaches that can be taken to reduce the effect of temperature changes on the acquired images. First, by thermally isolating the STM with an insulating box, the temperature fluctuations in the laboratory can be significantly reduced. The STM described in this thesis sits inside a custom built environmental isolation box with fiberglass insulation [Brenan et al., 1992].

Second, by carefully designing the STM, it is possible to compensate for the thermal expansion (see for example [Pohl, 1986], [van Kempen and van de Walle, 1986], [Lyding et al., 1988], [Albreksten et al., 1989], [Gaisch et al., 1992]). If the frame of the STM (which connects the sample and the end of the piezo tube) is made of a material with the same thermal expansion coefficient as the piezo actuator, the length change of the piezo tube with temperature will be exactly compensated and the tip to sample distance will stay constant.

Finally, by giving the STM a relatively large thermal inertia (by connecting the STM to a large heat sink for example), rapid fluctuations in the temperature can be

⁷ Some STM designs use a second piezoelectric tube as the STM frame to match the thermal expansion coefficient exactly.

minimized and only very slow temperature changes that change the heat sink temperature will cause microscope length changes.

For the microscope described in this thesis, it was found that the combination of the thermal mass of the microscope structure and the insulation in the environmental isolation box were sufficient to give stable images if the imaging time was short (< 10 minutes). For longer imaging times, thermal drift was found to affect some of the images but could almost always be corrected for by a simple linear slope removal since the drift was generally close to linear over the acquisition time (< 1 hour).

3.5 Microscope Tip

In order to get atomic resolution images of a surface, the microscope tip needs to have a single stable atom at its apex. Many methods have been used to sharpen tips but, as of yet, there is no procedure that guarantees a perfect monatomic tip. The tip material is generally chosen to provide fairly good conductivity (the resistance of the tip must be much less than the resistance of the tunneling gap) and high stiffness so that interatomic forces do not cause bending which will change the observed image. The ideal STM tip is conical with a large apex angle to increase the stiffness and has a single atom at the end.

Determining the sharpness of an STM tip is not easy. Light microscopes can only observe features sizes of hundreds of nanometers. Standard electron microscopes are limited to several nanometers resolution. Transmission electron microscopy is the most common method used to determine the tip shape, with resolution below 1 nanometer.

Early attempts by researchers to make sharp tips for field ion microscopy and field ion spectroscopy used mechanical grinding to create a conical profile. However, mechanical grinding did not give sufficiently sharp tips and electrochemical etching quickly became the favoured method for tip preparation.

The most commonly used materials for STM tips are Platinum/Iridium alloys or Tungsten, both chosen because of their high stiffness. Gold is also used for STM tips because it is very inert.

The most often used electrochemical method is the drop-off method. A thin wire of the tip material is partly submerged into an electrolyte and an etching voltage is applied between the wire and a counter electrode. The etching occurs fastest at the air-electrolyte surface, forming a thin neck in the wire that eventually breaks under the weight of the wire hanging in the solution. Tungsten tips are typically etched at 4 to 12 Volts (tungsten tip positive) in a 2M aqueous solution of NaOH [Chen, 1993][Ibe et al., 1990]. For Pt/Ir tips (typically 80% Pt arc 20% Ir), a solution of 3M NaCN and 1M NaOH can be used with an alternating 20 V applied [Nagahara et al., 1989]. Ibe et al. obtained tips with radii of curvature of between 20 nm and 300 nm by varying the conditions of the etching.

Fotino developed a two-step method of tip etching that routinely produces tips with nanometer and sub-nanometer radii of curvature at the apex [Fotino, 1992], [Fotino, 1993]. In the first step, Fotino etches tungsten tips with an AC voltage of 0.1 to 0.5 V to get a tip with curvatures of hundreds of nanometers. Then, the tip is etched with the tip completely immersed and pointing *upwards*, at similar or lower voltages.

Tips etched using both the standard drop-off method and Fotino's method were used as the probes for the STM built in this thesis. However, even with Fotino's ultrasharp tips, the stability of the tunneling gap and atomic resolution were not guaranteed.

While etching tips is not complicated, it was often easier to simply clip the tip with snips just prior to use. For Pt/Ir tips, clipped tips gave atomic resolution about half the time. Since the microscope is operated in air, if the tip does not give atomic resolution, it is easy to cut a new tip and try again, and so the reliability of each individual tip was not important. While clipping is very easy, the tips produced are not good for imaging very rough surfaces (roughness of > 10 nm) because there are often multiple 'tips' created. As an image is being acquired, the tunneling current can switch between the different tips depending on which is closest. The image acquired is the convolution of the sample and the tip geometry.

3.6 Conclusions

In this chapter, special requirements for designing and STM were discussed. In order to image at the atomic scale, the magnitude of vibrations in the laboratory environment must be reduced to below a nanometer. The tip of the STM must be positioned with an accuracy much less than a nanometer and should be sharp with a single atom at its apex. Finally, temperature effects caused by thermal expansion must be minimized so that thermal drift does not cause significant image artifacts.

The STM that was built is shown in Figure 3-7. Construction drawings of the

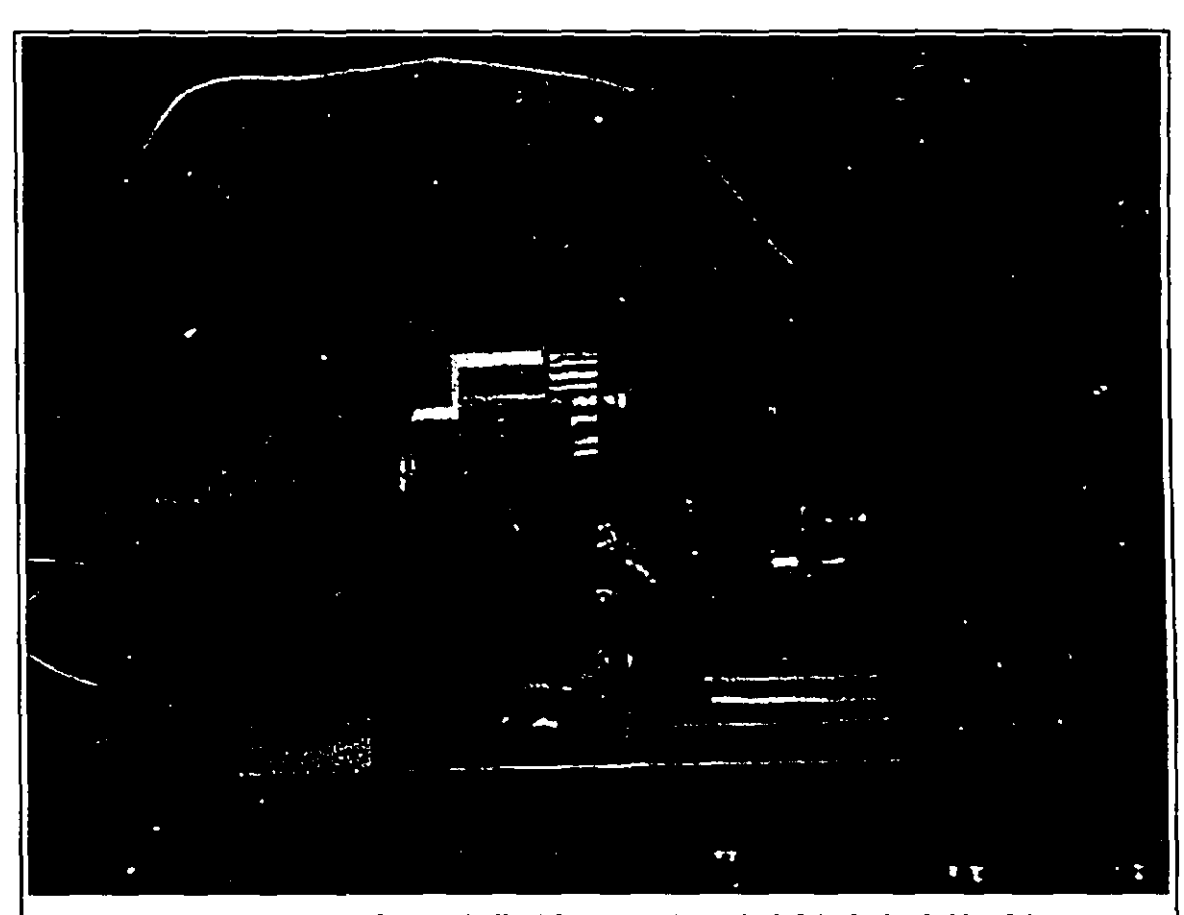


Figure 3-7: Photograph of the STM as built. The rectangle on the left is the backside of the current amplifier circuit board. The coarse approach nanosled is on the right, sitting on saphire rods. A 6.25mm diameter piezo tube actuator extends from the sled with a counterweight mounted on its end. A 12.7 mm diameter piezo tube actuator (center of image) holds the STM tip and scans the tip across the sample. For reference, the STM base is roughly 100 mm long and 60 mm high.

mechanical parts of the microscope are included in Appendix A. The following chapters discuss some of the specific details of the design.

Chapter 4: Coarse Approach - the Nanostepper

The piezoelectric actuators used for STM have a limited range of motion (about a micrometer). A mechanism is needed to bring the sample into position so it is within the range of the tip. Many different approaches have been taken to solving the 'coarse approach' problem for scanning tunneling microscopes.

4.1 Design

Binnig and Rohrer's first STM used a piezoelectric walker to move in two dimensions [Binnig et al., 1982], [Binnig et al., 1983]. Three walker feet, actuated with piezoelectrics, alternately slide over a flat supporting surface or are clamped to the supporting surface by an electrostatic force. Small step sizes, from nanometers to hundreds of nanometers, give very accurate position control. Similar designs have been used in many STMs (e.g. [Gerber et al., 1986], [Muralt et al., 1986], [van Kempen and van de Walle, 1986]). Uozumi built a similar piezoelectric stepper which used one piezo actuator to lift each leg away from the surface and another to move the legs parallel to the surface [Uozumi et al., 1988].

Burleigh Instruments (Fishers, New York) makes a piezoelectric stepper called the Inchworm® (described in [Chen, 1994], pp. 278-9). A small alumina shaft is mounted inside a three part piezoelectric sleeve. At each end of the sleeve the piezoelectric material is arranged so that an applied voltage clamps the sleeve to the alumina shaft. Between the two clamps, a piezo tube extends or contracts parallel to the alumina shaft. By activating the three parts in sequence (clamp the first end, extend the tube, clamp the second end, release the first end, contract the tube, ...) the inner alumina shaft can be moved in steps as small as 10 nanometers.

While both the Inchworm and the piezoelectric walker can make small steps and have a large range of motion, they have many moving parts and are relatively complicated to build. Many designs use simpler mechanical approaches to achieve the sub-micrometer resolution that is needed for the coarse approach.

For example, Steer et al. use a fine threaded screw followed in turn by a lever arm to make very small movements [Steer et al., 1990]. Davidsson et al. mount the sample on a base plate which is supported by three steel ball-bearings, one of which can be raised or lowered using a micrometer [Davidsson et al., 1992]. By putting the sample close to the two non-moving ball-bearings, which act as a lever fulcrum, the micrometer motion is reduced by ten times. A more complicated two lever system which ensures that the sample remains level as it is brought towards the tip was used by Grafstrom et al. [Grafstrom et al., 1990].

Coarse positioning has also been implemented using differential spring mechanisms. In the design used by Albrektsen et al., the sample mounts in the center of a thin triangular metal plate which is fixed at the corners [Albrektsen et al., 1989]. A helical spring pushes down at the center of the triangular plate. The other end of the spring is moved up or down by a micrometer. The ratio of the spring constants of the plate and helical spring determines how much the motion of the micrometer is reduced. Using a stiff plate and compliant spring, the micrometer motion can be scaled down significantly.

Jian et al. use gravity and an electromagnet for approaching the tip to the sample [Jian et al., 1990]. The tip is mounted on a small ferrite block which is held in place when the magnet is on and falls freely when the magnet is turned off. The step size is determined by the length of time that the magnet is off. Adamchuk uses a micrometer to push a wedge that raises the sample to within range of the tip [Adamchuk et al., 1992]. Carr and Thomson built a coarse approach that relies on the manufacturing errors in bearings [Carr and Thomson, 1992]. They rotate a thin shaft supported by bearings which are slightly canted due to asymmetries of manufacturing and cause the shaft to translate at 30 to 50 micrometers per turn.

A very successful type of coarse approach uses inertial steppers or 'slip-stick' mechanisms. In 'slip-stick' designs, either the tip or the sample is mounted on a sliding translation stage. By contracting a piezo tube to rapidly accelerate a counterweight, the frictional force of the stage can be overcome and the stage will slide. When the piezo tube is extended slowly, frictional forces keep the stage in place.

In the first piezoelectric inertial sliding design, Pohl put the stage to be moved on a track ([Pohl, 1987], [Pohl, 1987a]). The track is accelerated quickly by a piezo tube, causing the load to slip. A sawtooth voltage waveform was applied to the tube; during the linear rise in voltage, the track moves slowly and the load follows. The very fast change in the sawtooth voltage causes the tube to contract quickly and the track accelerates too abruptly for the load to follow (the ratio of friction force to weight exceeds the coefficient of static friction). Pohl measured step sizes from 40 nanometers to 200 nanometers and velocities up to 0.22 millimeters per second.

Lyding et al. use a small quartz sample holder on quartz rails for the coarse approach of their microscope [Lyding et al., 1988]. A piezo tube accelerates the quartz rails, moving the sample holder in steps of 0.5 nanometers to 1 micrometer. With step frequencies in the kilohertz range, the sample velocities reached 1 mm/s. Meepagala et al. use one 'slip-stick' stage for the sample and an orthogonal stage for the tip to get translation in two directions [Meepagala et al., 1990].

Neidermann built an inertial piezoelectric stepper that has the piezo actuator on the moving stage [Neidermann et al., 1988]. A piezoelectric plate, polarized so that an applied voltage causes a shear deformation, lies between two masses (see Figure 4-1). The lower mass is attached to three ball bearings which sit on a flat table. A sawtooth

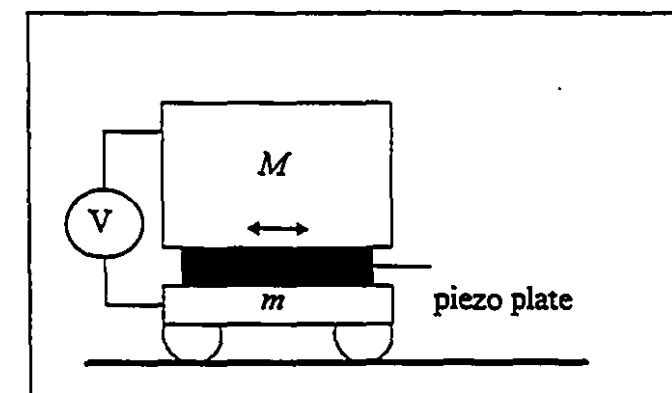


Figure 4-1: Stepper design used by Niedermann et al. (1988). When a voltage V is applied, the piezo plate undergoes a shear deformation. During slow changes in voltage, the ball bearings remain in contact with the supporting surface. When the voltage changes quickly, the inertial force exceeds the force of static friction and the ball bearings slide, making one step.

waveform applied to the piezo plate moves the large upper mass slowly to one side and then very quickly accelerates the lower mass to catch up. If two of the ball-bearings run in a V-groove on the supporting surface, the motion is constrained to one dimension.

Wildoer et al. and Smith et al. use similar designs for coarse approach/micro-positioning devices

[Wildoer et al., 1994], [Smith et al., 1994]. In both designs, the translation stage is supported on two rods, one of which slides in a V-groove to ensure that the motion is linear (as shown in Figure 4-2). By mounting a second stage on top of and perpendicular to the first, the two stages can move independently for movement in two dimensions.

Like Neidermann et al., Wildoer et al. use a piezoplate as the actuator. A disadvantage of using a piezoplate design is that there is a slight backlash because the load rides on top of the actuator. During the rapid acceleration, the large mass M (see Figure 4-1) moves slightly backwards as the smaller support mass m is pulled forwards. Each sharp acceleration gives a small backward motion before the mass is brought slowly back towards the tip.

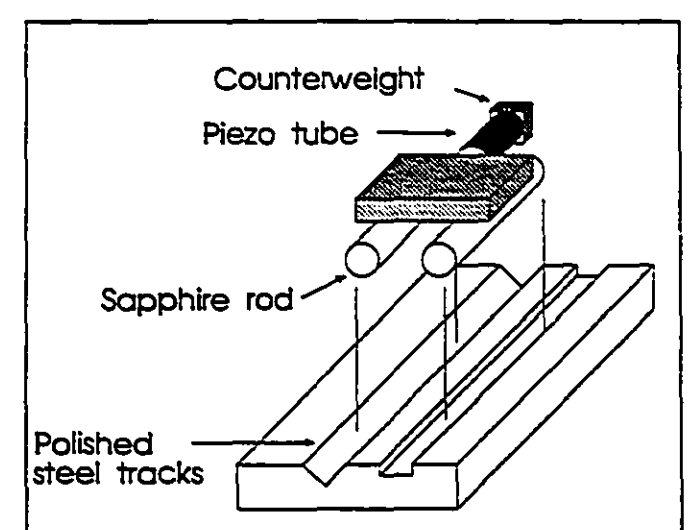


Figure 4-2: Stage for one-dimensional translation using the micro-positioning device of Smith et al. When the piezo tube is extended slowly, the stage does not slide. During a fast contraction of the piezo tube, the static friction is overcome and the stage moves. The microscope build for this thesis uses this design for the coarse approach.

The design of Smith et al. also incorporates two orthogonal motion stages piggy-backed one above the other. Smith et al. use piezo tubes as the actuators instead of a piezo plate (Figure 4-2 shows a one dimensional micro-positioner that uses the design of Smith et al.). With a counterweight at the end of the piezo tube. the rapid accelerations of the tube move the stage. During the slow extension of the piezo tube. only the counterweight moves. During the fast contraction, the force of friction

of the motion stage is exceeded and the stage slides along the track. Backlash is mostly eliminated because motion of the stage occurs only during the fast contraction phase. Smith et al. measured step sizes between 1 and 100 nanometers, depending on the applied voltage and frequency of the pulses.

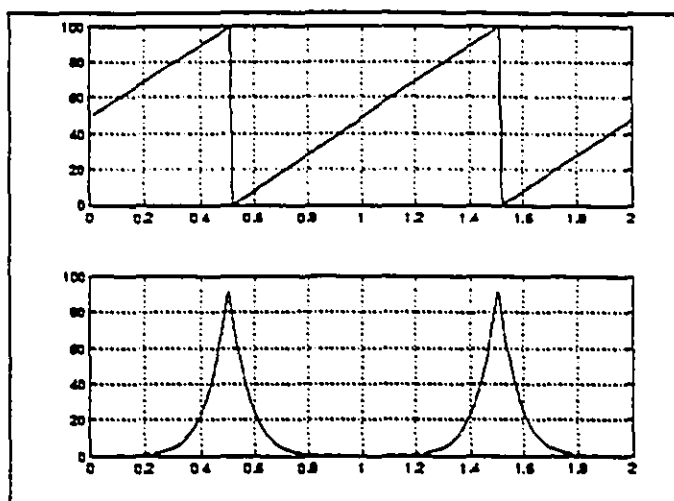


Figure 4-3: Plot of a triangular waveform (above) and a cycloidal waveform (below) that are applied to the piezo tube. The nano-motion stage moves when there is a sharp change in the velocity of the counterweight. The velocity of the piezotube is proportional to the slope of the applied waveform so the movement occurs at sharp changes in the waveform slope. Note that there is only one sharp acceleration per period of the cycloid waveform whereas the triangular waveform has two sharp accelerations.

Backlash can be further eliminated by using a waveform that has only one sharp acceleration per step. A sawtooth waveform results in two sharp accelerations: during the quick acceleration phase of the sawtooth, the counterweight can have momentum in the reverse direction. At the start of the slow motion section of the sawtooth the sharp change in direction of the counterweight causes momentum transfer to the stage. Smith et al. use a cycloidal waveform to get

only one large acceleration per step (see Figure 4-3).

4.2 Current Design

The scanning tunneling microscope built for this thesis uses a coarse approach that follows the design of Smith et al. The base is made from stainless steel. The V-groove and a flat track are machined directly into the base (see Figure 4-2). The 25 mm by 25 mm sled is epoxied (2 Ton Epoxy, Devcon, Danvers, MA) to two 6 mm diameter by 50 mm long ground saphire rods. A thin glass cover slide is expoxied between the sled and the piezo tube actuator to provide electrical isolation. At the end of the 6.35 mm diameter 12.5mm long tube, a 12mm long M4 bolt is glued as a counterweight. The mass of the counterweight can be adjusted by adding or removing M4 muts.

When fully assembled, the sled has a mass of 45 grams (including the sample holder and a sample). The counterweight, with four steel nuts, has a mass of about 4.5 grams. Electrical connection to the piezo tube is made by two very thin wires to minimize the force transmitted along the wires to the sled.

Smith's design was chosen over other designs because of its simplicity and the ease with which very flexible computer control can be implemented. For each stage, the nanostepper has only a single actuator and needs only two wires for electrical connection. By using an analog to digital converter, a computer can generate the applied voltage waveform, making it very easy to change both the amplitude and the period in order to generated different step sizes.

4.2 Interferometer for Calibration

The micropositioner step sizes are as small as 10 nanometers and the range of motion can be several millimeters. To determine both step sizes and the uniformity of step sizes, a measurement technique is needed that gives both high precision and large range of motion.

A Helium-Neon laser (λ =632.8 nm) Michelson interferometer was set up to calibrate the operation of the micro-positioning stage (see Figure 4-4). The laser beam is split into two paths by the beam splitter (BS). One path reflects off a reference mirror (M2) and returns to the beam splitter while the other path reflects off a small mirror (M3)

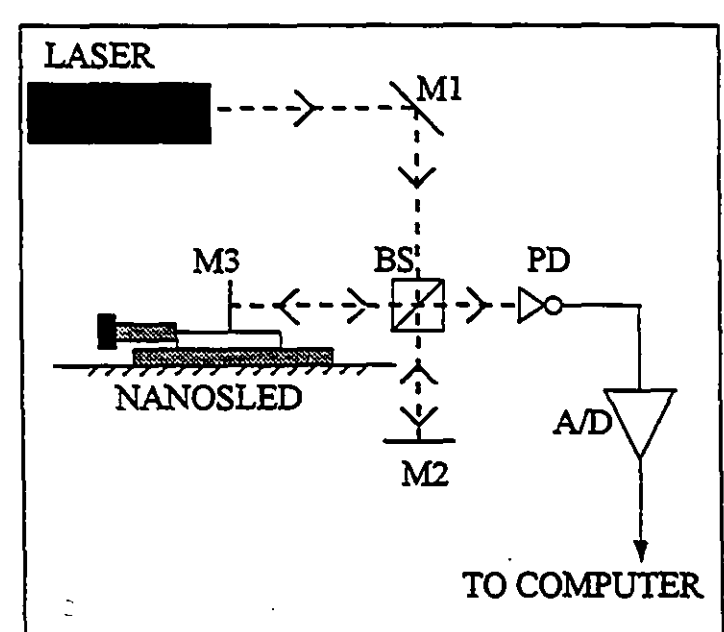


Figure 4-4: Interferometer layout. M1, M2, and M3 are mirrors, BS is a beam-splitter, and PD is the photodetector. M3 is mounted on the nanosled to measure the sled position. Not shown in the figure are two polarizers and a 45° rotator located between the laser and M1 (see text).

mounted on the moving stage. The two beams, recombined by the beam splitter, travel towards the photodetector (PD), which measures light intensity.

If the path lengths followed by the two separate beams are equal or differ by an integral number of wavelengths, the two beams will be in phase when they reach the photodetector and they will interfere constructively. The light intensity

measured by the photodetector will be high. As the micro-positioning stage is slowly moved so that the path lengths are no longer equal, the intensity will drop as the beams shift out of phase. If the path length traveled by each beam differs by half a wavelength $(\lambda/2)$, the two beams interfere destructively and the intensity at the photodetector is zero $(\lambda$ is the laser wavelength).

The intensity of the measured light is giving by the equation:

$$I_{\text{detected}} = \frac{1}{2} \left(I_{\text{max}} + I_{\text{max}} \cos \left(\frac{4\pi d}{\lambda} \right) \right),$$

where $I_{detected}$ is the detected intensity, I_{max} is the maximum detected intensity, d is the difference in path lengths, and λ is the laser wavelength. As the sled is moved over several wavelengths, the intensity rises and falls every $\frac{\lambda}{2}$. When the position of the sled changes by integral multiples of half a wavelength, the detected intensity before and after the position change is the same.

To measure the change in position of the sled, two different methods are used simultaneously. Large changes in position ($> \frac{\lambda}{2}$) are measured by counting fringes. Each light-dark-light transition corresponds to a movement of half a wavelength. Smaller changes in position are measured by inverting the equation for detected intensity:

$$\Delta d = \frac{\lambda}{4\pi} \arccos\left(\frac{I_{\text{detected}} - \frac{1}{2}I_{\text{max}}}{\frac{1}{2}I_{\text{max}}}\right),\,$$

to interpolate between fringes to get a measurement resolution well below $\frac{\lambda}{2}$.

The derivation of the equation for Δd ignores a number of complicating factors that produce errors when using an interferometer [Charette, 1990]. The effect of these errors is to limit the resolution that can be achieved. Misalignment of the mirrors, fluctuations of the laser light intensity and wavelength, and changes in path length due to thermal expansion all reduce the precision of the interferometer. Other sources of error are optical shot noise (fluctuations of intensity from individual photons being detected), electrical noise in the photodetector, and mechanical vibrations. Finally, there are

sampling errors caused by quantization when the voltage from the photodetector is sampled by the analog to digital converter.

In order to minimize errors caused by fluctuations in the environment, an environmental isolation box was used during measurements which provides thermal, electromagnetic, and vibration isolation [Brenan et al., 1992]. The laser generated significant heat during operation which led to varying thermal gradients inside the isolation box during experiments and caused significant drift in the measured position. To reduce the thermal gradients, the laser was wrapped in copper tubes carrying a flow of cold water. The overall dimensions of the interferometer were kept as small as possible to reduce thermal expansion effects from remaining temperature changes.

Instabilities in the laser intensity caused by laser light reflected back into the cavity were reduced by using two polarizers with a forty-five degree rotator. The polarized light from the laser passes straight through the first polarizer, is rotated by 45 degrees and passes through the second polarizer, which is aligned at 45 degrees. Light that is reflected back from the interferometer maintains its polarization and can pass back through the second polarizer. However, the light undergoes a further 45 degree rotation and, when it reaches the first polarizer again, is rotated by 90 degrees relative to the polarizer and cannot pass back through to re-enter the laser cavity.

The interferometer noise level for measured position was less than five nanometers over a range of 315 nanometers ($\approx \frac{3}{2}$) and less than ten nanometers for larger motions (the greater error for large motions is due mostly to difficulties in determining the exact location of the fringe peak; a small error in the interferometer intensity near the fringe peak gives a large error in the calculation of the inverse cosine). The interferometer signal drifted over time by less than 80 nm per hour. Typical experiments to determine the coarse approach step size took well under one minute and so the drift over time did not contribute significantly to the error (a maximum of 1.33 nm/minute).

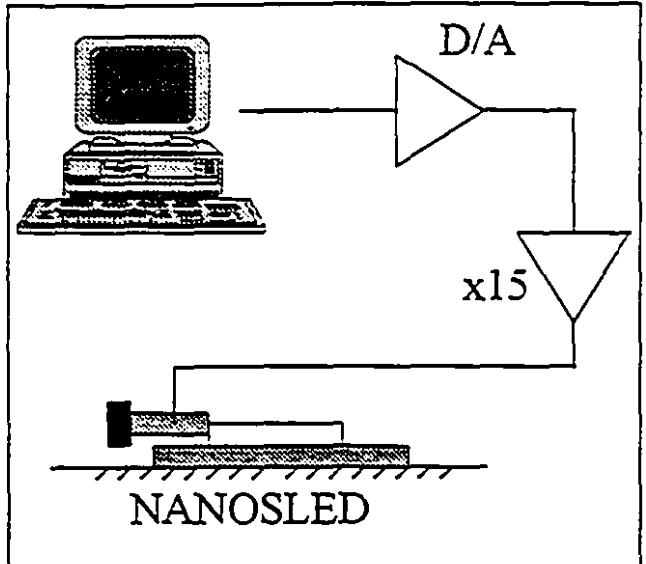


Figure 4-5: Computer control for the nanostepper. The cycloid waveform is output using the digital to analog converters and then amplified 15 times for a maximum peak to peak voltage of 300 V at the stepper piezo tube.

4.3 Calibration

Several measurements were made in order to predict the step size from the applied voltage waveform. Both the frequency and the amplitude of the applied voltage were changed. In all the measurements, the voltage waveform applied to the piezo tube was a sixth order polynomial least squares fit to a cycloid (only even coefficients were used because the function is symmetric around zero).

The equation of a cycloid is:

$$V = \sin u,$$

$$t = \cos u + u,$$

where V is the voltage, t is time, and u is a parametric variable. A polynomial approximation giving V as a function of t is:

$$V(t) \approx at^2 + bt^4 + ct^6,$$

where a = 6.3898, b = -21.0841, and c = 106.0182. The shape of the waveform is shown in Figure 4-3 above and, for the values of a, b, and c given has an amplitude of 100 and a period of 1.

The values V(t) are calculated by computer for discrete values of t and are saved in a lookup table so that they can be quickly referenced when a step is being made. During a step, the computer uses the table to set the voltage of a digital to analog converter¹ every ten microseconds (the maximum output rate of the D/A) until the complete waveform has been output. The computer can multiply the table values by a gain value to scale the waveform up to a maximum 20 V peak to peak at the output of the

¹ TVXI/DAC 16, Tasco Electronics, Plainview, New York mounted in VXI crate HPE1401A, Hewlett Packard.

digital to analog converter. A high voltage amplifier with a gain of 15 times increases the maximum piezo voltage to 300 V maximum peak to peak (see Figure 4-5) which increases the range and maximum velocity that can be given to the counterweight.

Using a computer to control the stepping waveform makes the coarse approach very easy to adapt. The amplitude, period, and the shape of the pulse applied to the piezo tube can be changed by rewriting a few lines of a computer program. However, the digital nature of the computer output creates differences between the desired waveform and the resulting waveform.

First, because the voltage is only updated every 10 µs, the voltage from the D/A converter will be a series of steps and so the approximated cycloid will not be continuous. The actual response of the voltage at the piezo tube will be smoothed somewhat from the discrete steps that come out of the D/A converter because of the limited bandwidth of the high-voltage amplifier and of the piezo tube. The stepped nature of the output waveform will affect the operation of the micro-positioner more when voltage changes between each D/A update are large. For waveform periods of a millisecond or longer which have hundreds of voltage updates per pulse, the voltage applied to the piezo tube is smooth enough to have little effect on operation of the stepping motor.

There are also errors in the output waveform that are caused by the quantization inherent in digital representation. The digital to analog converters used to control the micro-positioner are 16 bit (14 bits linearity) converters with a range of \pm 10 V. With a high-voltage amplifier gain of 15 times, the smallest change in voltage applied to the piezo tube will be $\Delta V = 15 \times 20 \text{V}_{214} = 18 \text{mV}$. When ΔV is the same order of magnitude as the voltage pulse, the minimum change in voltage can cause significant distortion of the output. In practice however, the amplitudes needed to drive the piezo tube are large enough (> 45 V) that the D/A quantization is not significant. In fact, the step changes in the voltage due to the discrete time updates of the output are typically much larger than ΔV .

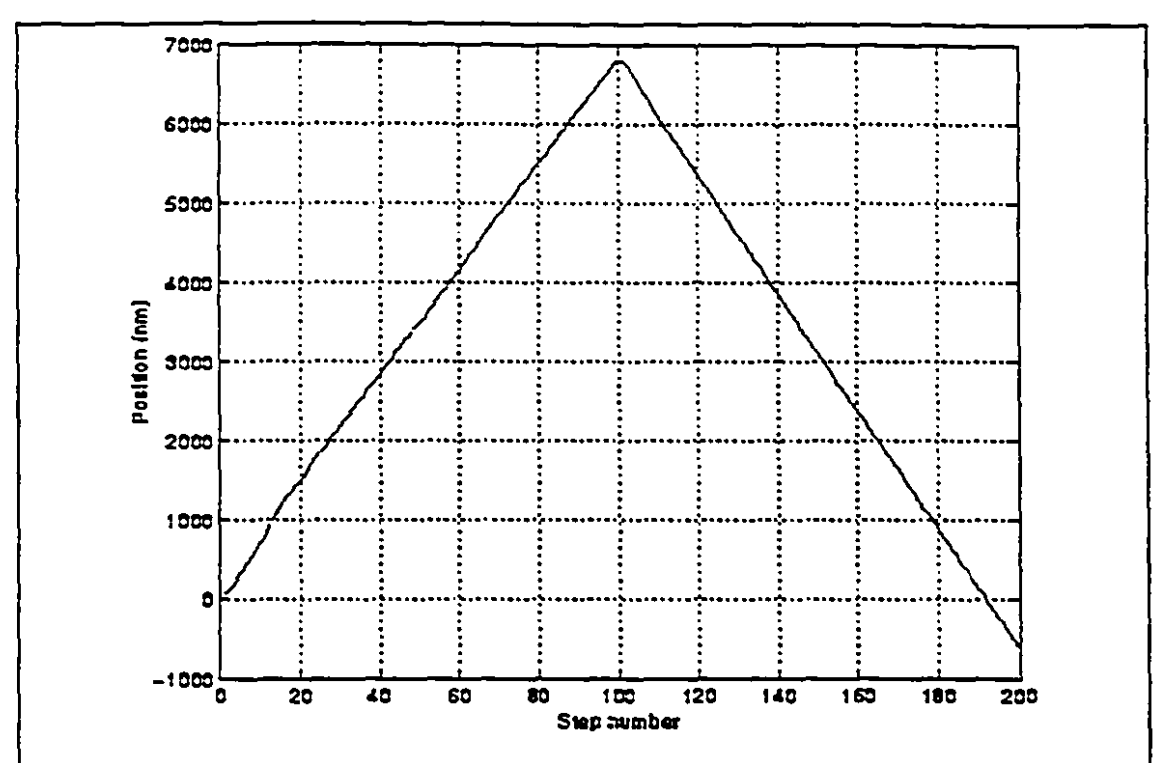


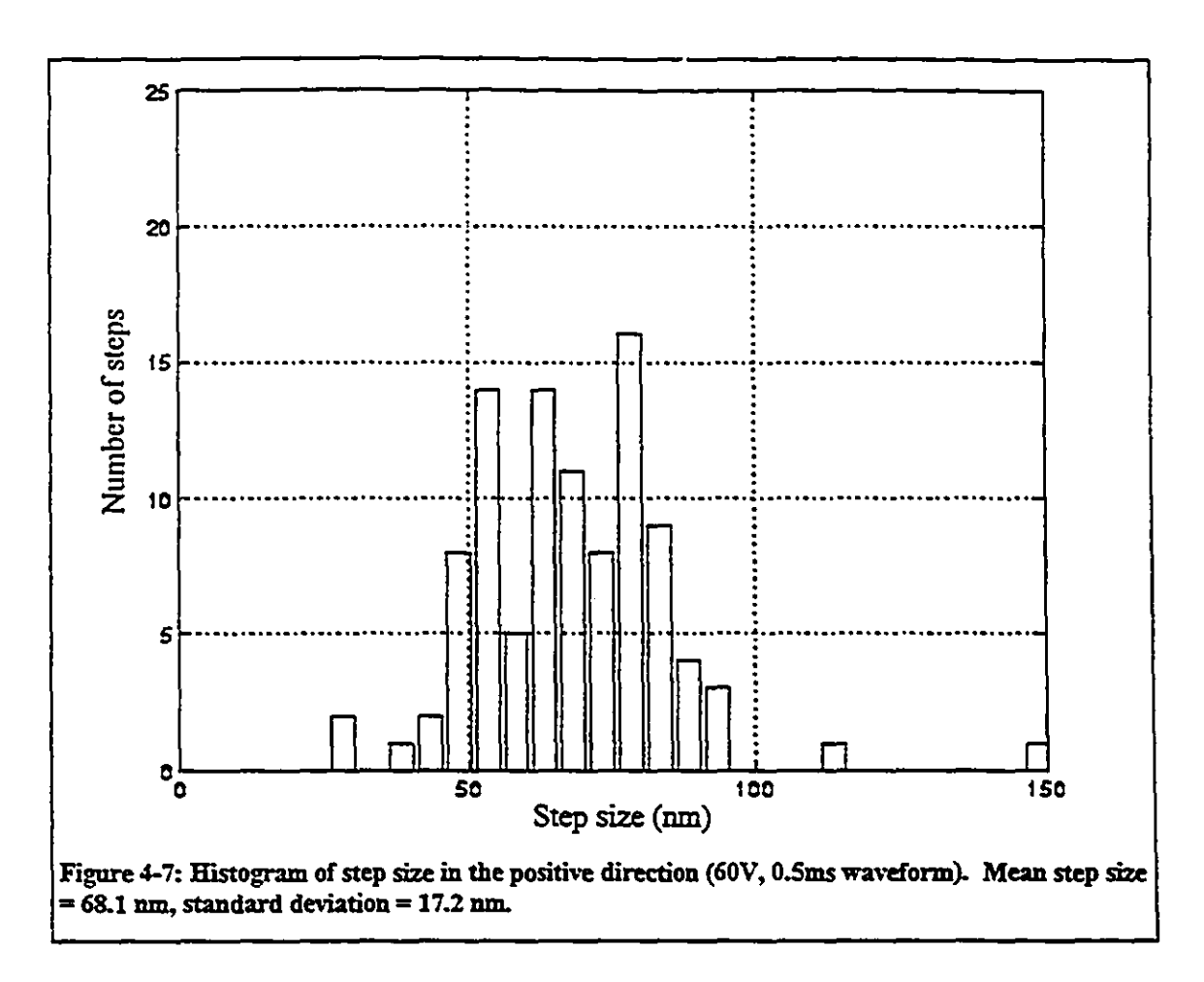
Figure 4-6: Position vs. step number of the micro-positioner. The waveform has an amplitude of 60V and a pulse duration of 0.5 ms.

Some results of the calibration experiments are shown in Figure 4-6, Figure 4-7, and Figure 4-8. Figure 4-6 shows the measured position of the sled over 100 steps forward and 100 steps backwards for a 60 V, 0.5 ms waveform. Both the forward and reverse directions are close to linear, which allows accurate control of the position even after many steps. A few things should be noted. First, after 100 steps forward followed by 100 steps in the reverse direction the coarse positioner does not end up in the same place that it started. The difference in step size between the forward and reverse directions is due to in part to slight asymmetries in construction but is caused mostly by a small bias force that is transmitted along the connecting wires. By slightly bending the connecting wires, the bias force can be either increased or decreased. Care must be taken not to bend the wires once the step size has been calibrated because the step size in both directions changes.

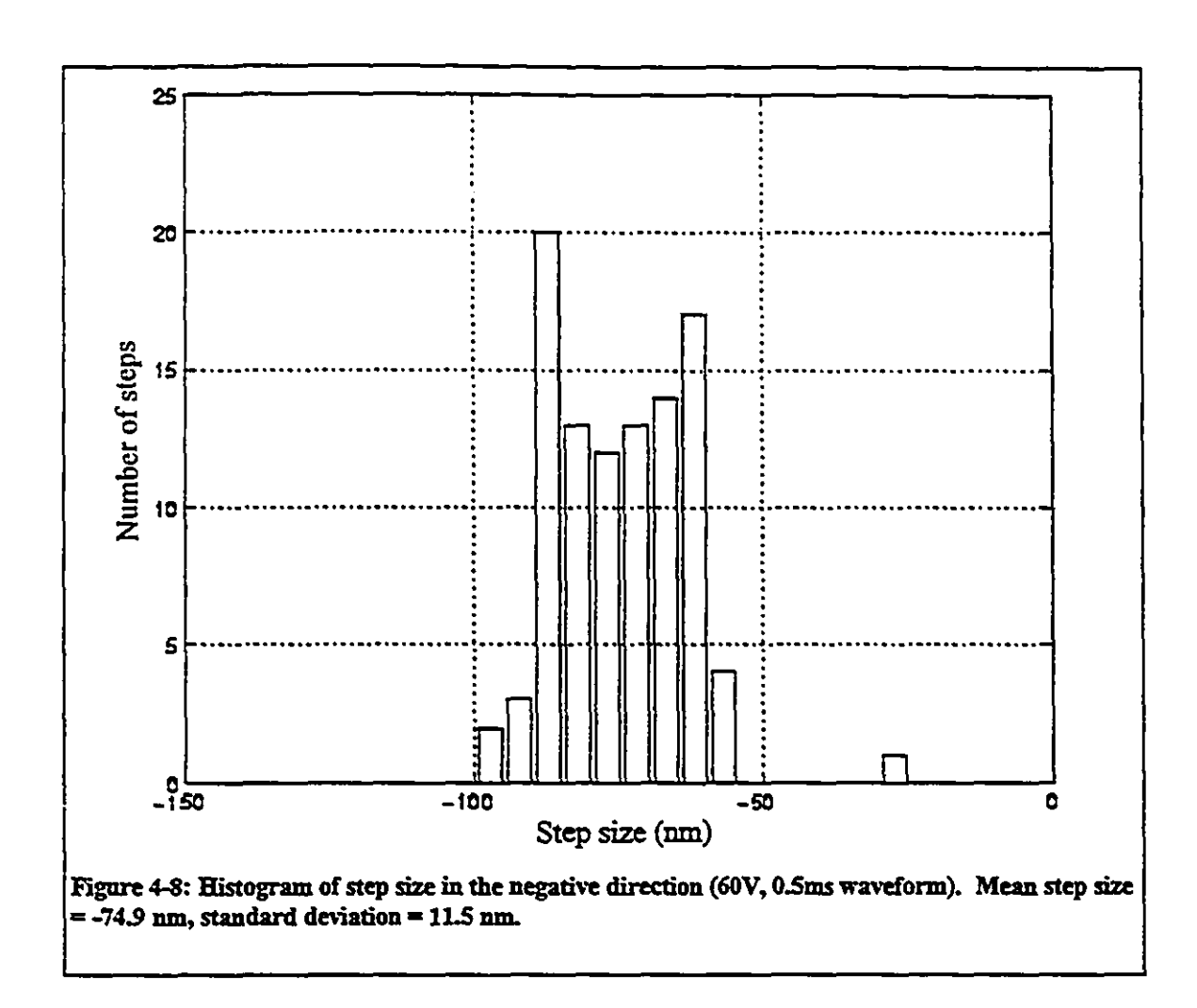
Second, the step sizes are not perfectly uniform. Figure 4-7 and Figure 4-8 show histograms of the step sizes in each direction for a 60 V cycloidal pulse of 0.5 ms duration

(results for other waveform amplitudes and pulse durations are similar). The average step size in the forward direction is slightly different from the step size in the backward direction (68 nm versus 75 nm). The standard deviations of the step sizes are 17 nm and 12 nm for the forward and backward directions respectively. The variations in step size in a given direction are due to surface inhomogeneities. Because the steel track is not perfectly smooth, different parts of the track will have slightly different coefficients of friction, which in turn causes different step sizes. Future versions of the coarse approach may use ground saphire flats for the track in addition to the saphire rods that are already used in the sled so that the smoothness of the track is better controlled.

Precise positioning can be achieved by using waveforms with different amplitudes and pulse durations. Measurements of step size vs. pulse duration (for a 60 V amplitude) and step size vs. voltage amplitude (for a 0.5 ms pulse) are shown in Figure 4-9 and Figure 4-10. Above a voltage of 50 V, the step size increases almost linearly with the pulse amplitude. On the other hand, for pulse lengths less than 0.5 ms, the step size decreases with increasing pulse size. The drop in step size below 0.5 ms (a maximum rate of 2000 Hz) is caused by limited bandwidth of the piezo actuator, which is on the order of kilohertz for the tube actuators used for STM. Above 0.5 ms, the maximum velocity of the counterweight decreases with increasing pulse length and so the momentum transferred from the counterweight to the sled also decreases, reducing the step size.



Using the software written for the STM, the pulse duration and amplitude are specified at the start of each coarse approach. A single voltage amplitude is used for steps until the tip is within a preset range and then the tunneling feedback is engaged. Typically, a step size of about 100 nm is used. Variable step size and combined motions in the forward and reverse directions could be used to fine tune the stage position but the experiments so far have not required positioning to within better than 100 nm. If needed, the position at which tunneling current starts could be measured by the STM tip and used as a feedback to position the sample with an accuracy better than 10 nm.



As a coarse position mechanism, the micropositioner works extremely well. When new samples are mounted on the coarse approach, they are quickly brought into range of the piezo tube for imaging. The combination of large range of motion, repeatable step sizes down to almost 10 nanometers, and computer control of the stepping makes the automated coarse approach easy and reliable

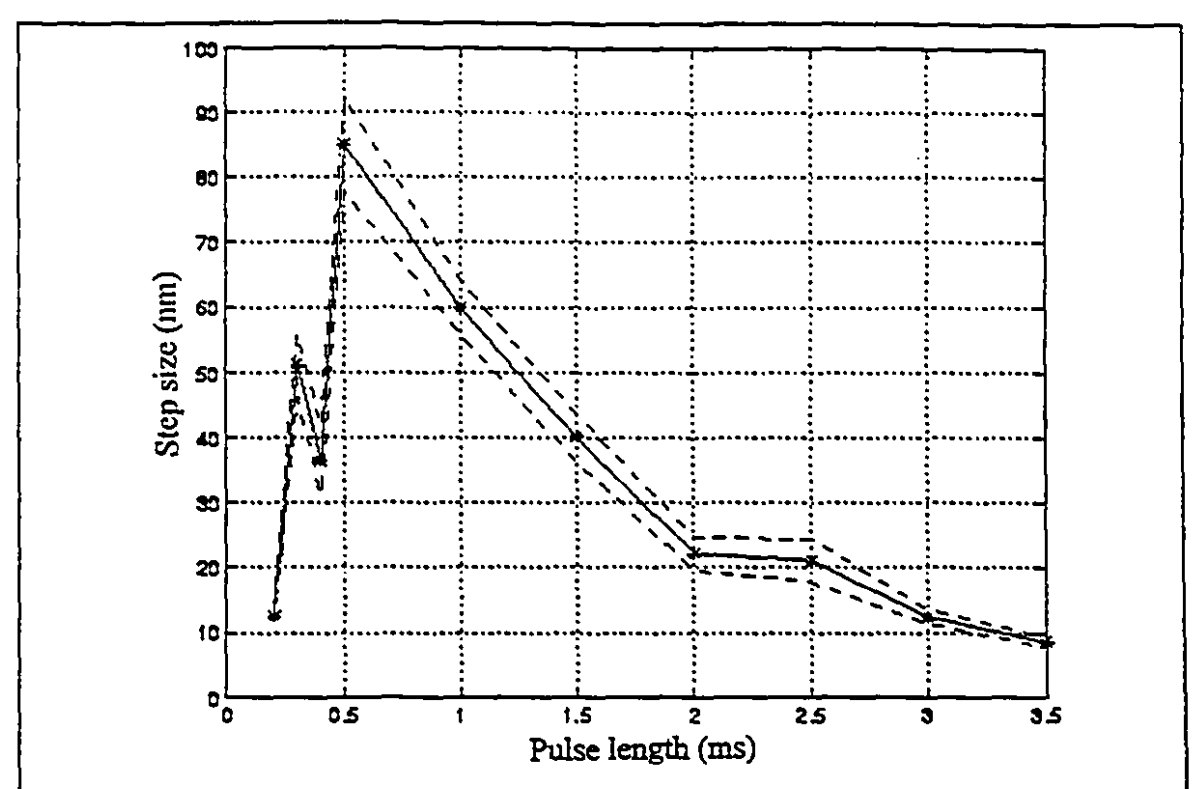
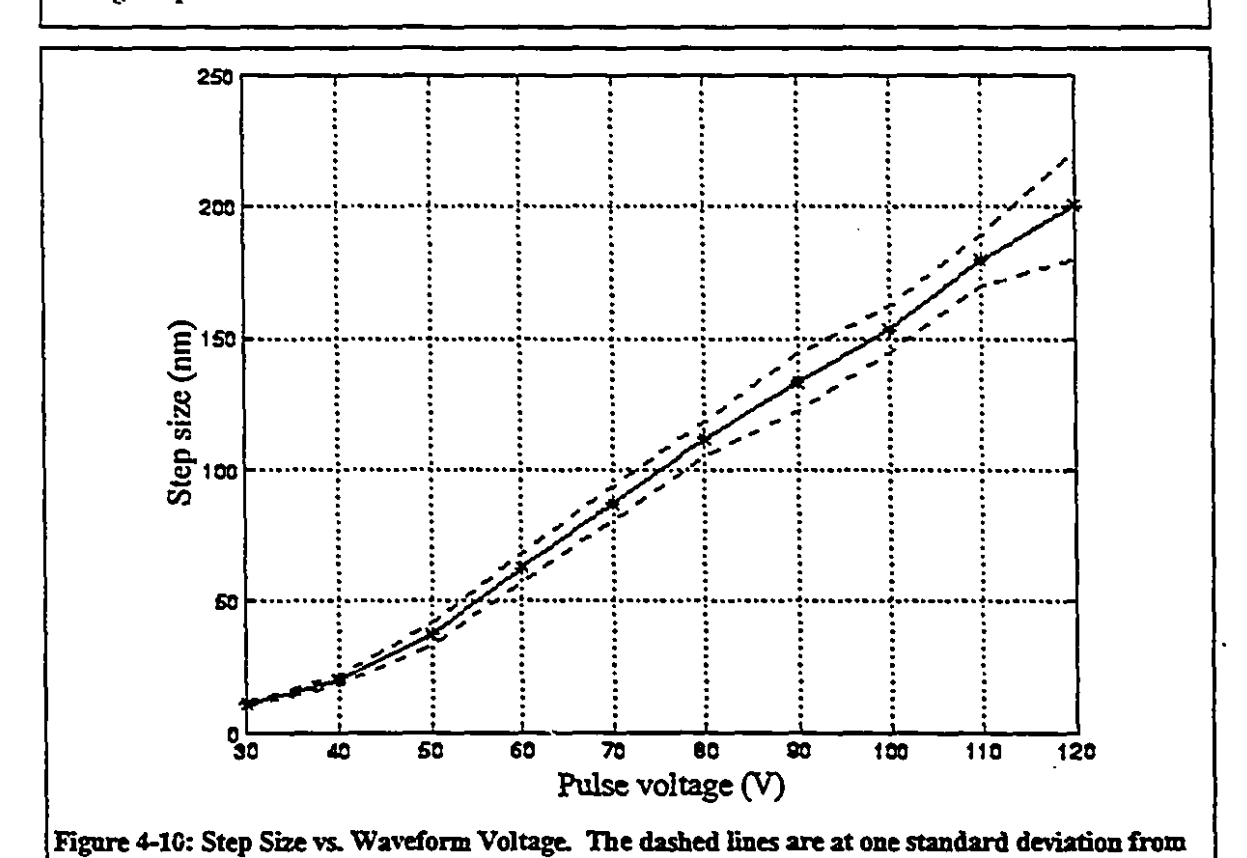


Figure 4-9: Step Size vs. Pulse Duration. The dashed lines are at one standard deviation from the average step size.



the average step size.

In the next chapter, the components of the electrical system that are required for an STM are discussed. The contributions of different components to the noise in the tip position and measured current are calculated and serve as a guide to the performance that can be expected of the microscope.

Chapter 5: Electronics

The electronics of the scanning tunneling microscope are a key part of the imaging process (see Figure 5-1). When an image is being acquired, the magnitude of the current flowing between tip and sample is used control the position of the tip. The electronics first amplify the tunneling current and then digitize and send the value of the current to the computer. The computer determines new x and y scan positions for the tip and calculates the new tip height (z position) needed to keep the tunneling gap constant. Once the computer has calculated the new tip position, the electronics convert the computer's

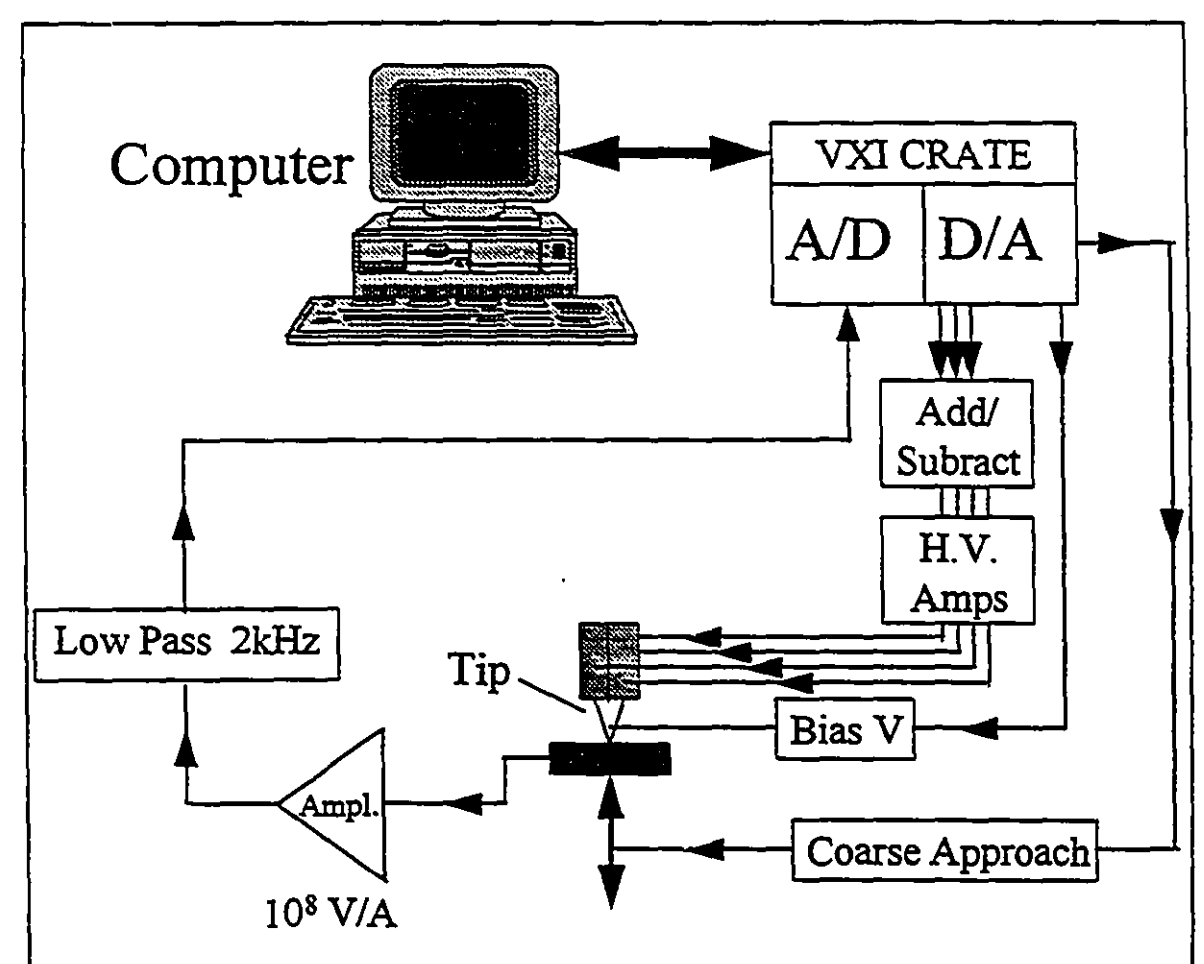


Figure 5-1: Electronics for the STM. The computer sends and receives data from analog to digital and digital to analog converters in a VXI crate and also controls the piezo tube position via an add/subtract circuit and high voltage amplifiers. The bias voltage is directly controlled from the D/A output. The tunneling current is amplified by 10⁸ gain current to voltage amplifier and low-pass filtered before being read by the A/D converter.

digital signals into analog voltages and amplifies them before they are applied to the piezo tube quadrants. Thus, for a digitally controlled scanning tunneling microscope, there are two parts to the feedback. One is the software that calculates a new position given past inputs (discussed in Chapter 6) and the second is the electronics that measure the current and control the tip and coarse approach positions.

5.1 Current to Voltage Amplifier

Perhaps the most important component of the STM electronics is the current to voltage amplifier. The amplifier must be capable of converting the very small tunneling

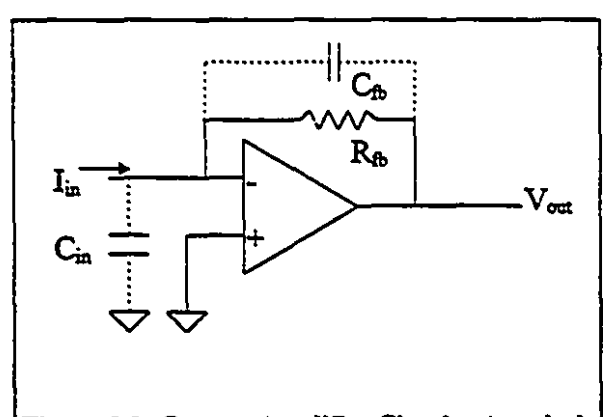


Figure 5-2: Current Amplifier Circuit. A typical value for the feedback resistance is 108 Ohms.

currents (10 pA to 10 nA) into a voltage. A poorly designed current amplifier can give noisy tunneling current measurements, which make the gap distance difficult to control or can limit the speed of data acquisition because of limited bandwidth. The basic operational amplifier circuit is shown in Figure 5-2.

The capacitors shown in the circuit (with dotted lines) are parasitic

capacitances caused by unavoidable coupling between circuit elements. Ignoring the parasitic capacitors for the moment, the transfer function of the amplifier is:

$$\frac{V_{out}}{I_{in}} = -R_{jo},$$

where V_{out} is the output voltage, I_{in} is the input current (from the tunneling junction), and R_{jb} is the resistor in the feedback loop. For $R_{jb} = 100 M\Omega = 10^8 V_A$, a one nanoamp current is amplified to 100 mV.

The parasitic capacitances cause the gain of the amplifier to roll off as the frequency increases. Since the negative terminal of the op-amp is kept very close to

ground, the effect of the input capacitance is not noticeable up to very high frequencies (close to 100 kHz). The capacitance C_{fb}, which is in the feedback path, in combination with the very large feedback resistance, can cause a roll-off at several kHz. With the feedback capacitance included, the amplifier transfer function becomes:

$$\frac{V_{out}(s)}{I_{in}(s)} = \frac{R_{fb}}{1 + sC_{fb}R_{fb}},$$

where s is the Laplace variable (and $s = j\omega$, where ω is the frequency). Typical values of C_{fb} are around 1 pF [Chen, 1993, section 11.1]. For $R_{fb} = 100M\Omega$, $C_{fb}=1$ pF, the roll-off is at $f = \frac{1}{2\pi C_{fb}}R_{fb} \approx 1.5kHz$.

The behaviour of the amplifier is also affected by the non-ideal characteristics of operational amplifiers. The non-ideal characteristics of real op-amps include non-zero input bias current (the current that leaks into the positive and negative input terminals), non-zero input bias voltage (the voltage between the input terminals), and finite frequency response.

For most op-amps, the frequency cut-off of the op-amp is well above the frequency roll-off caused by parasitic capacitance and so does not affect the current amplifier characteristics. However, the bias current and input bias voltage do affect the

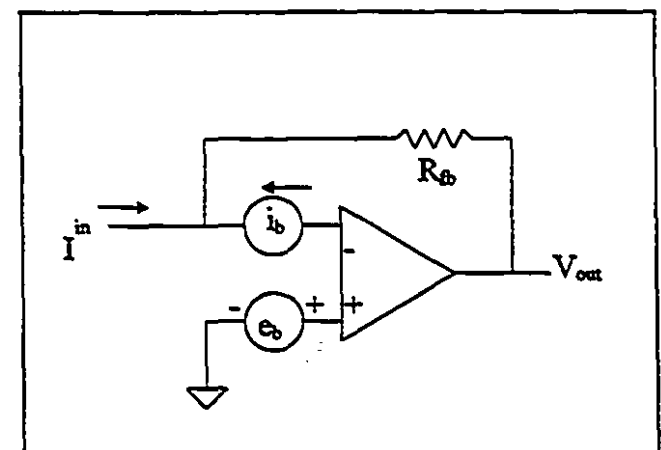


Figure 5-3: Sources of Noise and Offsets in the Current Amplifier. i_b and e_b are current and voltage sources. They include both DC and random noise terms $(i_b=I_b+i_n, e_b=V_b+e_n)$.

operation of the current amplifier (see Figure 5-3).

The input bias voltage will change the voltage across the tip-sample junction, in turn changing the current that flows. For normal operation of a scanning tunneling microscope, precise control of the tunneling voltage is not required. The effect of a constant non-zero input bias

voltage is not important for most experiments. A small change in the bias voltage will result in a small change in the tip sample distance during a scan. As long as the change in tip-sample bias voltage is constant, the measured image will be unaffected. Fluctuations of the input bias voltage, however, cause changes in the tunneling current which are interpreted as changes in the surface height.

When measuring very small currents, the input bias current can have a very large effect. Op-amps can have bias currents of hundreds of nanoamps (the 741, a general purpose operational amplifier, has a maximum bias current of 500 nA) which is many orders of magnitude larger than the picoamp to nanoamp tunneling currents. Very small bias current is one of the primary concerns in choosing an op-amp for the current amplifier. Burr-Brown¹ and Analog Devices² both make very low bias current FET input op-amps that are well suited for use in the tunneling current amplifier (see Table 5-1).

Table 5-1: Op-amps for Tunneling Current Amplifiers. (adapted from [Chen, 1993, App. H]). i, and e, are the noise in the bias current and voltage respectively.

OP-AMP	max I _{bias} (fA)	max V _{bias} (μV)	$i_n \left(\frac{fA}{\sqrt{Hz}} \right)$	$e_n \left(\frac{nV}{\sqrt{Hz}} \right)$
Burr Brown OPA128LM	75	500	0.12	92
Analog Dev. AD549L	60	500	0.11	90

With the bias current and bias voltage included in the circuit analysis, the transfer function becomes:

¹ Burr Brown, Tucson, Arizona.

² Analog Devices, Norwood, Massachusetts.

$$V_{out}(s) = (I_{in}(s) + I_b + i_n \times \sqrt{BW}) \frac{R_{jb}}{1 + sC_{jb}R_{jb}} + V_b + e_n \times \sqrt{BW},$$

where I_b is the bias current, i_n is the noise in the bias current (per square root Hertz), V_b is the bias voltage, e_n is the noise of the bias voltage (per square root Hertz), and BW is the bandwidth of the amplifier. The noise in the signal consists of a DC offset and a random component:

$$\begin{split} &V_{\textit{noiseDC}} = I_b R_{fb} + V_b \,, \\ &V_{\textit{noiseAC}} = \left(i_n \frac{R_{fb}}{1 + s C_m R_{fb}} + e_n \right) \times \sqrt{BW} \,, \end{split}$$

The expected DC voltage offset is (using the AD549L which has slightly better characteristics and is used for the STM described here) $V_{noiseDC} \le 6.5 \mu V$ and the AC noise is $V_{noiseAC} \le 100 nV / \sqrt{Hz}$. The errors in the measured currents caused by the noise sources are given by $I_{noise} = \frac{V_{noiseDC}}{R_{pb}}$, $I_{noiseDC} \le 65 fA$ and $I_{noiseAC} \le 1 fA / \sqrt{Hz}$. Even for a 100 kHz bandwidth ($I_{noiseAC} \le 315 fA$), both of these noise sources are below the minimum tunneling current resolution of around 10 pA that needs to be detected for atomic resolution.

Other sources of noise in the current amplifier are Johnson noise [Horowitz and Hill, 1980], which results from the thermal motion of the electrons in a resistor, and shot noise, caused because current flow is made up of discrete electric charges. Johnson noise through a resistor adds a root-mean-square (RMS) current $I_j = \sqrt{\frac{4k_bT \times BW}{R}}$, where k_b is the Boltzmann constant and T is the temperature. The peak to peak noise can be taken as eight times larger than the RMS amplitude (four standard deviations for a Gaussian distribution). At room temperature (T=300 K) a feedback resistance of 10^8 V/A has a Johnson current noise of $I_j = 100fA/\sqrt{Hz}$. For a 2 kHz bandwidth (close to the bandwidth of the current amplifier), the Johnson noise is 4.5 pA. To reduce the Johnson noise, the gain of the amplifier (i.e. the value of the feedback resistor) needs to be

increased. However, there is a tradeoff between reduced Johnson noise and the bandwidth which decreases with an increase in feedback resistance.

The shot noise for a mean current \vec{I} is

$$I_{shot} = \sqrt{2e\overline{I} \times BW}$$
,

where e is the charge of an electron. For a 2 kHz bandwidth, $I_{shot} = 2.5 \times 10^{-10} \sqrt{\bar{I}}$ which is negligible for \bar{I} greater than 1 pA (I_{shot} increases as the square root of the mean current so shot noise expressed as a percentage of mean current decreases as the mean current increases; at $\bar{I} = 1$ pA, the shot noise is 2.5% of \bar{I}).

Table 5-2: Current Amplifier Noise Sources and their Magnitudes (for T=300K, $R_0=10^8 \Omega$, BW = 2 kHz, and an AD549L op-amp).

Noise Source	Magnitude	
DC Voltage & Current Bias	<65 fA	
AC Voltage & Current Noise	<50 fA	
Johnson Noise	4.5 pA	
Shot Noise	$<2.5\%, \bar{I} \ge 1pA$ $<1\%, \bar{I} \ge 10pA$	

The different sources of noise and their magnitudes are shown in Table 5-2.

In choosing the components for the amplifier, the effects of different types of noise need to be taken into account. The Analog Devices AD549L op-amp was chosen because it has slightly better characteristics than the Burr Brown

OPA128LM. The resistance was chosen to be $10^8~\Omega$ for an amplifier gain of $10^8~V/A$ and acceptable bandwidth and noise characteristics.

The transfer function of the amplifier was measured using a Hewlett Packard Dynamic Signal Analyzer (HP 3562A). The magnitude and frequency response are shown in Figure 5-4. The amplifier has a first order cut-off frequency of 1.9 kHz, very close to the 2 kHz used for the noise calculations above.

From Table 5-2, the minimum detectable current of the current amplifier will be limited by the Johnson noise to > 4.5 pA. The amplifier voltage noise for a current of 4.5 pA is 4.5 mV. Typical currents used for imaging of surfaces are on the order of hundreds

of picoamps to several nanoamps and so the amplifier current noise is acceptable. For very high precision current measurements, the feedback gain would need to be increased and/or the bandwidth decreased to reduce the Johnson noise.

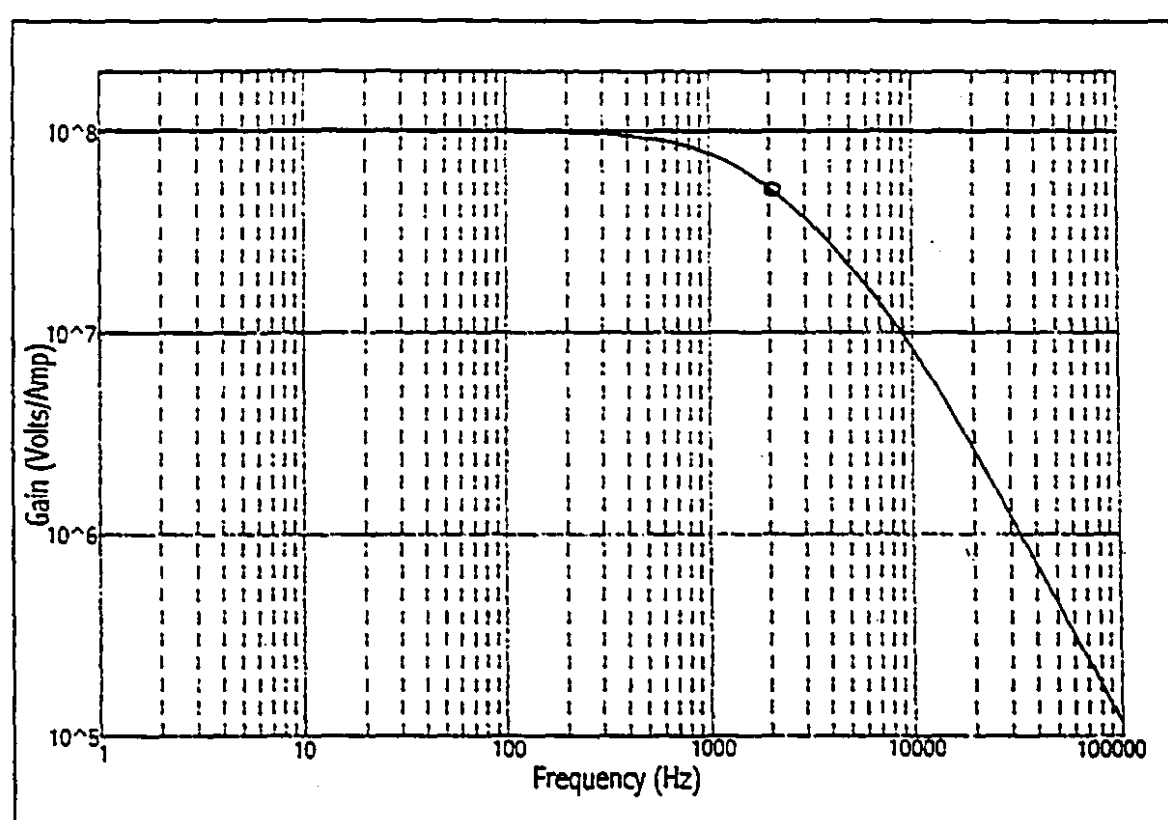


Figure 5-4: Measured frequency response of the current to voltage amplifier. The amplifier has a first order roll-off at a cut-off frequency of 2 kHz.

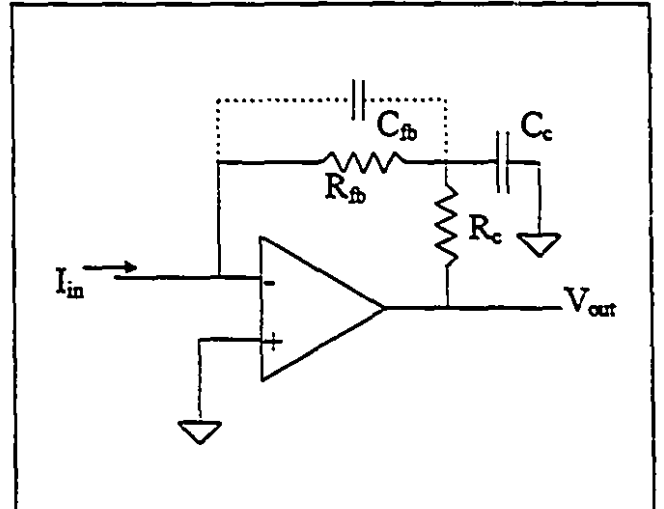


Figure 5-5: Compensation circuit for current amplifier.

If higher bandwidth desired, a compensation circuit can be added to the amplifier in order to reduce the effect of the parasitic capacitances. A higher bandwidth current amplifier has been constructed using a circuit described by Chen (see Figure 5-5) [Chen, 1993, Chapter 11]. The extra capacitor and resistor cancel out the low-pass effect of the parasitic feedback capacitance. The output voltage as a function of the input current is:

$$V_{\text{out}} = I_{\text{in}} \left(R_c + R_{\text{jb}} \left(\frac{1 + sR_cC_c}{1 + sR_{\text{jb}}C_{\text{jb}}} \right) \right),$$

where R_c and C_c are the compensating resistor and capacitor. Choosing $R_c = 1 \text{ M}\Omega$, and trying various different capacitor values, a new STM current amplifier has been built with a bandwidth of 21 kHz with $C_c \approx 0.91$ pF. The measured frequency response of the amplifier is shown in Figure 5-6. At the time of writing, the new current amplifier has not yet been integrated into the STM.

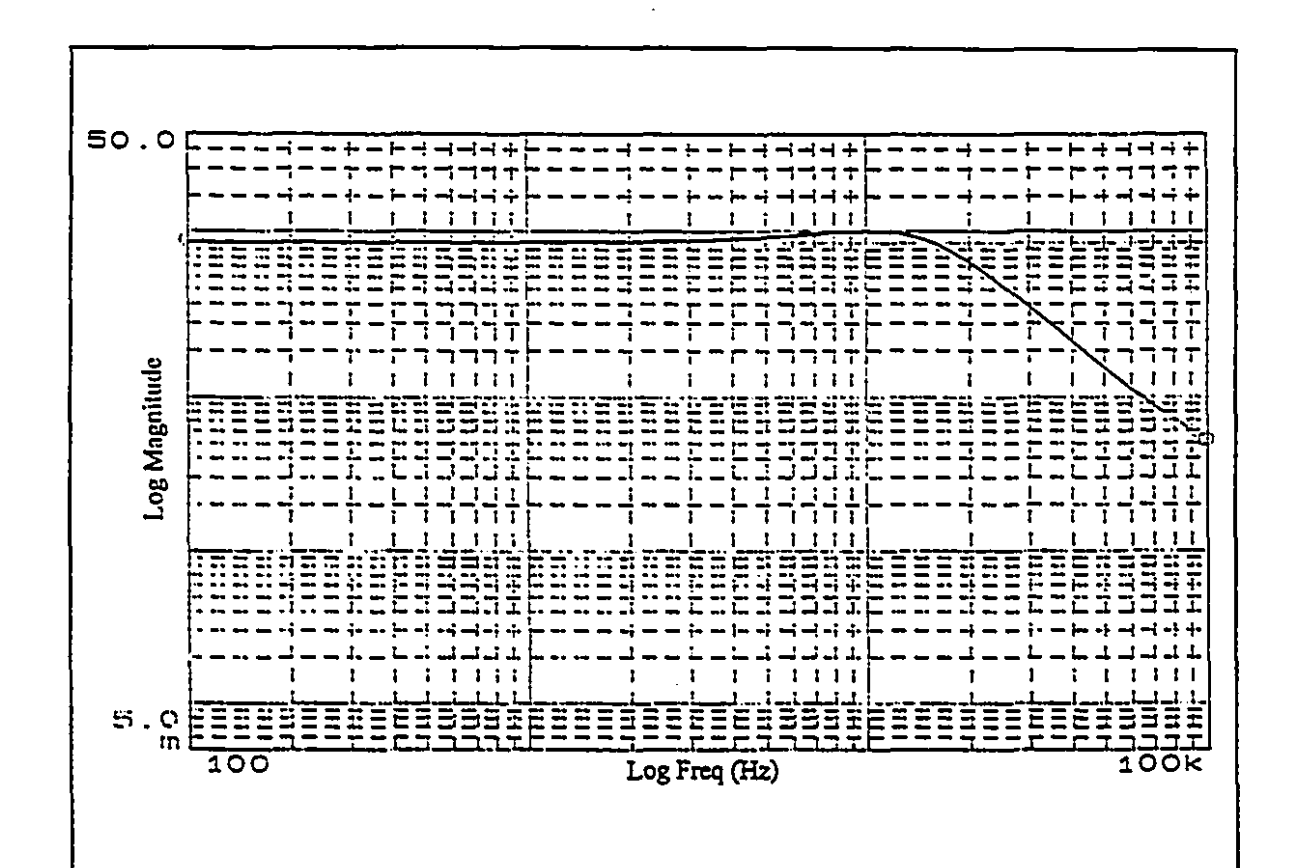


Figure 5-6: Measured transfer function of the compensated current amplifier with a bandwidth of 21 kHz.

5.2 Analog to Digital and Digital to Analog

Once the current has been converted to a voltage, the voltage needs to be digitized and sent to the computer. The analog to digital converter used is a Hewlett Packard³ model E1413A 64 channel analog to digital converter in a VXI crate (Hewlett Packard E1401A VXI mainframe).

The two most important characteristics of the A/D converter are the sampling rate and the number of sampling bits. The E1413A has a maximum sampling rate of 100 kHz and resolution of 16 bits. The sampling rate is important because it determines the maximum frequency that can be measured and reconstructed by the computer. By the Shannon-Nyquist theorem, the original signal can only be reconstructed exactly if its component frequencies are all less than half the sampling rate (the 'Nyquist rate') [Oppenheim and Schafer, 1989]. At the maximum sampling rate for the E1413A, the Nyquist rate is maximum 50 kHz. If the signal contains frequencies above the Nyquist rate, they will be aliased down to lower frequencies, where they combine with the existing low frequencies, making it impossible to reconstruct the original signal.

To avoid aliasing, a low-pass filter is required to remove any high frequency components. If a perfect bandpass filter could be made, then the cut-off frequency of the filter could be set to just below the Nyquist rate. However, practical filters have finite roll-off rates and so the cut-off frequency of the anti-aliasing filter is usually less than half of the Nyquist rate (or one quarter of the sampling rate).

The current to voltage amplifier of the STM has a 1st order roll-off from a frequency of about 2 kHz. The current to voltage amplifier is followed by a 2nd order Butterworth low-pass filter⁴ that also has a cut-off frequency of 2 kHz to further attenuate high-frequency components.

During STM imaging, the sampling rate is limited not by the maximum A/D rate but by the computer time taken for calculations for tip position control, for sending the

1

³ Hewlett Packard, Fullerton, CA.

⁴ The shape of the Butterworth filter is optimized to be maximally flat in the pass-band.

desired tip positions to the digital to analog (D/A) converters, and to store the image data. The measured times for the different operations that the computer must perform for each sample are shown in Table 5-3. The combined time taken to do all of these operations limits the sampling frequency to about $\frac{1}{23.6\mu\text{s}} \approx 40 \text{ kHz}$ (and the Nyquist rate to about 20

kHz). For a third order filter (the combination of the current amplifier and the Butterworth filter is third order), the output magnitude falls of by one thousand times for each ten times increase in frequency beyond the cut-off. As a quick estimate of the attenuation of the signal at the Nyquist rate, using a Nyquist rate (20 kHz) of ten times the cut-off frequency (2 kHz), the attenuation of frequencies at and beyond the Nyquist rate is 1000 times or more.

The number of bits from the analog to digital converter determines the minimum change in signal that can be detected. The E1413A samples with 16 bits or 2¹⁶ different

Table 5-3: Time for computer operations in the feedback loop. For each new z piezo voltage that is calculated, the tunneling current must be sampled (AD read), several floating point calculations and a logarithm must be computed, some timing functions are executed, and the updated x, y, and z positions must be output (three DA writes).

Operation	Time µs	Total time µs
AD read (x1)	5.5	5.5
DA write (x3)	4.4	13.2
floating point calculations	0.3	0.3
logarithm	1.5	1.5
timing functions	0.6	0.6
miscellaneous (loops, bookkeeping)	2.5	2.5
TOTAL TIME		23.6

levels. The voltage range over which measurements can be made is ± 16 V. The smallest change in signal that can be detected is $32V/_{2^{16}} = 0.488\,\text{mV}$. The corresponding change in tunneling current is $\frac{0.488\,\text{mV}}{10^6V/A} = 4.88\,\text{pA}$. If more precise measurements of the tunneling current are needed, the amplitude range can be reprogrammed from ± 16 V to ± 4 V, ± 1 V, ± 0.25 V or ± 0.0625 V. Since the Johnson noise contributes 4.5 pA (see Table 5-2), reducing the range below ± 16 V, where the minimum detectable change in tunneling current is 4.88 pA, does not

improve the measurement accuracy very much.

Once the A/D converter has digitized the current, the computer reads the value of the current and performs a series of calculations to determine how the position of the tip should be changed to maintain constant height above the surface. The computer calculates a voltage for the deflection of the piezo tube in each direction x, y, and z and sends the voltages to the D/A converter.

Like the A/D converter, the D/A converter is limited by a maximum frequency at which it can update the output voltage and by the number of bits of resolution that it has. In the microscope built, a 16 bit DAC VXI crate module (TASCO model TVXI/DAC 16) is used with a reviewum update rate of 100 kHz for one channel. The TVXI-16 has an output voltage range of ± 10 V, giving a minimum voltage step of 0.31 mV. But the TVXI-16 has only 14 bits of linearity, so the smallest guaranteed linear output change is 1.2 mV.

5.3 Add and Subtract Electronics

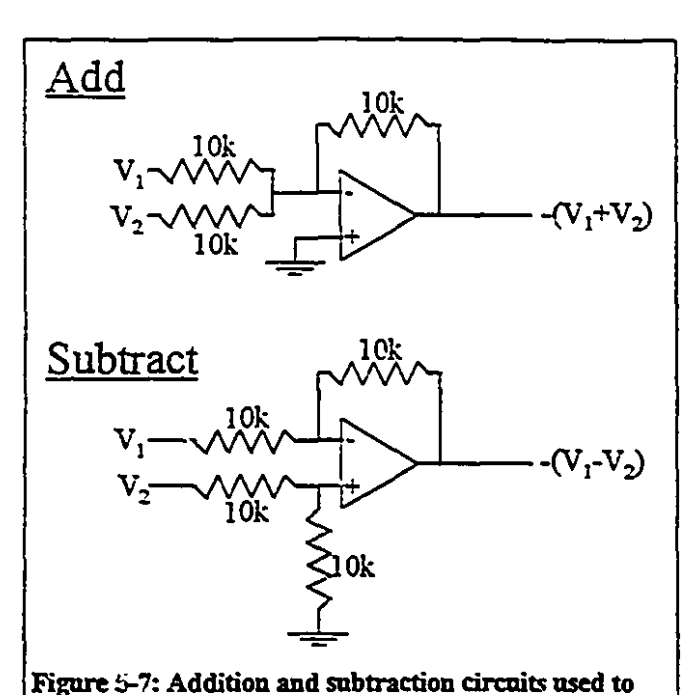
In the first iteration of the electronics constructed for the STM, a voltage was computed and written to the D/A converters for each of the four piezo quadrants. However, each write operation to the D/A converters takes time (Table 5-3) and so reduces the maximum rate at which the system can update the output.

Although there are four voltages applied to the piezo tube (one for each quadrant), only three independent variables are needed to describe them. The voltages on the quadrants are:

$$\begin{split} &V_{1}=V_{x}+V_{z},\\ &V_{2}=V_{y}+V_{z},\\ &V_{3}=-V_{x}+V_{z},\\ &V_{4}=-V_{y}+V_{z}, \end{split}$$

where the subscripts 1, 2, 3, and 4 refer to the quadrants of the tube, and the subscripts x, y, and z refer to the independent voltages required to move in the x, y, or z directions. For example, to extend the piezo tube in the z direction, the voltage on all four quadrants must

be changed by an equal amount. To move the piezo tube in the x direction, the voltage on piezo quadrant 1 must be increased by the same amount that the voltage on piezo quadrant 3 is decreased.



combine V_x , V_y , and V_z into the piezo quadrant

voltages.

Since there are only three independent variables, the computer algorithm was changed to output only V_x , V_y , and V_z . Two addition and two subtraction op-amp circuits were built to add and subtract the x, y, and z voltages to obtain the desired voltages for each quadrant (see Figure 5-7).

The circuits were built using the Linear Technologies LT1007 opamp (Linear Technologies, Milpitas, CA). The bandwidth of the addition and subtraction circuits far exceeded

the bandwidth of the following high-voltage amplifiers of 2 kHz (discussed in the next section) and so does not limit the performance of the STM in any way.

The noise at the outputs of the addition and subtraction circuits comes from two sources. The first source is at the inputs to the circuits or, rather, the noise in the output from the DA converters. The second source of noise is the input bias voltage noise from the op-amps used in the circuit. If each of the DA converter outputs has a noise of 1.2 mV (as determined in the previous section), then the noise at the add/subtract outputs is:

$$\begin{aligned} v_{noise} &= v_{input1} + v_{input2} + v_b, \\ v_{RMS \, noise} &= \sqrt{(12mV)^2 + (12mV)^2 + (0.13\mu V)^2} \\ &\approx 1.7mV, \end{aligned}$$

where v_{input} and v_{input} are equal to the output noise from the DAs, and v_s is the input

bias voltage noise of the op-amps used for the circuits, and $v_{noiseRMS}$ is the root-mean square noise at the circuit output. The measured RMS noise at the output of the add/subtract circuits was less than 0.01 mV (with inputs zeroed, 300 kHz bandwidth) and so the add/subtract circuits do not contribute significantly to the electrical noise at the piezo tube.

5.4 High-Voltage Amplifiers

The voltages applied to the piezoelectric tube to move the tip can be as high as ±150 V. At these voltages, the tube extends or deflects in the x, y, or z direction about

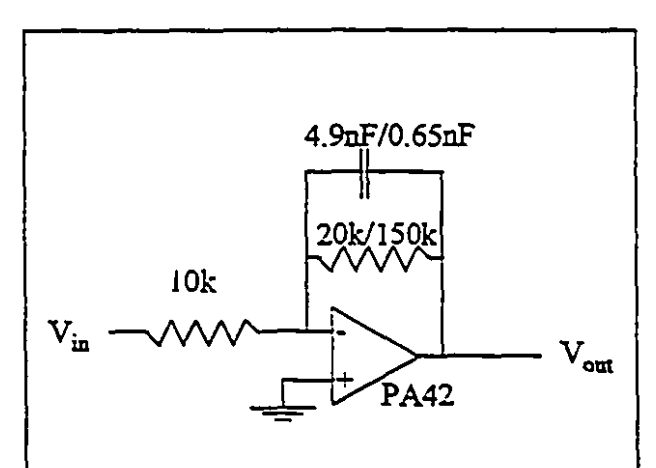


Figure 5-8: High Voltage Amplifier Circuit. The capacitor limits the output bandwidth to close to 2 kBz.

half a micrometer. The control signals for the tube position come from the computer via the digital to analog converter (described in the next section) which has a voltage range of ± 10 V. If the voltage from the D/A converters were directly applied to the piezo tube, the range of motion would only be about 60-70 nanometers.

The circuit used for the high

voltage amplifiers is shown in Figure 5-8. The operational amplifiers are APEX⁵ PA42 which have a maximum voltage range of ± 150 V.

For the circuit in Figure 5-8, the transfer function is:

$$\frac{V_{out}}{V_{in}} = -\frac{R_2}{R_1} \left(\frac{1}{1 + j\omega CR_2} \right),$$

giving a gain of $-\frac{R_2}{R_1}$ at low frequencies $(j=\sqrt{-1} \text{ and } \omega \text{ is the signal frequency})$. The gain of the amplifier can be set to either 15.00 times (with $R_1=9.98k\Omega$ and

⁵ APEX Microelectronics, Tucson, Arizona.

 $R_2 = 149.7k\Omega^{-6}$) in order to maximize the voltage range that could be applied to the piezo tube (\pm 150 V) and hence the size of the images that can be obtained, or to 2.00 times (with $R_1 = 9.98k\Omega$ and $R_2 = 19.96k\Omega$) in order to improve resolution. The transfer function of the amplifier is bandwidth limited by the capacitance to about 2 kHz.

The noise level at the output of the high voltage amplifier does limit the performance of the microscope. The noise level is:

$$v_{noise} = G \times (v_{noise in} + v_n),$$

where G is the amplifier gain, v_{noise_m} is the voltage noise at the input to the amplifier and v_b is the voltage noise at the input to the op-amp. When applied to the piezo tube, the voltage noise causes a variation in the position:

$$x_{noise} = K_x V_{noise},$$

$$y_{noise} = K_y V_{noise},$$

$$z_{noise} = K_z V_{noise},$$

where K_x , K_y , and K_z are the piezo constants (in units of m/V). The PA42 input voltage noise is equal to the output noise from the add/subtract electronics of 1.7 mV.

To determine the noise in the z position of the STM tip due to the electronics, the voltage noise at the input is multiplied by the high voltage amplifier gain and the piezo constant:

Table 5-4: Piezo position error for x, y, and z.

	K (nm/V)	G=2 (nm)	G = 15 (nm)	
х	3.3	0.011	0.085	
y	4.5	0.015	0.11	
Z	5.4	0.018	0.14	

$$\Delta z_{noise} = K_z \times G \times (\nu_{in} + \nu_{bias}),$$

$$\Delta z_{RMS noise} = K_z \times G \times \nu_{RMS in},$$

For a $K_z = 5.4$ m/V (measured in Chapter 7) and a gain of 2 or 15 times, the RMS position noise is $\Delta z = 0.018mm$ or $\Delta z = 0.14mm$

respectively. The position noise in the x, y, and z direction for high voltage gains of 2 or 15 are shown in Table 5-4.

⁶ The resistors used were hand selected to give the correct gain to within 0.1%.

To reduce the noise at the tunneling tip, either the noise at the input or the high voltage gain needs to be reduced. To image the hexagonal structure of highly oriented pyrolytic graphite (known as HOPG) which has an atomic spacing of 0.25 nm, a lateral resolution on the order of 10 pm is needed. The vertical resolution required depends on whether the image is being taken in constant height mode or constant current mode. For constant current mode, the vertical resolution also needs to be about 10 pm while for constant height mode, vertical resolution can be lower because it is the change in current that is being measured. A high voltage gain of 2 times gives position noise between 11 and 20 pm which is acceptable. The increase in resolution is accompanied by a corresponding decrease in the range of motion of the tip because the maximum voltage that can be applied to the piezo tube is lowered to only 20 V. The maximum scan size is reduced from about one micrometer (±150 V) to about 120 nm (±20 V). Atomic resolution on HOPG was never achieved with a gain of 15 times but was achieved when the lower gain of 2 times was used.

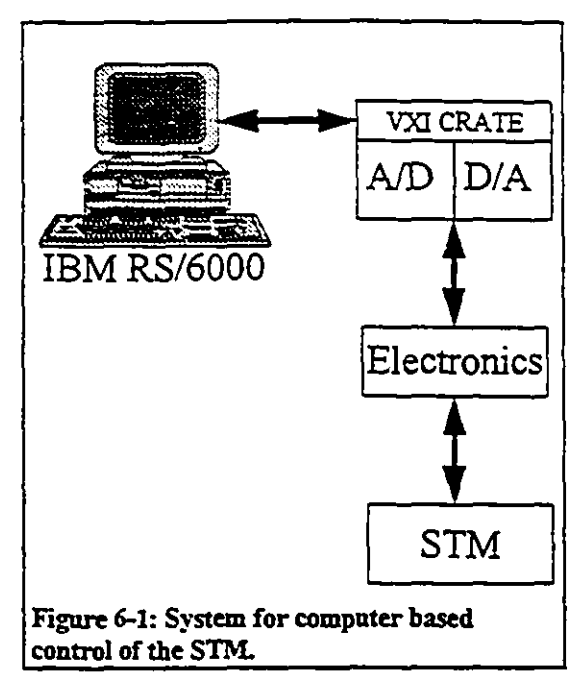
The above discussion has focused on the noise contributions from the electronics. However, as discussed in Chapter 3, mechanical vibrations contribute to the tip to sample position noise and atomic resolution was only obtained consistently late at night or early in the morning when the lab environment was quiet, even with the considerable effort that was put into vibration isolation.

Chapter 6: Computer Feedback Control

Most of the scanning tunneling microscopes that have been described in the literature use analog feedback control to maintain a constant tunneling gap. Analog control is easy, requiring only a proportional, integral, derivative (PID) controller made from a few op-amps, resistors, and capacitors. However, an analog feedback system lacks flexibility. If the feedback can be implemented digitally, the feedback gains can be easily and automatically adjusted (even during the scan if needed) and the feedback loop can be interrupted to perform local spectroscopy or other experiments. Full digital control also makes it easier to quickly change the scanned area or to program a special scanning path (such as a spiral scan). Because of the added versatility, the microscope built for this thesis uses digital control.

However, there are a number of potential problems with digital control. Low precision A/D and D/A converters are very fast but do not have adequate resolution. On the other hand, very high precision converters trade off speed for accuracy. As the speed and dynamic range of digital to analog and analog to digital converters has increased, digital feedback has become a feasible alternative to analog feedback for high-speed, high accuracy control, but the cost of fast, high-accuracy A/D converters can still be prohibitive.

By analyzing the precision and dynamic range needed for piezo tube positioning, Piner and Reifenberger identified the minimum requirements for digital feedback control as 12 bits A/D conversion for current measurement and 16 bits D/A conversion for the z direction (12 bits D/A is sufficient for the x and y directions but for the z direction, an increased dynamic range is needed for extra precision) [Piner and Reifenberger, 1989]. The time taken for A/D conversion, computer calculations, and D/A conversion should be small enough to allow at least a 10 kHz bandwidth to achieve scan rates comparable to analog control scan rates. Piner and Reifenberger used a VME bus system to run their digitally controlled STM.



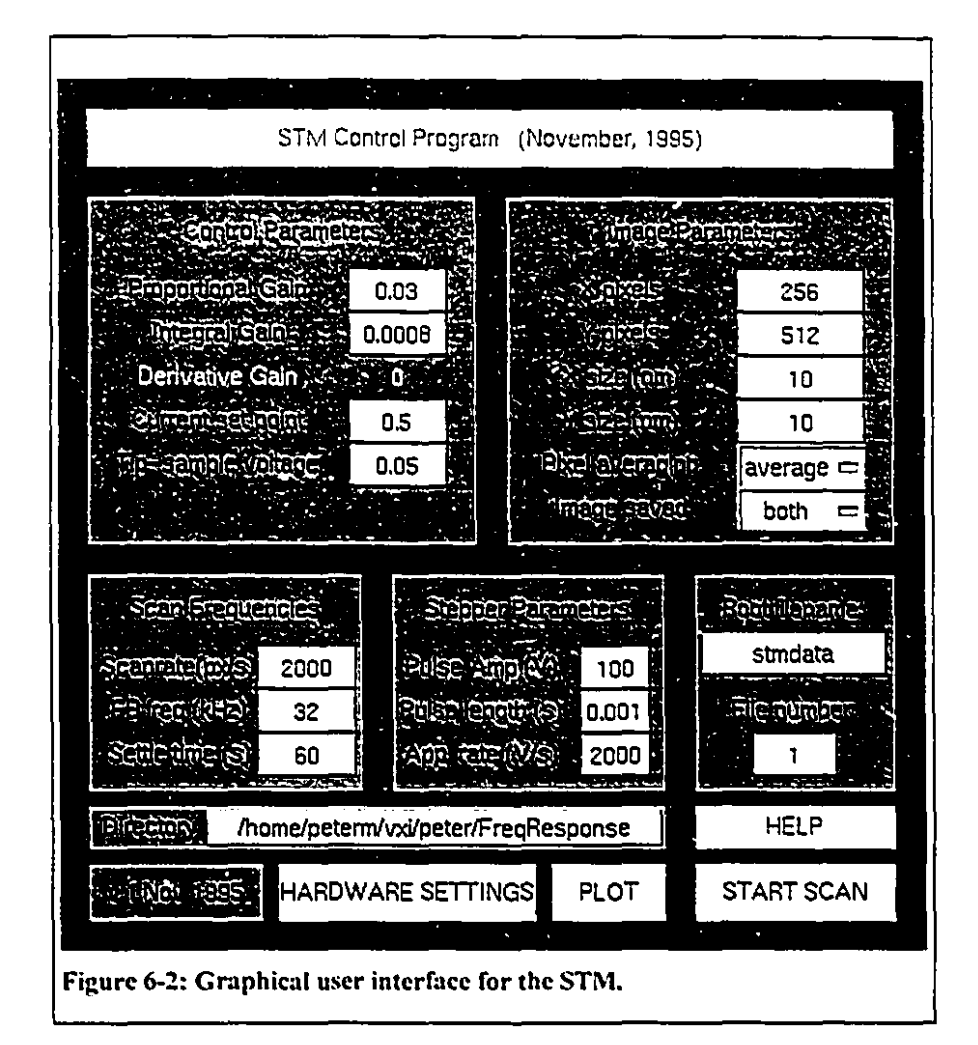
Clark et al. use an IBM PC/AT computer with a dedicated digital signal processing (DSP) board based on the Texas Instruments TMS 320C30 digital signal processor [Clark et al., 1992]. The DSP board performs all the floating point calculations required for feedback and controls the x and y raster scan. 18 bit D/A converters are used, giving a dynamic range large enough to get atomic resolution on graphite even for very large scan areas¹. The system of Clark et al. can sample at up to 100 kHz, limited by the speed of the A/D

converter. Only for very complex control algorithms is the scan rate reduced because the DSP can not perform all the required computations quickly enough.

The paper by Baselt et al. describes some feedback tuning algorithms used in a their DSP based digital control system [Baselt et al, 1993]. Baselt et al. use a computerized optimization procedure to find good values for the PID feedback parameters and discuss some techniques for hysteresis compensation and sample tilt removal. Algorithms for measuring the barrier height image (the effective work function of the tip and sample) by measuring $\frac{dI}{dz}$ and even $\frac{d^2I}{dz^2}$ are also discussed, demonstrating the flexibility of the digital control approach for local spectroscopic imaging.

The microscope developed for this thesis uses A/D and D/A converters in a VXI bus crate that is connected to an IBM RISC/6000 computer (see Figure 6-1). The multitasking IBM AIX (UNIX) operating system includes our own special kernel extensions to allow (single-tasking) real-time control of devices with timing of events to less than one

Often, to achieve atomic resolution, the high voltage gain of the STM piezo tube is reduced to lower the noise levels at the tube. The lower gain gives better precision for positioning but also reduces the maximum scan area. With 18 bits of precision in the output, large voltages can still be used to image large areas without sacrificing atomic resolution.



microsecond. Precise timing is important because the stability of digital control algorithms is dependent on having a uniform sampling period and minimal delay in the feedback.

The control program is written in C. The program performs the following functions: 1) control of the coarse approach micro-positioner to position the tip within the range of the piezo tube, 2) linearization of the tunneling signal, 3) feedback control to maintain a constant current, 4) control of the X and Y coordinates of the tip for the raster scan, and 5) saving of the image data to disk. A simple graphical user interface was constructed in Matlab which runs the C program and displays the images (see Figure 6-2). The C code is included in Appendix B.

6.1 Coarse Approach

The software written to perform the coarse approach uses a simple algorithm that steps the micropositioner toward the tip until the sample is within range. The STM tip is retracted away from the surface before each step is taken. The computer sends out the step waveform to the micropositioner, moving the sample one step toward the tip, and then extends the tip toward the sample. If a tunneling current is detected within a specified range of the piezo tube extension, the coarse approach is stopped. If, on the other hand, the tube is extended to its limit and no current is detected, the tube is fully retracted and another approach step is taken.

As implemented, the step size is set before the program is run and there is no way to change the step size or step direction during the coarse approach. However, the approach algorithm could be changed by rewriting the code so that the step size is reduced when the micropositioner gets close to the desired position. Future refinements of the software will include the ability to decrease the step size or even step backwards when the sample is close to the desired position so that the starting position can be specified to within 10 nm (10 nm is the minimum coarse approach step size). Better positioning of the sample should reduce the effects of hysteresis and piezo drift, as discussed in Chapter 3.

6.2 Linearization

During imaging, the tunneling current is amplified by the current-to-voltage amplifier and then digitized by the A/D converter. The measured current varies exponentially with the tunneling distance because of the current to distance relationship across the tunneling gap:

$$I(z) \propto e^{-\kappa}$$
,

where z is the tunneling gap and κ is the decay constant (see Chapter 2). The computer uses the measured value of the current to control the position of the tip. To make the control loop linear, the logarithm of the current is taken to yield a value that is proportional to the position (since $z \propto \log_{\kappa} I$).

The standard C algorithm to compute logarithms uses a converging series solution which requires many multiplications and additions. Log calculations take 4 µs, which is a significant fraction of the control loop execution time (about 25 µs). Instead of using the standard algorithm, a lookup table of logarithm values is created before the feedback is started. When a new value for the current is read by the computer, the computer uses that value to determine an address in memory where the logarithm is stored. For currents that lie between two stored values, linear interpolation is used to approximate the correct log value. If the table size is reasonably large, the error in the linear approximation is very small. In the STM control program, a table with 16384 elements is used. The maximum error between the table lookup values and the value calculated by the computer algorithm is less than 1.3 percent. The lookup table takes 1.5 µs to calculate the logarithm, saving 2.5 µs per loop.

The error of 1.3 percent is acceptable because the exact value of the gap width is not important. Rather, it is important to keep the current close to a constant set point so that the gap width is constant and the tip closely follows the surface profile during a scan. The error in the calculated position might introduce a small difference between the desired set point and the actual tunneling current when feedback is engaged but will not cause noticeable distortion of acquired images.

6.3 PID Control

Effective control of the tunneling gap is crucial to getting good images. Surface height in STM images is calculated from the voltage applied to the piezo tube. If the voltage applied to the piezo tube doesn't keep the tunneling gap constant, the change in the gap width will result in a distortion of the true sample shape.

Since $I(t) \propto e^{-\kappa(z(t)-z_0(t))}$, changes in the gap width cause a change in the current (z(t)) is the height of the tip and $z_o(t)$ is the height at which the tip touches the surface). $z_o(t)$ changes as the tip scans across the sample being imaged because of the surface height variations. If the current increases due to a decrease in gap width (increase in surface height), the control system compensates by increasing the gap width. If the

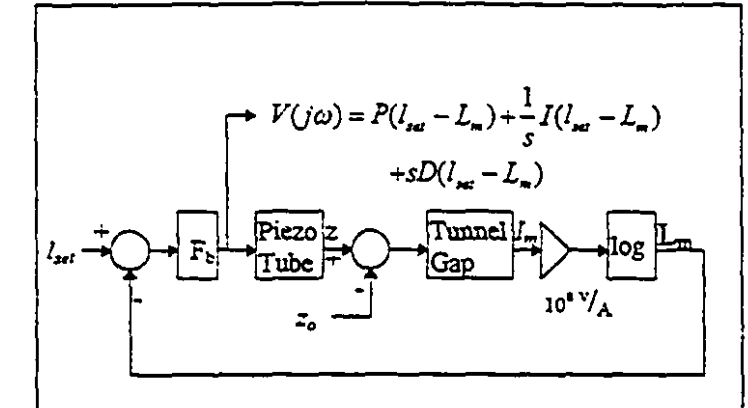


Figure 6-3: Block diagram of feedback for STM. F_b is the feedback transfer function. P, I, and D are the proportional, integral and derivative gains, and s is the Laplace transform variable. For proportional integral derivative (PID) feedback, $F_b = P + I/s + sD$.

current decreases (increase in surface height), the control system acts to decrease the gap width. To make the system linear with respect to gap width, the logarithm of the current is taken, as described above.

Proportional integral derivative (PID) control is used to maintain a constant current.

A block diagram of the feedback system for the STM is shown in Figure 6-3. The output of the

PID controller is:

$$v(t) = P(l_{set} - l_m(t)) + I \int_0^t (l_{set} - l_m(t)) dt + D \frac{d}{dt} (l_{set} - l_m(t)),$$

or in the frequency domain (found by taking the Laplace transform):

$$V(s) = P(L_{set} - L_m(s)) + \frac{1}{s}I(L_{set} - L_m(s)) + sD(L_{set} - L_m(s)),$$

where $l_{set} = \log i_{set}$, $l_m(t) = \log i_m(t)$, $i_m(t)$ is the measured tunneling current, P, I, and D are the proportional, integral, and derivative gains respectively, and L_{set} and $L_m(s)$ are the Laplace transforms of l_{set} and $l_m(t)$. (The current to voltage gain of 10^8 V/A cancels out of the equation: $\log 10^8 i_{set}$ - $\log 10^8 i_m(t) = \log i_{set}$ - $\log i_m(t)$, and so need not be included.)

The value $l_m(t)$ depends on the gap width $z-z_o$:

$$l_m(t) = \log_e I_0 e^{-\kappa(z(t) - z_0(t))}$$

= $\log_e I_0 - \kappa(z(t) - z_0(t))$.

Since $l_{set}(t) = \log_0 l_0 e^{-sct}$, where d is the set point tunneling gap width, we can write:

$$l_{m}(t) - l_{set} = \log_{e} I_{0} - \log_{e} I_{o} e^{-\kappa t} - \kappa(z(t) - z_{0}(t)),$$

= $-\kappa(z(t) - z_{0}(t) - d),$

or taking the Laplace transform,

$$L_m(s) - L_{set} = -\kappa (Z(s) - Z_0(s) - d),$$

and so the controller output in terms of the tip position and sample height is:

$$v(t) = P\kappa(z(t) - z_0(t) - h) + I\kappa\int_0^t (z(t) - z_0(t) - h)dt + D\kappa\frac{d}{dt}(z(t) - z_0(t) - h),$$

or

$$V(s) = P\kappa \left(Z(s) - Z_0(s) - h\right) + \frac{I\kappa}{s} \left(Z(s) - Z_0(s) - h\right) + sD\kappa \left(Z(s) - Z_0(s) - h\right).$$

The proportional (P) term responds to fast changes in the input. Increasing the P term generally increases the speed of the response but also reduces the stability of the system.

Increasing the P term also decreases the tracking error. However, if $z_o \neq 0$, the tracking error can be significant, even for very large values of P. By adding an integral (I) term to the control, offsets or slow changes in z_0 can be compensated.

Finally, the derivative (D) term increases the magnitude of the response if the system is moving away from the set point at a high rate. When the system is only moving away from the set point slowly, the derivative term contributes little to the control output. Derivative control helps to reduce oscillations around the set point by reducing the overshoot.

However, if the signal includes high frequency noise, derivative control can amplify the noise and reduce the stability of the system. When trying to keep the tip to sample gap constant as the STM tip is scanned over a surface, the measured current changes primarily at low frequencies because of changes in the gap width, but noise is present at all frequencies (Johnson noise, shot-noise, coupling from external vibrations, etc.). The derivative term amplifies the higher frequency noise more than the low frequency noise, reducing the signal to noise ratio.

Often STM control uses a very small or zero derivative term to avoid amplifying high frequency noise. Baselt et al. occasionally use a negative derivative term to attenuate the high frequency noise although this can increases the magnitude of oscillations around the set point [Baselt et al., 1993].

To calculate the control output, the computer program uses a discrete approximation to continuous time PID that was presented above (see Table 6-1). The

Table 6-1: Discrete app. ximation to continuous time P, L, and D gains. This the sampling period of the digital system.

discrete	approximation	to	the	PID
feedback				

$$V_i = V_{i-1} + P(E_i - E_{i-1}) \div$$

$$ITE_i + \frac{D}{T}(E_i - 2E_{i-1} + E_{i-2}),$$
where T is the sampling interval.

Following Baselt et al., the feedback is calculated as

$$V_{t} = V_{t-1} + aE_{t} + bE_{t-1} + cE_{t-2}$$

where a = P + IT + D/T, b = -P + IT - 2D/T, and c = D/T. Thus each new value of the output voltage for the pieze tube requires a knowledge of the errors from the newest and previous two samples and of the previous voltage output. Once the new voltage is determined, the voltage is output using the D/A converter. The voltage is also saved in a matrix from which the sample image is later reconstructed.

The error between the set point and the measured current can also be saved in a matrix. The matrix of the errors can be used to obtain an image at very fast scan rates on flat surfaces. By setting the feedback gains to be small, only very slow changes in the surface can be tracked and the higher spatial frequencies appear as feedback errors. The error matrix therefore gives an image that depends on the quickly changing features. An atomic resolution image of this type (called constant height imaging as opposed to constant current imaging) is shown in Chapter 9 for an HOPG (graphite) surface.

6.4 Raster Scan

The computer not only runs the control algorithms to maintain a constant gap width but also controls the scan position. The x-y scan is controlled open loop by varying the voltages on the piezo quadrants. During acquisition of an image, the x and y voltages must be updated to trace out a path over the image area. The raster scan position is updated once per feedback control loop.

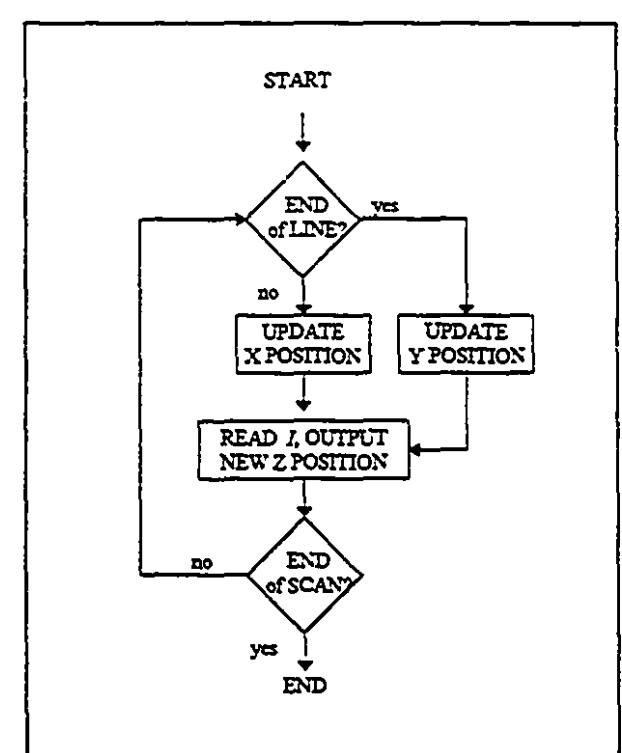


Figure 6-4: Flow diagram of the control loop and scanning algorithm. I is the amplified tunneling current as measured by the AD converter.

To reduce the time per control loop, only the x raster value is updated inside the main control loop (see Figure 6-4). The y raster value is only updated at the end of each line. The y raster value could be updated in the main control loop to allow diagonally scanned lines (or images scanned with an arbitrary path) but this would reduce the maximum control Each D/A rate of the microscope. conversion takes 4.4 µs out of a total of about 25 µs for the entire control loop. Updating the y value as well as the x value would add 4.4 µs or close to 20 percent to the period of the control loop.

The scanning algorithm is written so that the control loop is executed many times for each saved image pixel. The control loop frequency is typically set at 40 kHz while pixels are sampled at less than 2 kHz.

The piezo voltage and current error values that are saved in matrices can be either from a single point or they can be averaged along the scan line over many iterations of the control loop in order to reduce the effects of high frequency noise. For most images, the average is taken along the scan line to reduce noise levels by averaging.

Chapter 7: Piezo Tube Calibration

The piezo electric materials used for actuation in STM exhibit significant non-linearities that generate unwanted imaging artifacts. Various groups have tried to model piezo electric behaviour with the aim of compensating for non-linear distortion once an image has been acquired.

In this chapter, some examples of piezo-electric non-linearities are presented first and are followed by a brief description of the attempts to model the hysteresis and why so far they have not been satisfactory.

7.1 Piezoelectric Calibration and Observed Non-Linearities

For an STM actuator, the displacement must be known as a function of applied voltage. The piezo constant d_{31} is the ratio of the material stress along the axis of the piezo tube to the (radial) electric field applied between the inner and outer electrodes. The piezo displacement is:

$$\Delta z = d_{31} L E = d_{31} V \frac{L}{h},$$

where Δz is the change in length, L is the initial length, V is the voltage applied to the tube, and h is the thickness of the tube. To make quantitative measurements with STM, d_{31} must be measured.

Once d_{3l} is known, accurate measurements are still difficult to make because of the complicated behaviour of piezoelectric materials. Several different types of non-linearities are discussed in the literature, ranging from hysteresis and creep to variations of properties with temperature and long term aging effects.

Hysteresis and creep are the two dominant causes of image artifacts in STM. Hysteresis is a lag or difference between the command voltage applied to the piezo tube and the expected (generally linear) length change of the tube. Creep is a slow time-dependent change in the length of the tube that occurs after an initial much faster (less

than 1 millisecond) displacement. Creep is manifested either as a decaying response to a step change in voltage that eventually comes to equilibrium, e.g. a displacement of the form $\Delta x = x_i + x_{creep} e^{-t/x_{creep}}$, as a continual increase (typically linear or logarithmic) in the displacement, or a combination of both. Creep of any form will always result in some (time dependent) hysteresis because of the time lag between the initial change in voltage and the final position change. Hysteresis can be independent of creep (static friction for

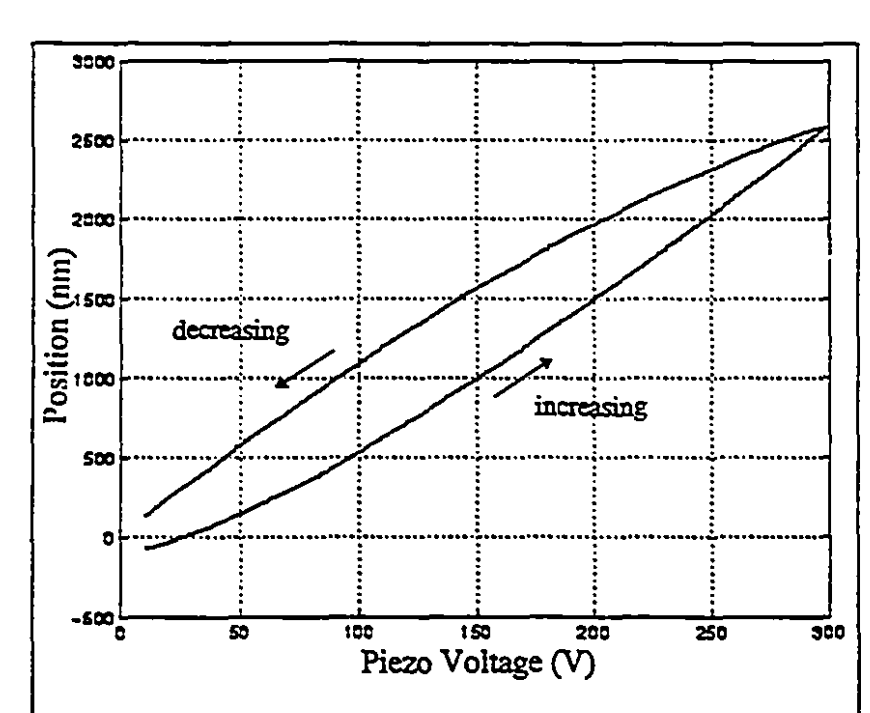


Figure 7-1: Hysteresis of the Piezo Tube. As the voltage ramps up to 300V, the position follows the lower curve. When the voltage is ramped down to its starting value, the position follows a different path and returns to a different starting point.

-

example causes creep independent hysteresis in a force position relationship).

A typical example of hysteresis is shown in Figure 7-1. The curve shows the of displacement STM piezo tube versus voltage and was measured using the interferometer described in Chapter 4. As the voltage applied to the piezo tube increases, the piezo tube position

follows the lower curve. When the voltage applied starts to decrease, the return path differs from the rising voltage path by more than 20% of the maximum length change. The applied voltage was a triangular waveform increasing for 50 s and decreasing for 50 s.

Measured creep is shown in Figure 7-2 through Figure 7-5. In Figure 7-2, the interferometer was used to measure the response of the piezo tube to step changes in voltage. In order to increase the signal to noise ratio of the measurement, the mean responses of one hundred steps were calculated for 6 V and 12 V steps. (The noise level of the interferometer is about 10 nm (Chapter 4). By averaging over one hundred trials, the noise level is reduced to about 1 nm.)

The two step responses scale almost linearly with the applied voltage. The 6 V response settles to a magnitude of 31.2 nm, or 5.2 nm/V, and the mean of the 12 V response 65.1 nm (measured from 0.4 s to 1 s), or 5.4 nm/V. The mean value 5.3 nm/V is used in all the calculations of the piezo tube or tip position from the applied voltage.

The higher frequency oscillations that are present in both step responses and that

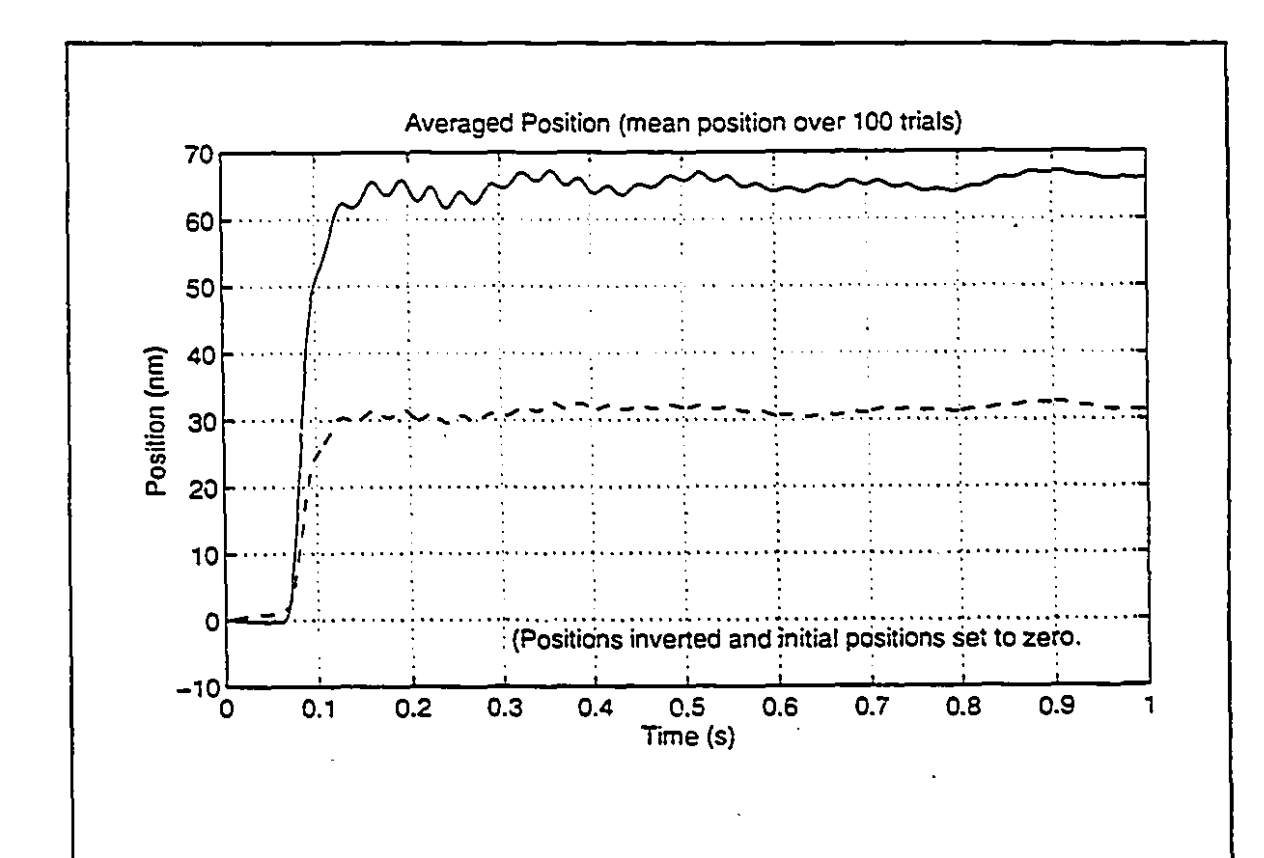


Figure 7-2: Creep measured with an interferometer for 30 and 60 nm steps. For both curves, 100 trials were averaged to reduce the interferometer noise levels. The zero position point in these measurement sets was chosen to minimize the interferometer measurement error and does not correspond to zero volts applied to the piezo tube.

decay towards zero are present in every one of the unaveraged step responses. The oscillations are at a frequency of about 30 Hz and are in almost in phase in every measurement. There is no 30 Hz component before the step and the amplitude decays almost to zero in one second. The source was not determined but it could be a mechanical resonance of some part of the interferometer (possibly a part that was not securely fastened).

It is useful to compare the experimentally measured results with the material properties that are given by the piezo tube supplier, Stavely Sensors. The length change of a piezo tube is given by:

$$\Delta z = d_{31} L E = d_{31} V \frac{L}{h},$$

and so d_{31} is found from:

$$d_{31}=\frac{h}{L}\frac{\Delta z}{V},$$

where for the piezo tube used, h = 0.51 mm and L = 12.7 mm. The experimental value of d_{31} is 212×10^{-21} m/V. Stavely Sensors specify $d_{31} = 173 \times 10^{-12}$ m/V, almost 20% lower than the experimentally measured value. Given the large deviation from the manufacturer's specifications, it is clearly very important to individually calibrate each piezo tube.

While the interferometer provides a good independent measure of the piezo constant, measurements are hampered by low resolution (10 nm for single measurements) and drift over time (1.3 nm / minute) that make it difficult to observe slow effects such as creep. To get around the limitations of the interferometer, measurements were made using the STM tunneling junction.

In Figure 7-3, the position of the STM tip is plotted against time. The tip is initially as far away from a gold sample as possible (the voltage applied maximally retracts the tip). In the plot the zero position is the position at which zero volts is applied to the piezo tube and the positive direction is away from the sample. The tip is brought towards

the sample until tunneling starts (the position change of the tube is calculated as $\Delta z = \frac{d_{31}LV}{h}^{-1}$). Feedback is then engaged to maintain a constant tunneling gap width. After the initial extension, the tube continues to extend because of creep. Since the sample position is fixed, the feedback compensates by changing the voltage to keep the piezo tube length constant. When taking an image, if the scan is started immediately after the initial (large) step change in position, the creep that results will appear in the image as an apparent variation in surface height. Figure 7-4 is an expanded view of the creep after the largest initial step of 780 nm shown in Figure 7-3. After 100 s, the creep is less than 0.1 nm/s. In Figure 7-5, an expanded view of the 400 nm step from Figure 7-3, the creep over the last 40 of the 100 seconds is smaller than the peak to peak noise level of roughly 0.3 nm (the creep is smaller than 8 pm/s).

¹ The experimental value of d_{31} is used.

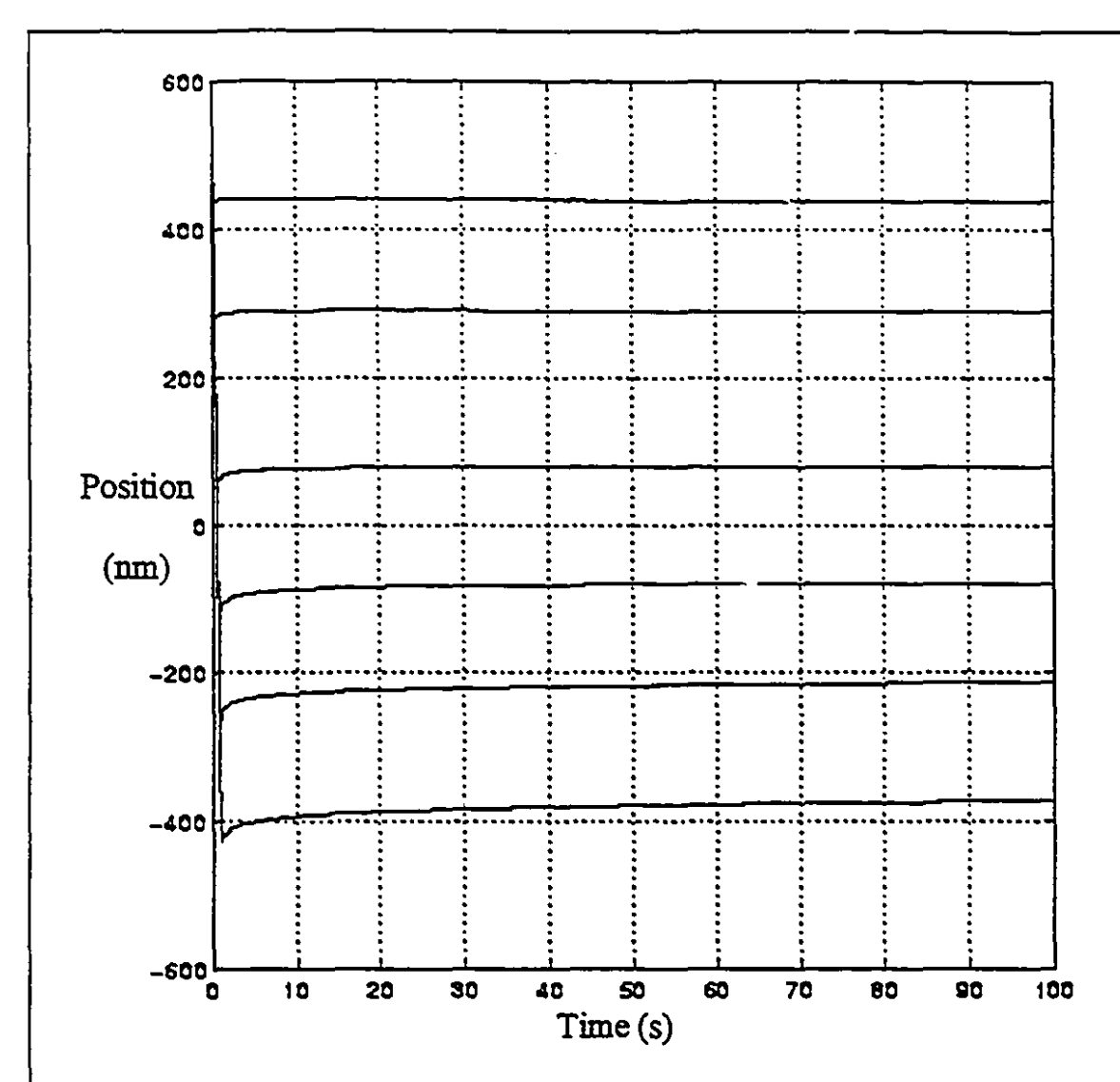


Figure 7-3: Measurement of Piezoelectric Creep. The position is calculated from the voltage applied to the piezo tube to keep the tunneling gap constant. After the initial change in length, the tube gets longer because of creep. To compensate, the voltage applied to the tube decreases and so the apparent position of the tip also decreases. For small initial changes in position, the creep magnitude is very small. Large initial changes in position show much larger creep. After 100 seconds, the creep is less than 0.1 nm/s in all cases.

Note that for the smallest step (about 30 nm), the apparent position first increases (the effect of creep from the 30 nm step) but then starts to decrease after about 10 s. The overall response is actually a combination of the response of the piezo material to the 30 nm step and to the initial large step that pulled the tip away from the sample. All of the three top curves in Figure 7-3 show a reversal in direction of creep. The rate of creep after 100 s becomes smaller for the curves as they move closer to the zero position. In the fourth curve (the step that is closest to the zero position) the creep can not be seen above

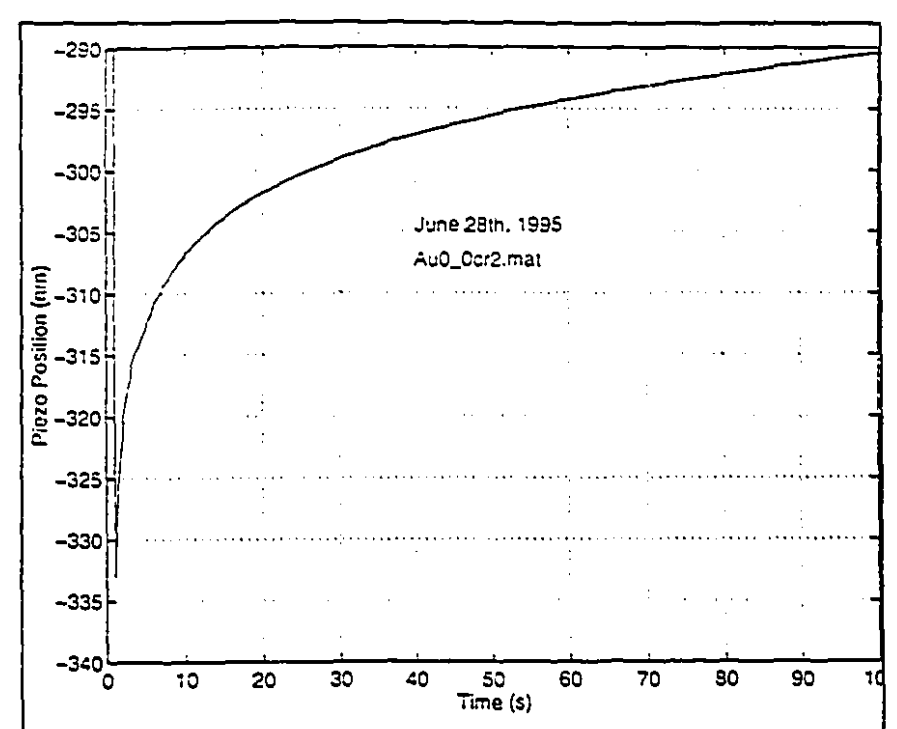
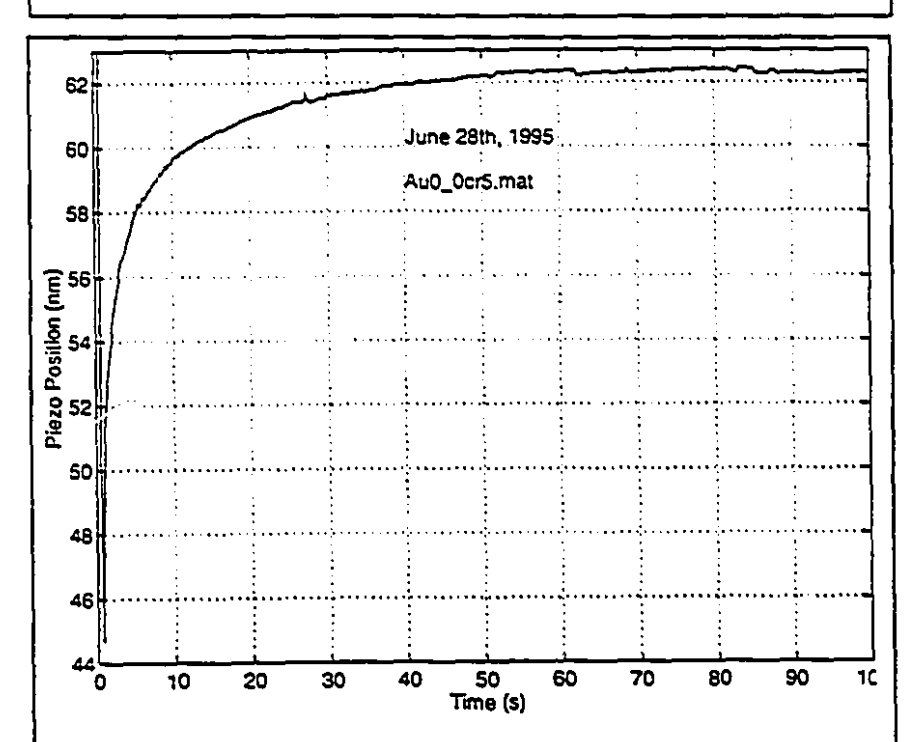


Figure 7-4: Expanded view of creep measured while tunneling for the largest initial position change. After 100 seconds, the piezo tube is extending at a rate of less than 0.1 nm/s.



rigure 7-5: Expanded view of creep measured while tunneling for the position step that ends closest to zero volts applied to the piezo tube. Even after 60 seconds, the piezo tube creep is unnoticeable.

the noise level. The curves that pass beyond the zero position (the polarity the applied of voltage changes) all show a creep that does change not direction but that increases in rate after 100 s) with increasing step size.

The rate of creep measured in Figure 7-3 after 100 s is always smaller for curves close to the zero position. The conclusion is that creep is smallest close to the zero position. By using the coarse approach mechanism to keep the STM tip piezo tube voltage close to zero volts. the effects of slow creep can be minimized.

The minimal creep near the zero position explains why almost no creep was observed in the 6 V and 12 V step responses (Figure 7-2) measured with the interferometer. Both step responses were measured at positions close to zero volts.

Among the other non-linearities, temperature effects tend to increase d with increasing temperature [Stavely Sensors, 1994]. Certain ceramic mixtures are optimized to give low variation near room temperature (e.g. Stavely Sensors EBL #1 and EBL #4 ceramics). However, even for materials with very high temperature sensitivity, the change in d per degree Celsius is only one or two percent. For experiments conducted at a constant temperature (within a few degrees), image artifacts caused by variations of the piezo constant with temperature are dwarfed by hysteresis and creep.

Long term aging changes the piezo constants over time periods of weeks or months. The changes in piezo-electric parameters are very close to logarithmic with time over large time scales. The variations, especially a few days or weeks after the piezo electric material is poled, are negligible compared to hysteresis and creep.

7.2 Models of Creep

If good mathematical models of creep could be found, the distortions caused by creep could be removed from images. However, determining a good model is not an easy task.

One of the simplest models for creep in a material treats the material like a spring in series with a second spring and damper which are in parallel (Figure 7-6). Many materials, including piezoelectrics, show an initial almost

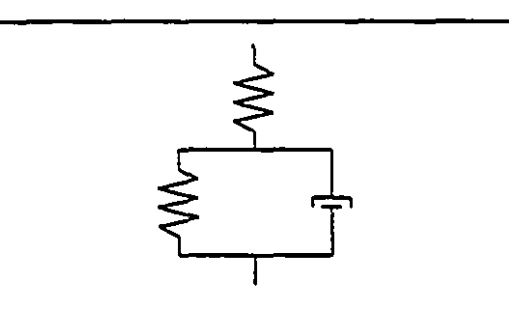


Figure 7-6: Simple model for creep in a material. A spring is in series with a second spring and a damper which are in parallel.

instantaneous response to an applied stress which is followed by a slower response that eventually reaches steady state. In Figure 7-2 for example, there is a fairly sharp rise (not instantaneous because of anti-aliasing filters) followed by a slower decaying response.

While this model is reasonably good for short time scales (less than 1 to 10 seconds), it does not explain creep of the form measured in Figure 7-3. Vieira found that the longer term creep was well described by the equation:

$$\frac{\Delta z}{L} = \frac{V}{d}(\alpha + \beta \ln t),$$

where α and β are chosen to best fit measured data, t is the time, and V is the applied voltage [Vieira, 1986]. In general, α and β are dependent on both the temperature and the electric field. The actual dependence on the electric field is very small.

Stoll used Vieira's model to implement a correction method for the distortions [Stoll, 1994]. Difficulties arise however because of singularities in the model at t=0 and at $t=\infty$. The logarithm term suggests that at t very close to zero, the step response of the tube is actually in the negative direction. This is not a physical response. Stoll got around the problems of singularities by introducing small time delays into his correction equations and by applying ramp changes in voltage instead of step changes.

Image distortion removal has not yet been added to the STM software written for this thesis. A second STM will likely be built in the near future and that will either incorporate an correction algorithm or will use a different actuator (probably electrostrictive) that avoids many of the hysteresis and creep problems associated with piezoelectric materials (this is discussed further at the end of Chapter 10).

7.3 X and Y Calibration

So far, this chapter has only discussed the calibration of the piezo tube in the z direction. An interferometer can also be used for the x and y calibration. Alternatively, the x and y scan range can be calibrated by imaging a sample with known periodicity and determining the piezoelectric coefficients by calculating the voltage change between periods. Examples of surfaces with known periodicity that can be imaged are HOPG

(highly-oriented pyrolytic graphite), which has an atomic spacing well known from x-ray diffraction, or gold plated holographic gratings. The calculation of x and y piezoelectric coefficients is done in the chapter on imaging results (Chapter 9). Using HOPG (Burleigh Instruments, Fishers, NY) as the calibration standard, it is found (see Chapter 9) that $K_x = 3.33$ nm/V and $K_y = 4.46$ nm/V. Large difference in the x and y coefficients are not unusual [Chen, 1993, p. 233]. The difference between K_x and K_y once again highlights the importance of calibrating the piezo tube if the STM is to be used for quantitative analysis.

7.4 Summary

Piezoelectric materials are able to generate very small motions with high precision. However, their use is complicated by a number of non-linear and non-ideal behaviours. The two most significant problems are hysteresis and creep. Experimentally measured hysteresis and creep were shown and some models were presented that try to explain the creep behaviour. However, the models do not fully explain the observed behaviour.

Measurements of short term creep (6 and 12 V step responses) were used to determine the piezo electric coefficient that relates voltage to displacement. The piezo coefficient K_z (extension of the tube) is 5.3 nm/V. The piezo coefficients for the x and the y directions (bending of the tube) are found in Chapter 9 to be $K_x = 3.33$ nm/V and $K_y = 4.46$ nm/V.

Chapter 8: System Characterization

In this chapter, measurements of the behaviour of the STM and of its components are shown that shed light on what level of performance can be achieved. The measurements also show which system components limit the performance so that future work can focus on improving those elements.

8.1 Frequency Response

The STM system can be split into five major components, each of which can be characterized by its frequency response. The frequency response gives an indication of the frequencies over which each component can be easily controlled. For a particular frequency, if the magnitude of the response is small or the phase lag is big, very large control signals or special compensators are needed to get the component to track the control input well. Disturbance noise can also cause problems at frequencies where the response is small or the phase lag is big.

The five different components of the STM are 1) the mechanical structure, which includes the piezoelectric tube, the STM base, the coarse approach, the sample holder, and the vibration isolation system, 2) the high voltage amplifiers for the piezo tube, 3) the tunneling junction, 4) the current to voltage amplifier, and 5) the computer based feedback.

The transfer function of the mechanical structure is difficult to calculate from first principles because of the complicated geometry and the many different parts. Neither is the transfer function easy to measure because of the difficulty of generating an appropriate input. To get a rough idea of the mechanical bandwidth, an approximation to a position impulse was generated by dropping a brass ball onto the aluminium plate that sits on the inner tube. (The STM in turn sits on spring suspended platform that is mounted onto the aluminium plate).

The response of the STM feedback and the feedback error are shown in Figure 81. The plot on the left is the voltage at the output of the computer feedback (converted to the piezo tube displacement). The plot on the right shows the feedback error. The large oscillations in the feedback error show that the feedback is unable to completely compensate for the dynamics of the mechanical impulse response (the disturbance rejection bandwidth of the STM is lower than the oscillation frequency). The frequency of oscillation, which is attributed to mechanical resonance, is 650 Hz. Any actuator

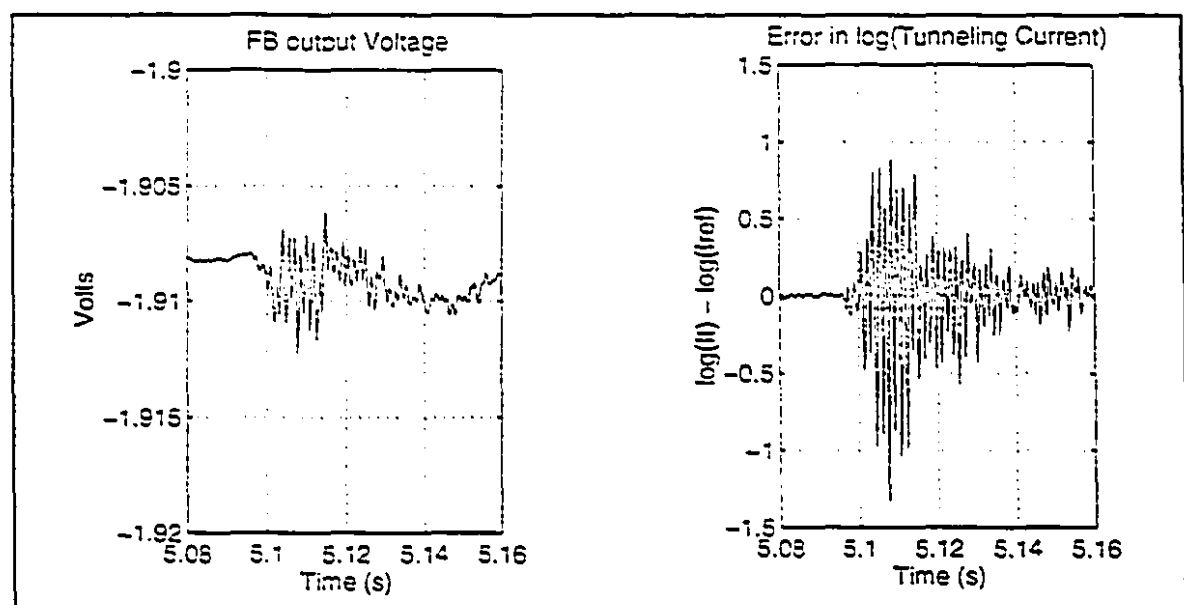


Figure 8-1: Position impulse response of the STM. The impulse was generated by dropping a brass ball onto the aluminium plate that supports the STM. The plot on the left shows the position command generated by the STM feedback. The plot on the right shows the feedback error.

displacements or vibration noise at this frequency will couple into the STM system and distort measurements. The resonant frequency is probably related to the structure of the STM base or of the STM coarse approach. The piezo tube actuator itself has calculated lateral (bending mode) and longitudinal resonant frequencies of about 22 kHz and 58 kHz respectively¹. The base structure of the STM is significantly larger and will thus have a

¹ The lateral resonant frequency of the piezo tube is given by $f = \frac{0.56\kappa c}{L^2}$, where $\kappa = \frac{\sqrt{D^2 + d^2}}{8}$ and $c = \sqrt{Y/\rho}$, Y is the Young's modulus, L is the tube length, and ρ is the density (see [Chen, 1993], p. 234).

much lower resonant frequency. In future designs, it should be possible to increase the mechanical resonant frequency by reducing the overall size of the entire STM structure. Finite element analysis may be used as a design aid towards this end.

The high voltage amplifiers convert the DA output voltage, which ranges from -10 to +10 V, to the high voltages needed to get the maximum displacements from the piezo tube. The high voltage amplifiers have a designed first order roll-off at 2 kHz (see Chapter 4). Above 2 kHz, the magnitude of the frequency response drops by one order of magnitude per order of magnitude of frequency (the slope of the log-log plot is -1). As discussed in Chapter 4, the 2 kHz bandwidth was chosen to match the bandwidth of the current amplifier and of the anti-aliasing filters.

The dynamics of the tunneling junction are significantly faster than the dynamics of any of the other major system components. Experiments that have been done to measure the electron tunneling time across the gap yield values on the order of femtoseconds [Nunes and Freeman, 1993].

The analysis of the STM system is complicated somewhat by the tunneling junction's exponential current to gap width relationship. The computer takes the logarithm of the amplified current once the value has been digitized but the amplification process itself will distort the observed current because of the finite bandwidth of the current amplifier.

The current to voltage amplifier converts the nanoamp tunneling currents into hundreds of millivolts, with a gain of 10⁸ V/A. The bandwidth of the current amplifier was measured in Chapter 5 to be 2 kHz (the improved current amplifier that has not yet been used with the STM has a bandwidth of 21 kHz). Because the logarithm is taken after the current amplifier, the high frequency components of the current that have been attenuated by the amplifier will not be reconstructed correctly. However, by keeping the cut-off

For the piezo tube, D=12.7mm, d=12.14mm, Y=6.4x 10^{10} N/m², and $\rho=7500$ kg/m³. The longitudinal resonant frequency is given by $f=\frac{c}{4L}$.

frequency of the current amplifier much higher than the STM system bandwidth, the distortion should not be significant. Furthermore, in constant current mode the deviations of the current from the set point should be small which in turn ensures that the distortions are negligible.

The fifth and final major component of the STM system is the feedback compensator. The implementation of the PID feedback compensator was discussed in Chapter 6.

When building a system with feedback control, the optimum feedback gains can be determined using the measured frequency response of the open loop (no feedback) response. However, in a scanning tunneling microscope, it is very difficult to keep the tunneling gap stable long enough to make a measurement of the frequency response. Slight changes in temperature, acoustic or floor vibrations, and drifts in the electronics can all change the gap width by enough to crash the tip into the sample or to move the sample out of tunneling range.

Instead, the feedback gains were tuned experimentally. Initially, a small integral term was included so that the controller can compensate for any position offset between the sample and the zero voltage position of the piezo tube. The proportional gain was

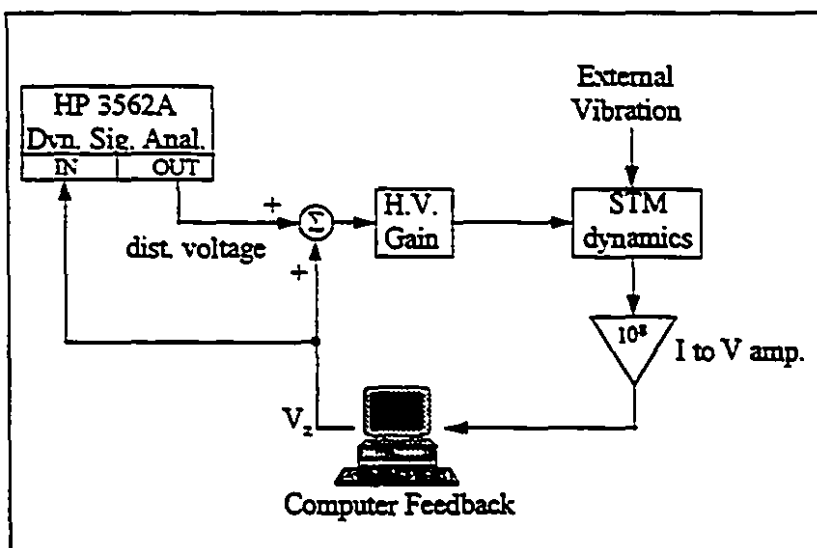


Figure 8-2: Experimental setup for measuring frequency response of the STM.

gradually increased from zero until the system became unstable. The proportional gain was reduced slightly to restore stability and then the proportional and integral gain were iteratively changed by small amounts to try to

reduce the tracking error.

The closed-loop response of the microscope to a known disturbance in the z direction was measured to determine system performance. The response of the system to a known disturbance added to the z direction piezo voltage (see Figure 8-2) is shown in Figure 8-3. Without feedback, the disturbance voltage applied to the piezo tube changes the gap width, simulating a change due to surface variation. With feedback engaged, the feedback voltage will try to cancel the disturbance to keep the tunneling current constant.

The disturbance frequency was varied between 10 Hz and 10 kHz and the response was measured using an HP 3562A dynamic signal analyzer. The dynamic signal analyzer output is a set of sinusoids of gradually increasing frequency. The output is used as the disturbance to the z piezo tube. The input to the HP 3562A is the output of the computer feedback which comes from the digital to analog converter. The tip was not scanned across the surface during measurements because variations in the surface height during a scan contribute frequencies to the tunneling gap width that could be confused with the known disturbance. By keeping the tip at a single point, any variations in the gap width are due to the disturbance voltage. The measurements shown in Figure 8-3 were made using a tungsten tip and a gold sample.

At each frequency, the magnitude of the computer controlled feedback is compared to the magnitude of the disturbance. At low frequencies, the microscope feedback easily compensates for the disturbance: the voltage output from the computer cancels the disturbance voltage so that the piezotube voltage is constant (see Figure 8-3a)). As the frequency is increased, the feedback is not able to keep up to the rapid changes in voltage applied to the piezo tube and the ratio of the feedback voltage to disturbance voltage falls.

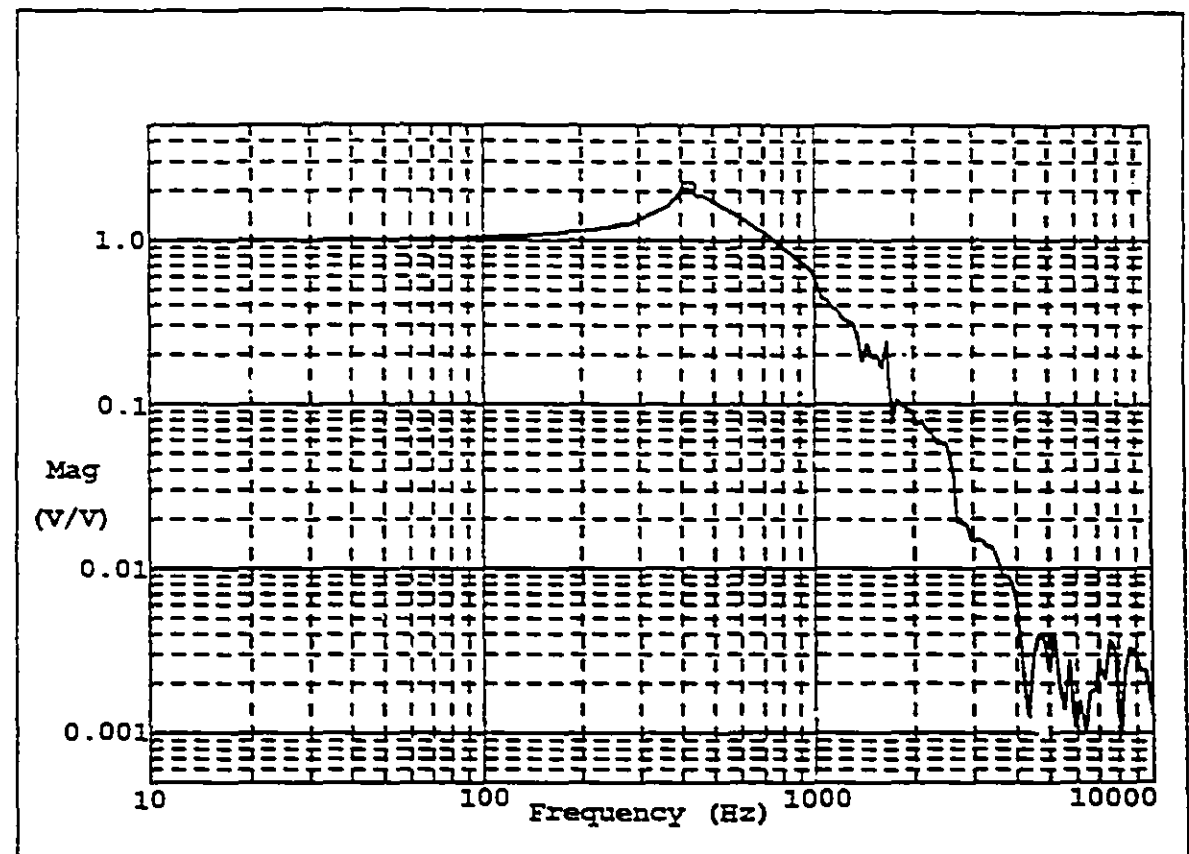
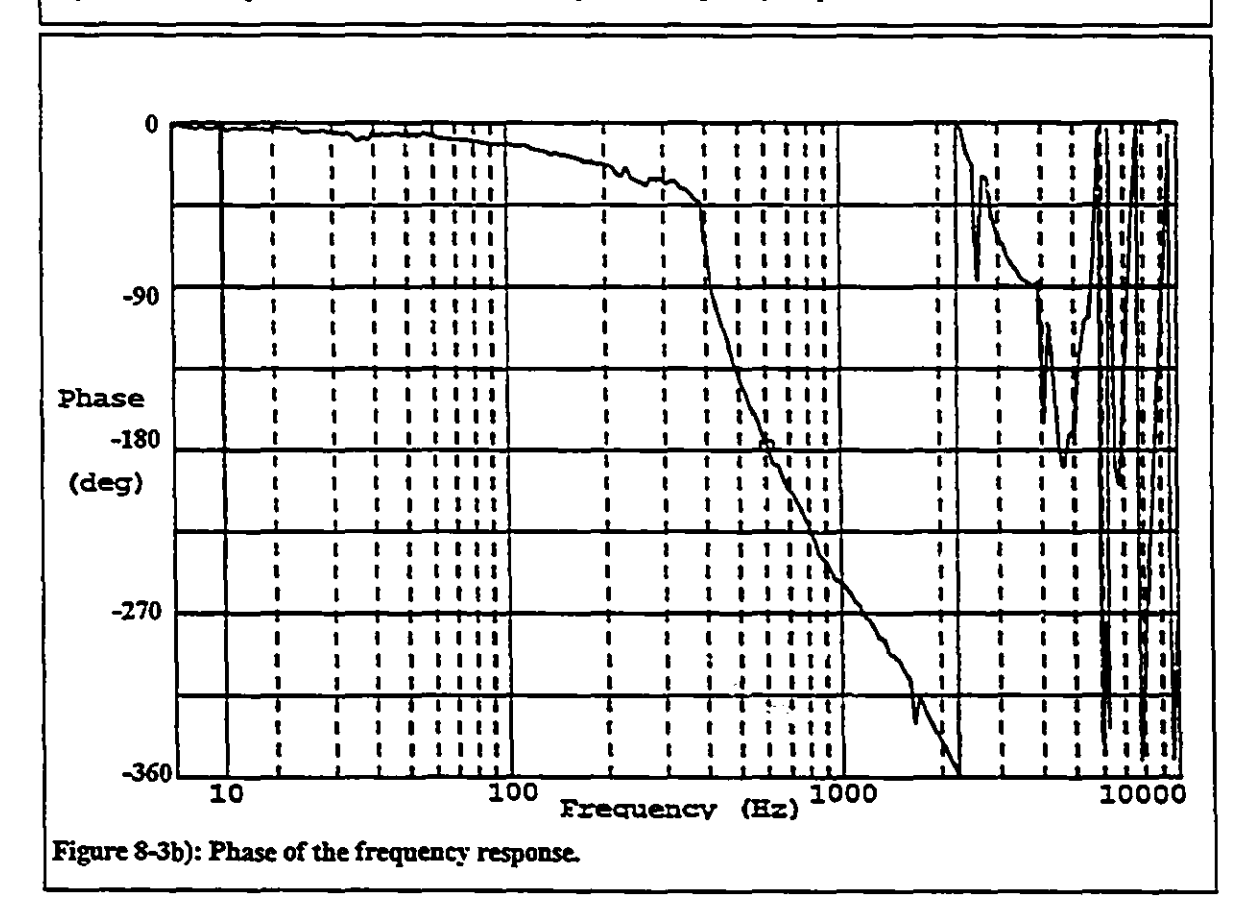


Figure 8-3a): Magnitude of the disturbance rejection frequency response.



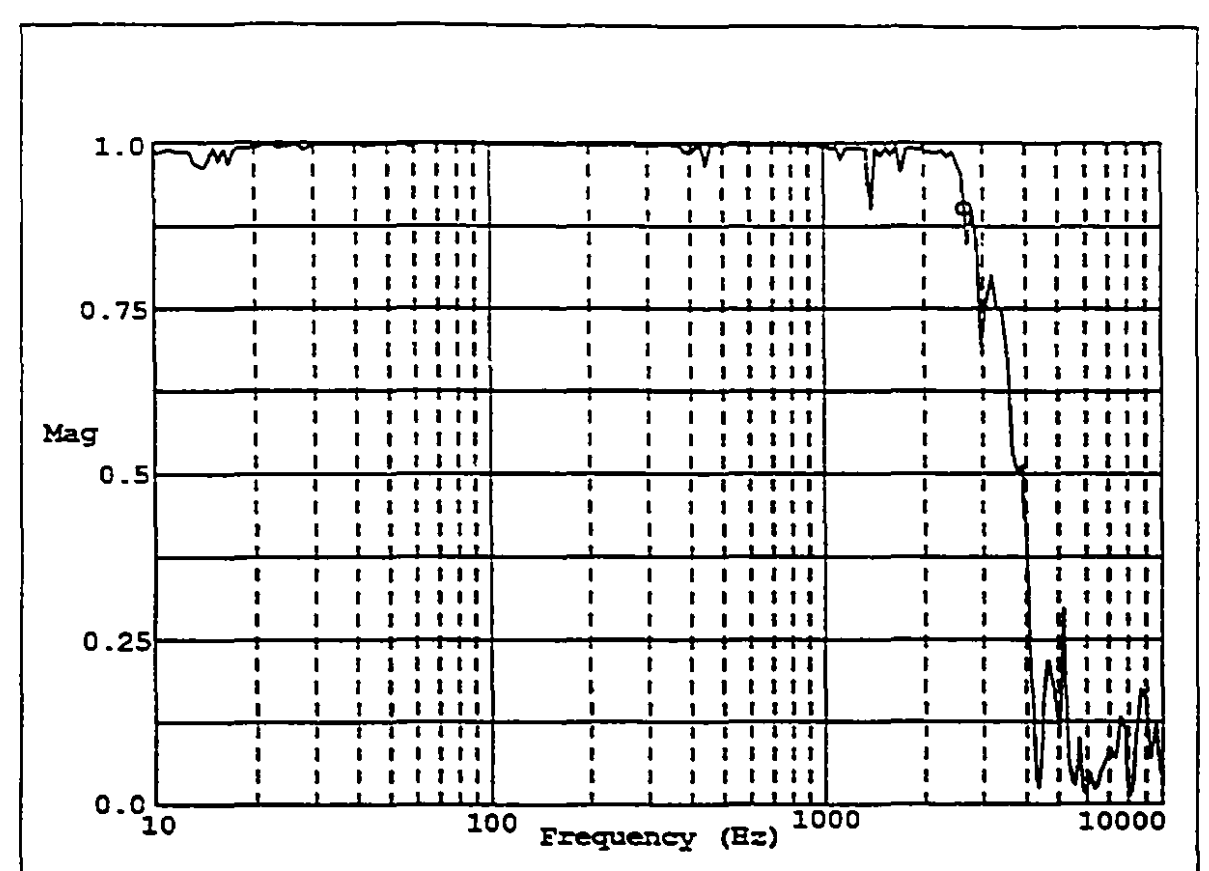


Figure 8-3c): Coherence of the frequency response. The coherence is very close to 1 up to a frequency of 2 kHz. Above 2 kHz, the coherence drops to zero, indicating that the measured frequency response above 2 kHz is very inaccurate.

The cut-off frequency (above which the microscope feedback can no longer compensate for the disturbance) determines the maximum frequency at which the microscope can track surface height changes. From Figure 8-3a), the cut-off frequency is found to be close to 500 Hz.

With the feedback loop closed, the cut-off depends on the proportional and integral gains. The proportional gain was set just below the value at which the system went unstable (the gain P = 0.01). The integral gain was set to 0.001 to reduce the low-frequency tracking error as much as possible while maintaining system stability (I = 0.001 for a feedback frequency of 40 kHz 2).

² The effect of the integral gain in a discrete time system depends both on the magnitude of the gain and on the sampling frequency, as discussed in Chapter 6.

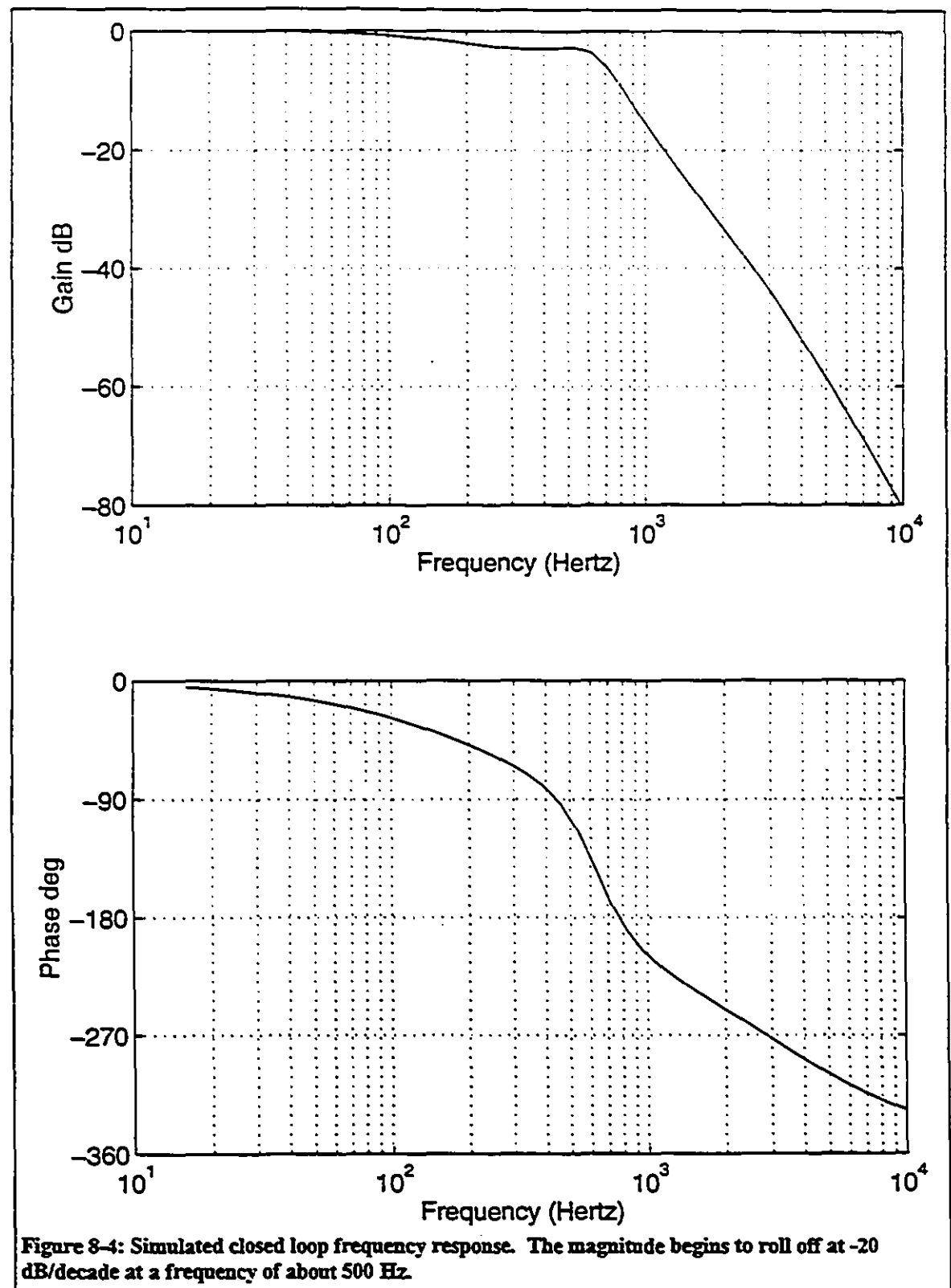
The coherence of the measurement was also measured to show the range over which the frequency response is meaningful (Figure 8-3c). Where the coherence is close to one, the frequency response measurement is accurate but as the coherence drops towards zero, the error in the response measurement increases. The coherence limit of about 2 kHz corresponds to the electronic filtering cut-off frequency.

The bandwidth or cut-off frequency of the constant current mode is limited by the dynamics of the system and the noise level. For STMs, the bandwidth is usually limited by mechanical resonances of the microscope structure itself. Small amounts of noise or motions of the piezo tube near the resonant frequency couple into the mechanical structure and can cause system instabilities.

8.2 Simulation

A model of the STM was created using the MatlabTM programming environment (MathWorks, Inc., Natick, MA) to check that the system was correctly characterized. The Matlab simulation models the mechanical system as a second order low-pass filter with a bandwidth of 650 Hz. The high voltage gain is modeled as a first order low-pass filter (bandwidth of 2000 Hz). The tunneling junction ($I = I_0 e^{-\kappa(z-z_0)}$) logarithm (log I) are lumped into a single (linear) system with a gain of κ Finally, the digital feedback is implemented in the Matlab simulation using an analog approximation (where $P_{analog} = P_{digital} = 0.01$, and $I_{analog} = \frac{I_{digital}}{I} = 0.001*40000$ since $I = I/f_{sample}$ and $I_{sample} = 40$ kHz). The Matlab language program for the model is included in Appendix C.

The closed loop transfer function (with PI control) is shown in Figure 8-4. The magnitude plot begins to roll off sharply above 500 Hz, in agreement with the measured frequency response. The simulated open loop transfer function is shown in Figure 8-5. The open loop transfer function includes the PI controller in the forward path but there is no feedback. With a gain margin of only 10 dB, the proportional gain can be increased only 3 times before the system will be unstable with feedback.



In Figure 8-5, the phase drops from -90 to -270 because of the mechanical resonance poles at 650 Hz. A controller can be designed (e.g. a lead compensator) that would increase the phase near 650 Hz, shifting the -180 degree phase point to the right and increasing the attainable bandwidth. However, even if the feedback system is stable above the mechanical bandwidth, there is no way to distinguish between the sample surface height variations and the mechanical vibrations. The only practical way to improve the bandwidth of the microscope is to increase the mechanical resonance frequency with a more compact design and stiff materials.

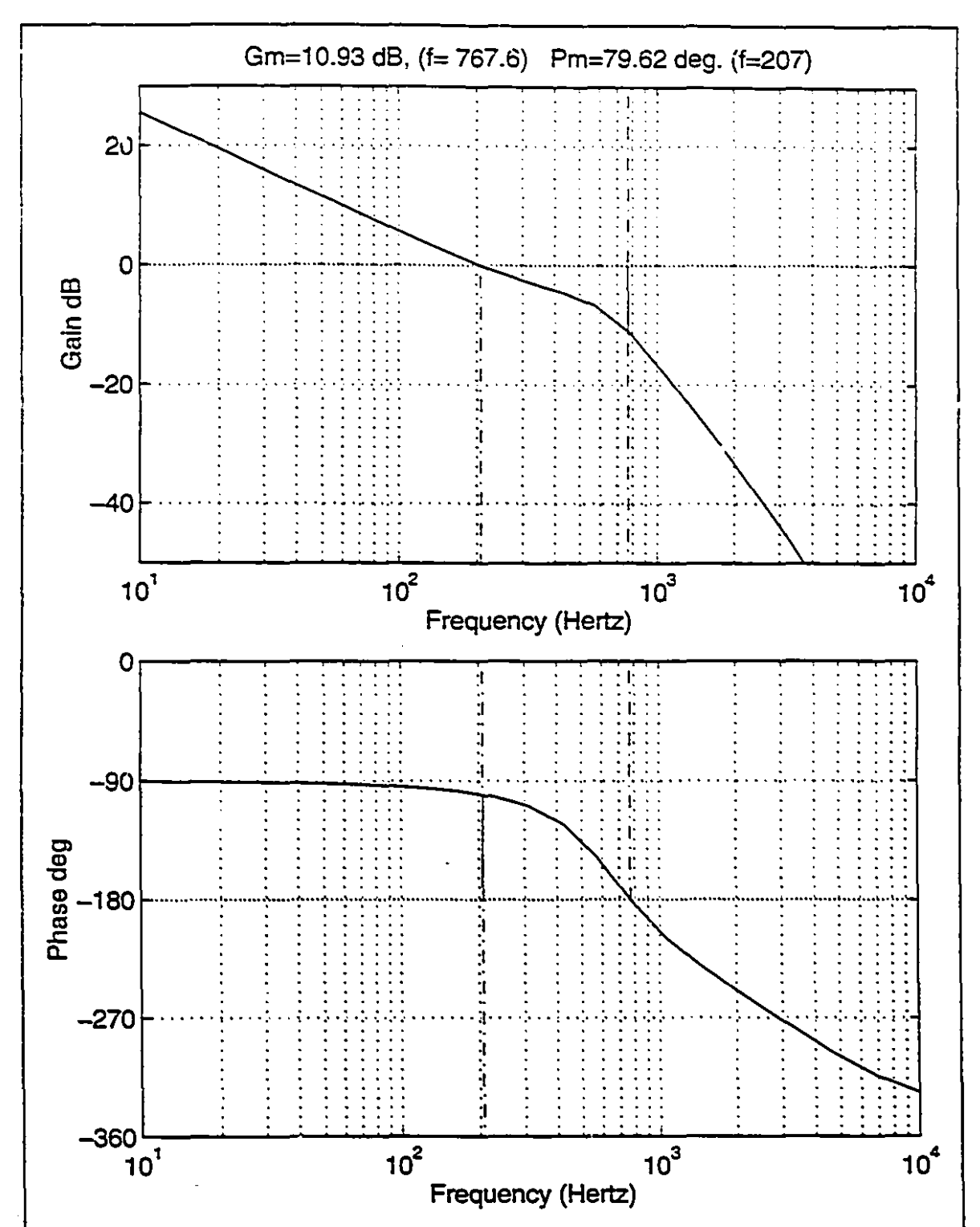


Figure 8-5: Simulated open loop frequency response (with PI controller included). The gain margin of 10 dB confirms that the experimentally determined gains are close to the maximum stable gains possible.

8.3 Scan Rates

In constant current mode, the maximum scan rate is proportional to the feedback cut-off rate and inversely proportional to the highest spatial frequency in the sample:

$$v_{scan} = \frac{f_{cut-o_s^{m}}}{\eta_{max}},$$

(v_{scan} is the scan rate, f_{cu-of} is the cut-off frequency, and η is the maximum spatial frequency). The total scan time is given by:

$$t = N \times \frac{l}{v_{\text{max}}} = N \times \frac{l\eta_{\text{max}}}{f_{\text{out-off}}},$$

where N is the number of lines being scanned, and I is the length of each line. The only way to reduce the constant current imaging scan time for a given sample is to increase the cut-off frequency.

To determine the maximum scan rate that can be used in constant current mode, the spatial frequencies present in the sample need to be known. For example, to get atomic resolution on graphite, which has a spatial frequency of 4 nm⁻¹ (an atomic spacing of 0.25 nm) the maximum scan rate is:

$$v_{scan} = \frac{2kHz}{4nm^{-1}}$$
$$= 500 \, \text{m/s}.$$

If a higher scan rate is used, the current amplitude changes will be attenuated and a phase lag will be introduced that will distort the image.

In constant height mode, where the tip height does not follow the surface contours and the image is constructed from the variations in the measured tunneling current, the limit to imaging speed is the maximum frequency at which variations in current can be measured. This frequency is the smaller of the cut-offs of the current to voltage amplifier cut-off or the low-pass anti-aliasing filter at the input of the analog to digital converters (both are about 2 kHz). For constant height mode, the proportional gain is reduced so that only slow surface variations are followed and the scan rate is increased.

8.4 Microscope Resolution

Microscope resolution determines how small an object can be observed. For the scanning tunneling microscope, two different resolutions exist. The first is the resolution in the plane of the sample (the lateral resolution) which determines the smallest separation between features that can be distinguished. The second is the resolution perpendicular to the sample (in the z direction, parallel to the piezo tube axis) which determines the smallest change in height that can be measured.

Resolution is often experimentally determined by measuring the impulse response or by measuring how far apart two (small) objects must be to be distinguishable. For STM, the smallest objects that can be observed are atoms and they are often used as an indication of good resolution. It is difficult to experimentally measure resolution smaller than the atomic spacing.

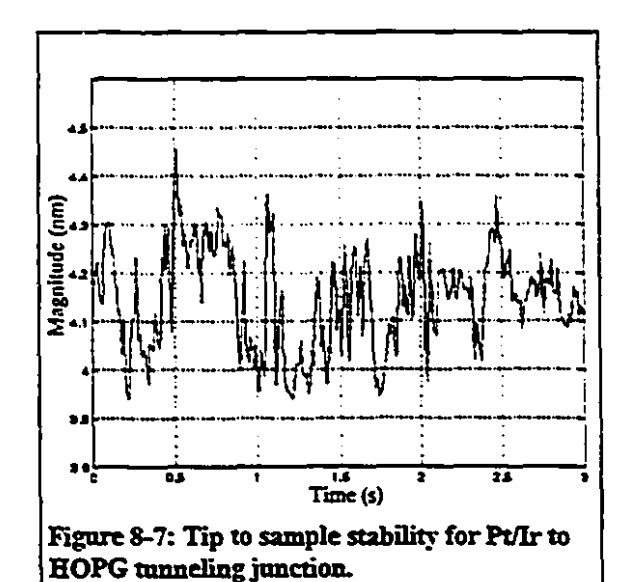
A lower bound for the lateral resolution can be calculated by measuring the noise levels of different parts of the microscope setup and calculating how they affect the position measurement. Such a calculation is more useful for the design stage of a microscope than it is for characterizing the system performance because it is an estimate rather than direct measurement of performance. This estimate is made in Chapter 5 in order to help predict whether or not atomic resolution will be obtained. The lower bound was calculated to be 0.14 nm for a high voltage gain of 15 times and 0.018 nm for a high voltage gain of 2 times. The most important source of noise not included in the calculations for these values is noise from vibrations that affect the tip position relative to the sample. The vibrations will move the tip both perpendicular to and parallel to the sample. The tip will also reduce resolution because it is not perfectly sharp.

Unlike the lateral resolution, the perpendicular (or z direction) resolution can be measured. Keeping the tip in a single position (not scanning) and determining the variation in the height of that point as measured by the microscope gives an accurate indication of the noise in the z direction. The smallest step change in height that can be measured, and hence the resolution, is limited by the noise amplitude.

The perpendicular resolution of the microscope depends a great deal on both the sample and the tip material because of distortion of the sample or tip from interatomic forces. Figure 8-7 shows a typical measured height through time of a point on an HOPG surface using a Pt/Ir tip. The measurement was made in the middle of the day. The standard deviation of the measured height is 0.11 nm. Measurements late at night or in the very early morning tended to have lower standard deviations of 0.03 to 0.05 nanometers. The difference in noise levels between the night and day is due to increased vibrations during working hours and explains why atomic resolution images could not be obtained consistently during the day.

The measured height of a point on a conducting polymer surface imaged during the daytime with a polymer coated Pt/Ir tip (Pt/Ir from Goodfellow, Berwyn, MA) is shown in Figure 8-6 (both polymers are polypyrrole). For the polymer to polymer tunneling junction the position variance is 1.12 nm, about an order of magnitude greater than for HOPG. For the polymer to polymer junction, the increased noise is attributed to the softness of the material.

In conclusion, numbers can be given for the best possible resolution of the microscope. The lateral resolution of the microscope will be no better than 0.011 nm (x direction) and 0.015 nm (y direction) and the perpendicular resolution of the microscope is



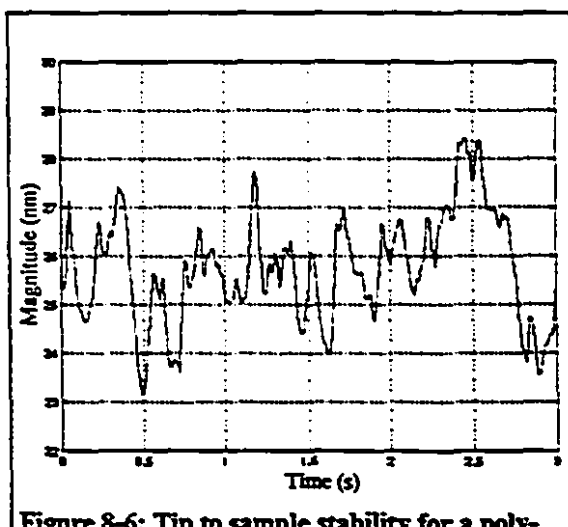


Figure 8-6: Tip to sample stability for a polymer to polymer junction (polypyrrole). Note that vertical scale is different from Figure 8-7.

dependent on the sample but will be above 0.011 nm. The calculation of the lateral microscope resolution ignored variations in the tip to sample distance due to vibrations and sample or tip distortion and so the actual resolution obtained will depend on the laboratory conditions during the measurement.

Chapter 9: Imaging Results

9.1 Current Distance Curve

The key to the extremely high sensitivity of the scanning tunneling microscope is the exponential dependence of the current on the gap width. The tunneling current flowing between the tip and the sample changes by an order of magnitude for a changes in the gap width of only a few tenths of a nanometer.

The current voltage curve was measured for a gold sample and a Pt/Ir tip. As was discussed in Chapter 2, the current-distance relationship should have the form:

$$I_s \propto V_b \rho_s |\psi(0)|^2 e^{-\kappa t}$$

where, $\kappa = \frac{\sqrt{2m\phi}}{\hbar}$, d is the gap width, V_b is the bias voltage, p_s is the electron density of states, and $\psi(0)$ is the electron wavefunction. For a gold to Pt/Ir tunneling gap, V_b , ρ_s , and $\psi(0)$ are constant. $m = 9.11 \times 10^{-31} \, kg$, $\hbar = 6.58 \times 10^{-16} \, eV \cdot s$, and ϕ is given approximately by the average of the work function of gold ($\phi_{Au} \approx 5.4 eV$) and of the Pt/Ir tip ($\phi_{Pt/Ir} \approx 5.7 eV$) giving $\phi = 5.55 eV$. Using these values, we expect the value for κ to be $12.5 \, \mathrm{nm}^{-1}$.

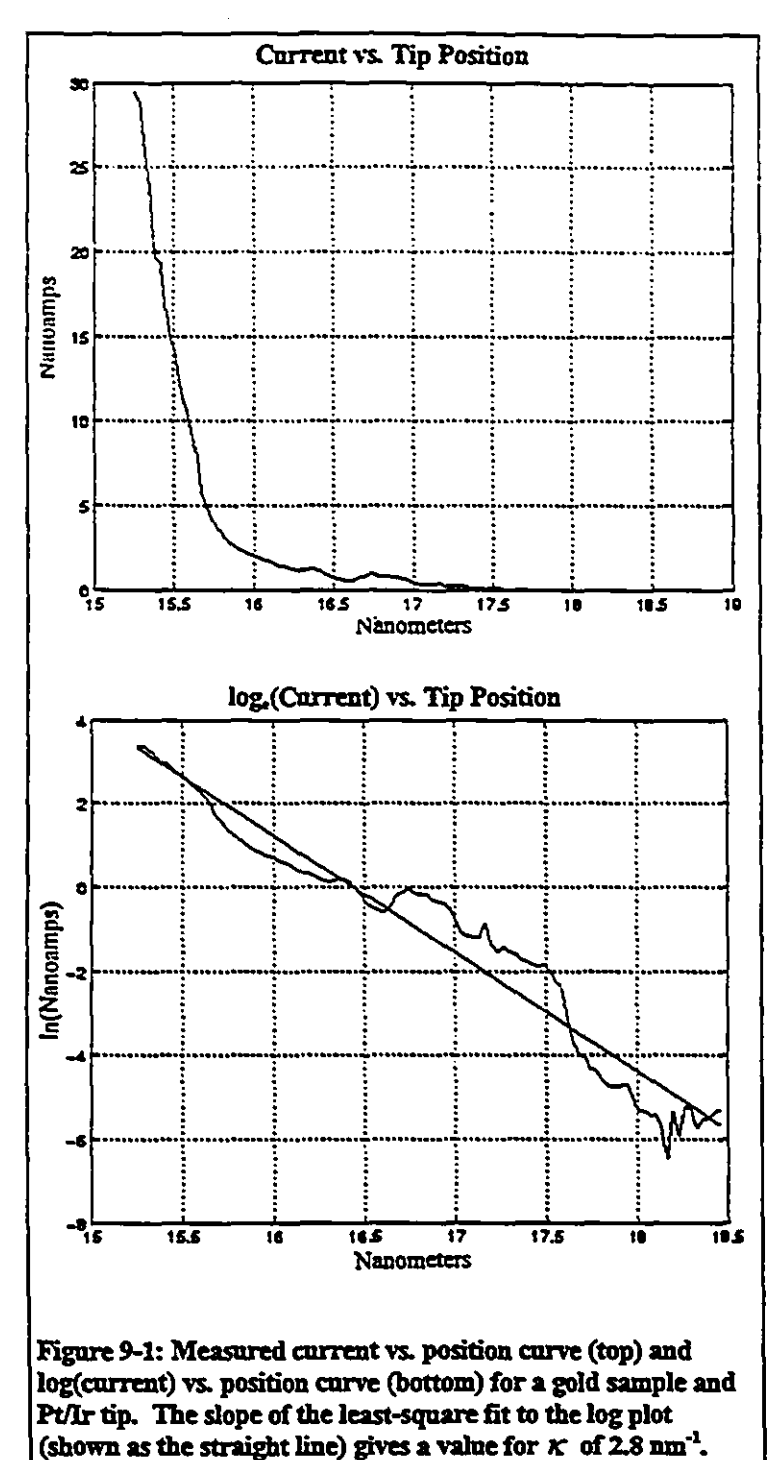
The measured curve is shown in Figure 9-1. The top plot shows the current plotted against the position. The lower plot shows the natural logarithm of the current plotted against the position.

It can be seen from the lower plot that the curve is close to exponential. To find an experimental value for κ , we need to take the logarithm of the current:

$$\log(I_t) = -\kappa d + \text{Constant}$$

and so $-\kappa$ is the slope of the $\log(I_t)$ versus position plot. A linear least squares approximation to the measured curve (Figure 9-1, lower plot) gives $\kappa = 2.8 mn^{-1}$, which is significantly different from the theoretical value of 12.5 nm⁻¹. The error between the line

٠.



fit and the logarithm of the current is most likely caused by noise in the position (typically 0.11 nm RMS as measured in Chapter 8).

The value for the work function calculated using the measured κ is 0.27 eV, much smaller than the expected 5.5 eV. In the original experiments done by Binnig and Rohrer, the value of the work function was also found to be low even in vacuum (Binnig et al. found work functions between 0.6 and 0.7 eV [Binnig et al., 1982]). After repeated cleaning of the sample surface, they measured a work function of 3.5 eV. The much lower than expected value for the work function observed when not in vacuum or when samples have not been properly cleaned is generally surface attributed to

contamination (air borne particulates or thin films of condensed water vapour).

9.2 Holographic Grating

The first images acquired with our scanning tunneling microscope were of a goldplated holographic grating with a spacing of 200 nanometers. One of the images taken is shown in Figure 9-2. Small crystallites of gold that form during the plating process can be clearly seen throughout and have grain sizes that are close to 10 nanometers (typical grain sizes are expected to be around 10 nanometers [Miller, 1994]). The image shown has not been filtered or processed in any way.

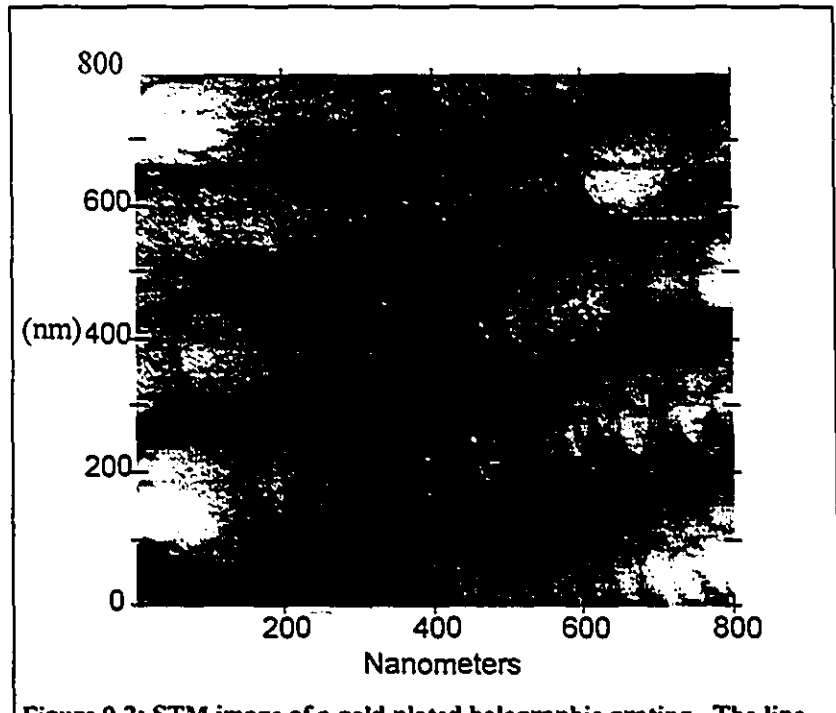


Figure 9-2: STM image of a gold plated holographic grating. The line spacing is 200 nm.

9.3 Graphite

Atomic resolution images of graphite (HOPG or highly oriented pyrolytic graphite) were taken in both constant current and constant height mode. In constant current mode, the scan speed was limited to about 10 nm/s in order to keep the current error low. The best images at constant current tended to be taken late at night when the lab environment was very quiet. Even late at night, images that were acquired often show streaking effects parallel to the raster scan direction. A constant current image of HOPG is shown in Figure 9-3. The image was acquired in 64 seconds. The vertical direction in the image corresponds to the direction along which the tip was scanned.

Figure 9-4 shows two cross-sections taken from Figure 9-3. The upper plot is a cross-section taken in the direction of the tip scan (up and down

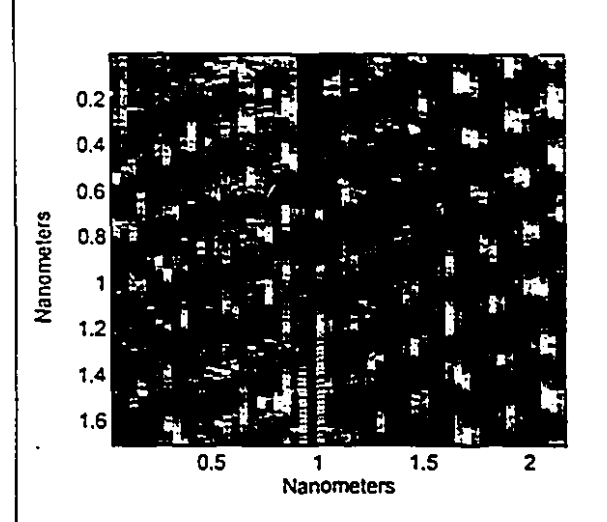


Figure 9-3: Constant current image of HOPG.

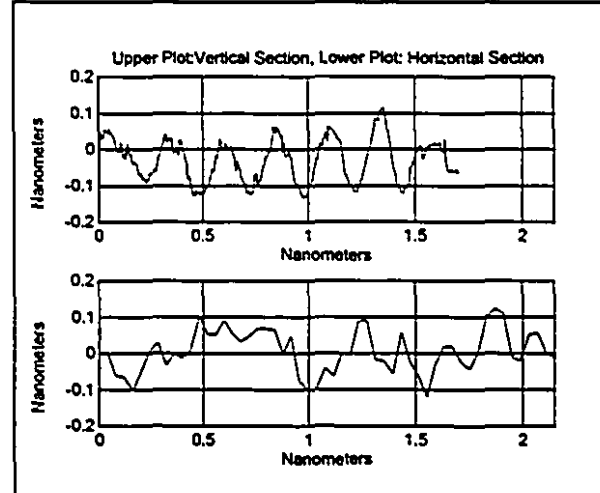
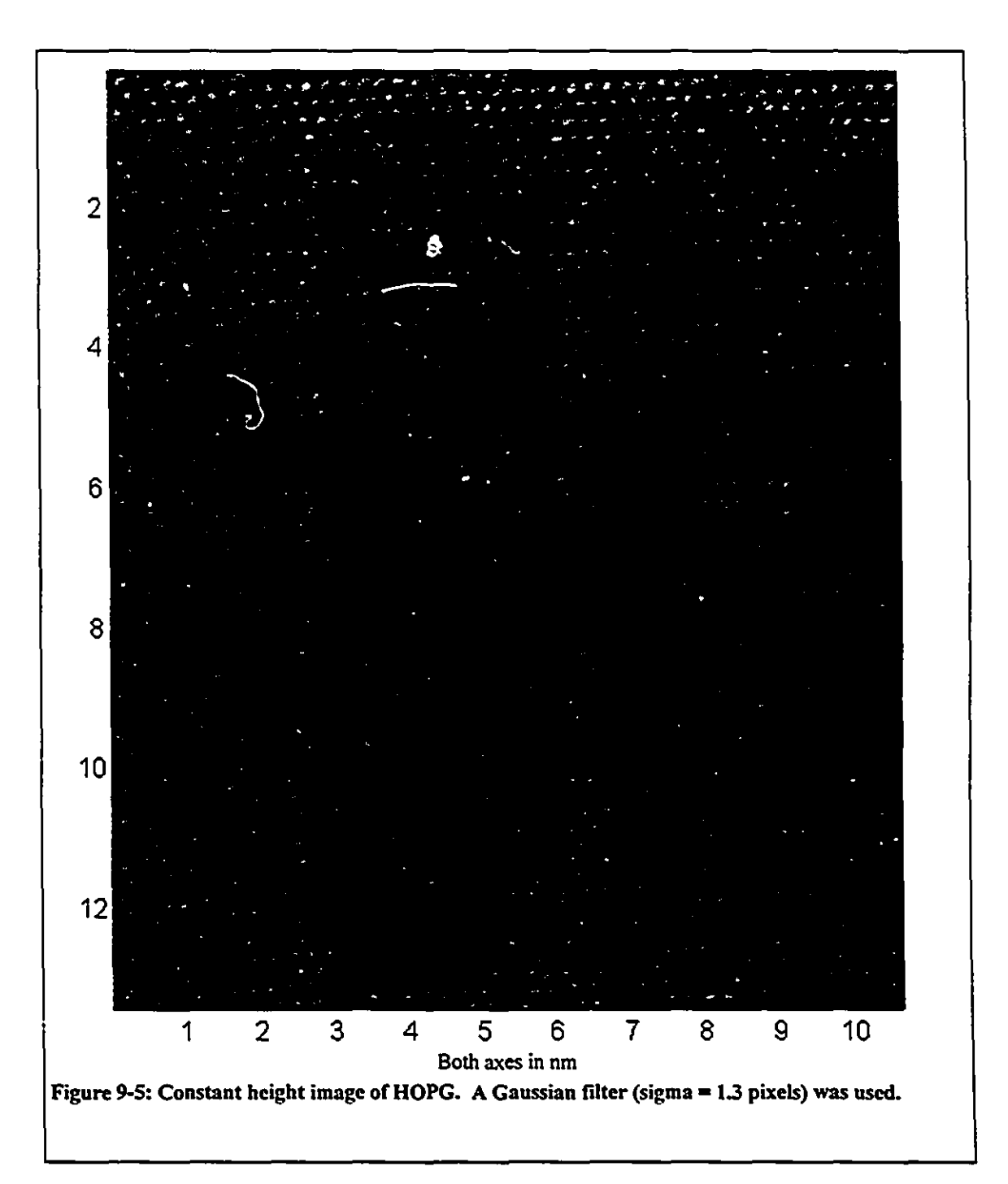


Figure 9-4: Two cross-sections from Figure 9-3. The upper cross-section is taken in the vertical direction parallel to the scan direction. The lower cross-section is taken in the horizontal direction perpendicular to the scan direction.

the page in Figure 9-3). The corrugation amplitude of the HOPG as measured by the STM is between 0.1 and 0.2 nm peak to peak. The lower plot is a cross-section perpendicular to the scan (going across the page in Figure 9-3). The position of peaks in the lower plot is very difficult to determine. Because the upper and lower cross sections were not along taken axes that are symmetric, the periodicity observed in the two plots is different.

Constant height images can be taken at much higher scan rates and are therefore more immune to low frequency vibration noise. Complete constant height images can be acquired in seconds as opposed to the minutes required to take a current image. The scan rate for a constant height image is limited by the 2 kHz bandwidth of the current measurement electronics to about 2000 pixels per second. For HOPG, which has an



atomic spacing of 0.25 nm, sampling at the (spatial) Nyquist rate gives a scan speed of about 250 nm per second. An 11 nm by 13 nm image acquired in 64 seconds is shown in Figure 9-5. Imaging an area the size of Figure 9-3 takes just under 2 seconds.

The constant height image was used to calibrate the horizontal (x and y direction) motions of the piezo tube. The atomic spacing of HOPG is well known and has been measured using x-ray crystallography. An accurate measure of the x and y piezo constants was made by determining the voltage change applied to the piezo tube for a movement across a certain number of carbon atoms. The calculated values for the piezo constants are $K_x = 3.33$ nm/V and $K_y = 4.46$ nm/V. The difference in the x and y piezo constants is probably due to damage to one of the piezo electrodes from soldering during assembly of the STM.

9.4 Polymer Tunneling Junction

If tunneling junctions are going to be miniaturized so that they can be easily integrated into small moving mechanisms such as micro-robots, a simple and effective manufacturing method is required. If the same manufacturing method can be used to build the entire micro-robot as well, then it may be possible to avoid many difficult assembly problems. Conducting polymer technology offers almost every different element that

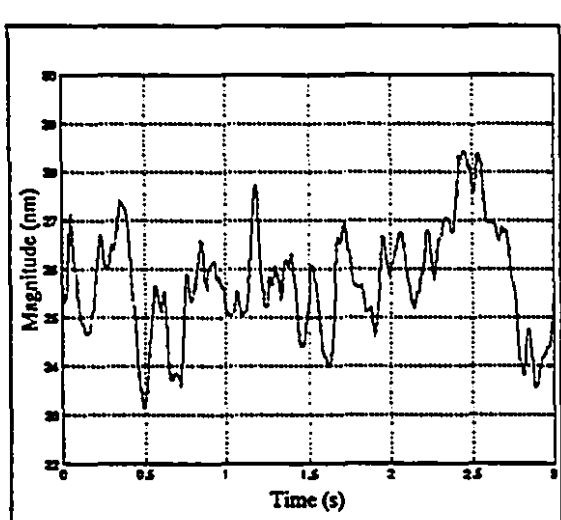


Figure 9-6: Gap width stability measured between a polypyrrole tip and a polypyrrole sample. The junction is stable to within 1.1 nm RMS.

might be required to build an independent micro- or nano-machine.

To test the feasibility of using a polymer to polymer tunneling junction as a sensor, the stability of a polymer tip to polymer sample junction was measured. Because polymers are very soft materials (typical Young's moduli are on the order of 1 GPa, a few hundred times smaller than typical metals) the interatomic forces between the tip and the sample can cause

significant distortion. As the tip moves towards the surface, the polymer sample molecules close to the tip may be either pushed away from the tip or pulled towards the tip. In some cases, a small movement of the tip towards the sample can cause a larger motion of the sample leading to instabilities when imaging [Chen, 1993, Chapter 8]. Thus, the gap stability for soft conducting materials such as polymer is lower than it is for harder conductors.

Results of gap stability measurements at a single point are shown in Figure 9-6 (this result was also shown in chapter 8). A layer (~10 micrometers thick) of polypyrrole was electrochemically deposited onto a tungsten STM tip. The polypyrrole tip was then used to measure gap stability at a single point of a polypyrrole sample (Figure 9-6) which was found to have a noise level (or stability) of 1.1 nm RMS, about an order of magnitude worse than the Pt/Ir to gold tunneling junction.

While the stability of the polypyrrole tunneling junction is not high enough to give atomic resolution images, it should be possible to improve the resolution by increasing the strength of the polymer used in the experiment. Polypyrrole was chosen because it was easily available in the lab but there are many other conducting polymers that can be tried.

Chapter 10: Conclusions and Future Work

10.1 Scanning Tunneling Microscope

The scanning tunneling microscope successfully acquired images with a total field of view from 1 nanometer up to 800 nm. The small scale images easily resolved atomic features on highly oriented pyrolytic graphite (HOPG). The STM operates in an environmental isolation box to shield it from electromagnetic, thermal, and mechanical disturbances and uses an integrated computer controlled coarse approach with a 10 nm step size to accurately position the sample within the range of motion of the tip.

10.2 Future Work

Future work to improve the microscope will proceed along several directions. First, the mechanical structure of the microscope will be redesigned to improve performance. By carefully choosing materials for their thermal properties, namely their coefficient of expansion and their thermal conductivity, it will be possible to design the microscope to have almost zero drift due to temperature changes. Low thermal drift is especially important for large range, high resolution images where imaging time can be an hour or more and the lab temperature can drift by a few degrees Centigrade.

Another aspect of the mechanical redesign will be to increase the resonant frequency of the STM structure. Reduction of the size of the structure while ensuring sufficient rigidity should allow increases in mechanical resonance to frequencies in the 10's or even 100's of kilohertz. Finite element modeling packages will be used to speed the design process by simulating mechanical behaviour before machining and construction. With the high mechanical bandwidth that we expect to achieve, resonance of the piezo tube actuator could become a limit to the microscope performance. In the final design, we may use a smaller piezo tube with a corresponding smaller total range of motion.

With the smaller range of motion, it will desirable to have better control over the coarse positioning of the sample. Ideally, the sample should be able to move along three

axes with close to nanometer resolution and millimeter or more range of motion. The coarse approach mechanism used by the current STM can easily be expanded to two degrees of freedom. Future work on the coarse approach will investigate how to extend movement to three degrees of freedom and integrate it into the microscope design.

The second direction of improvement will be to change the configuration of the computer software and hardware. With the anticipated performance improvements for the next-generation STM, real-time imaging or close to real-time (> 10 images per second) will become possible. The software controlling the microscope will be able to display images as they are acquired and allow real-time user control of the image position on the sample by both piezo tube and coarse approach positioning. Ultimately, the real-time user control will be implemented with a three degree of freedom, force feedback haptic interface so the user can 'feel' surfaces at the atomic scale. In order to accomplish these goals, the performance of the computer hardware will need to be increased. In particular, the D/A and A/D access times need to be reduced if their full 100 kHz bandwicth is to be used. The floating point and graphics performance of the computer will also need to be upgraded for display of images as they are being acquired. Also, higher resolution D/A converters will make possible atomic resolution for large field of view images.

Finally, the third direction for improvement is to get better actuator performance. Both hysteresis and creep cause significant distortions in images and make accurate quantitative measurements of samples very difficult. Improvement of actuator performance can follow one of two approaches. Either the hysteresis and creep need to be modeled or an alternative actuator should be used. Some work on modeling the creep of the piezoelectric material has already been started and it should be possible to correct in software for image distortion. However, a simpler approach is to use an electrostrictive material such as PMN (lead magnesium niobate), which has much lower hsyteresis than the piezoelectrics used for STM actuators.

10.2 Tunneling Sensors

The construction of a polypyrrole polymer to polymer tunneling junction (which I believe to be the first ever) is a small step towards micro- and nano-scale polymer sensors. The junction was stable to within about 1.1 nanometers (RMS).

Further work on the polymer to polymer junction will include trying different conductive polymers, obtaining images using polymer tips, and ultimately building a polymer actuated, polymer to polymer junction.

One of the causes of a polymer junction instability is the high material compliance. Many different conductive polymers have been synthesized and we will investigate using materials other than polypyrrole. While the material compliance is expected to be the dominant factor in determining the junction stability, other factors may also be important. In particular, the mechanism of conduction in polymers is not well understood, especially as it could relate to tunneling from a sharp tip. It may turn out that a polymer with a greater bulk compliance has a chemical structure that yields improved stability of the tunneling gap.

One of the goals of the polymer STM work is to image a polymer substrate with a polymer tip. Initial efforts have been unsuccessful because of the large variations in surface height of the samples imaged, due either to an uneven sample or to deformation from tip to sample forces. As an intermediate step, images of well known, more uniform surfaces, such as HOPG or the gold plated holographic grating shown in Chapter 9 will be acquired using a polymer tip. At the same time, attempts will be made to grow more uniform, smoother polypyrrole surfaces.

Once images of a conducting polymer are obtained, a polymer actuated STM will be built. The STM will use contractile polymers being developed by Professor Hunter's laboratory for position control of the tip. Eventually, even the mechanical structure of the STM, including a coarse approach mechanism, will be constructed from polymer to show that polymer STMs are a viable choice for sensors in micro- and nano-robots.

10.3 Conclusions

The process of building the scanning tunneling microscope and using it to image different materials brought to light many issues that will be very important when working at the nanometer scale.

The extremely high position sensitivity of the tunneling junction highlights the magnitude of the ambient vibrations in a typical laboratory environment. Vibrations on the scale of hundreds of micrometers are common and must either be attenuated by an isolation system or be rejected by the mechanical structure of the microscope. The former implies a relatively bulky mass-spring-damper or equivalent setup with a very low cutoff frequency. The latter necessitates building structures of small size so that the mechanical resonant frequencies are well above the dominant noise frequencies.

The tunneling junction sensitivity to position also highlights the variation of material dimensions with temperature. Temperature variations must either be attenuated or, by clever design, canceled out. Carefully matching temperature expansion coefficients in key parts of the design can reduce thermal expansion effects almost to zero.

Finally, interatomic forces seem to have a significant effect on the junction stability. Particularly for soft materials, interatomic forces are large enough to cause significant deflection. In the measurements of polymer to polymer tunneling, the forces lead to much larger oscillations in the gap width than with measurements using stiffer materials.

In the design and construction of the digitally controlled STM, the engineering obstacles arising from vibrations, thermal expansion, and interatomic forces were successfully overcome. But the performance of the STM can be improved. For future work on nanoscale systems, all of the lessons learned will need to be taken into account in order to achieve higher levels of performance.

Bibliography

- Abraham, D., Mamin, H., Ganz, E., Clarke, J. Surface Modification with the Scanning Tunneling Microscope. *IBM Journal of Research and Development*, 1986, 30, 492-499.
- Adamchuk, V., Ermakov, A., Fedoseenko, S. Scanning tunneling microscope with large scan range. *Ultramicroscopy*, 1992, 42-44, 1602-5.
- Aguilar, M., Pancorbo, M., Vazquez, F., Gomez, F., Anguiano, E., Gonzalez, J., Vazquez, F., Cebollada, F. Study of the surface roughness of Co-based amorphous alloys by STM. *Ultramicroscopy*, 1992, 42-44, 1329-1336.
- Albrecktsen, O., Madsen, L., Mygind, J. A compact scanning tunneling microscope with thermal compensation. *Journal of Physics: E, Scientific Instruments*, 1989, 22, 39-42.
- Baselt, D., Clark, S. Younquist, M., Spence, C., Baldeschwieler, J. Digital signal processor control of scanned probe microscope. *Review of Scientific Instruments*, 1993, 64(7), 1874-82.
- Binnig, G., Rohrer, H., Gerber, Ch., and Weibel, E., Tunneling through a controllable vacuum gap, *Applied Physics Letters*, 1982, 40(2), 178-180.
- Binnig, G., Rohrer, H.. Scanning Tunneling Microscopy. Surface Science, 1983, 126, 236-44.
- Binnig, G., Rohrer H., Gerber, C., Weibel, E.. 7x7 reconstruction on Si(111) resolved in real space. *Physics Review Letters*, 1983a, 50, 120-23.
- Binnig, G., Rohrer, H. Scanning Tunneling Microscopy. IBM Journal of Research and Development, 1986, 30(4), 355-69.
- Binnig, G., Smith, D. Single-tube three-dimensional scanner for scanning tunneling microscopy. *Review of Scientific Instruments*, 1986, 57(8), 1688-89.
- Boland, J.J. Evidence of pairing and its role in the recombinative desorption of hydrogen from the Si(100)-2x1 surface. *Physics Review Letters*, 1991, 67, 1539-42.
- Bocko, M. The scanning tunneling microscope as a high-gain, low-noise displacement sensor. Review of Scientific Instruments, 1990, 61(12), 3763-68.
- Bocko, M., Stephenson, K., Koch, R. Vacuum tunneling probe: a nonreciprocal, reduced-back-action transducer. *Physics Review Letters*, 1988, 61(6), 726-29.

- Brenan, C., Charette, P., Hunter, I. Environmental isolation platform for microrobot system development. Review of Scientific Instruments, 1992, 63(6), 3492-98.
- Carr, R., Thomson, R. Device for high resolution positioning. *Ultramicroscopy*, 1992, 42-44, 1606-9.
- Charette, P. An Integrated Fringe Counting and Interpolation Laser Heterodyne
 Interferometer for Micro-robot Position Measurement. M.Eng. Thesis, Montreal:
 McGill University, 1990.
- Chen, C. Electromechanical deflections of piezoelectric tubes with quartered electrodes. Applied Physics Letters, 1990, 60(1), 132-134.
- Chen, C. <u>Introduction to the Scanning Tunneling Microscope</u>. New York: Oxford University Press, 1993.
- Clark, S.M., Baselt, D., Spence, C., Younquist, M., Baldeschwieler, J. Hardware for digitally controlled scanned probe microscopes. Review of Scientific Instruments, 1992, 63(10), 4296-307.
- Davidsson, P., Olin, H., Persson, M., Pehrson, S. Design and operation of a low-temperature scanning tunneling microscope suitable for operation below 1K. Ultramicroscopy, 1990, 42-44, 1470-75.
- Eigler, D.M., Schweizer, E.K. Atomic and Molecular Manipulation with the Scanning Tunneling Microscope. *Nature*, 1990, 344, 524-6.
- Feynmann, R. There's Plenty of Room at the Bottom. Engineering and Science, 1960, 23(2), 22-36.
- Franklin, G., Powell, J., Emami-Naeini, A. <u>Feedback Control of Dynamic Systems</u>. 2nd ed. New York: Addison-Wesley Publishing Company, 1991.
- Gaisch, R., Gimzewski, J., Reihl, B., Schlittler, R., Tschudy, M., Schneider, W. Low-temperature ultra-high-vacuum scanning tunneling microscope. *Ultramicroscopy*, 1992, 42-44, 1621-1626.
- Garcia, R., Jiang, Y., Schabtach, E., Bustamante, C. Deposition and imaging of metal-coated biomolecules with the STM. *Ultramicroscopy*, 1992, 42-44, 1250-54.
- Gerber, C., Binnig, G., Fuchs, H., Marti, O., Rohrer, H. Scanning tunneling microscope combined with a scanning electron microscope. *Review of Scientific Instruments*, 1986, 57(2), 221-224.
- Grafstrom, S., Kowalski, J., Neumann, R. Design and detailed analysis of a scanning tunnelling microscope. *Measurement Science and Technology*, 1990, I, 139-46.

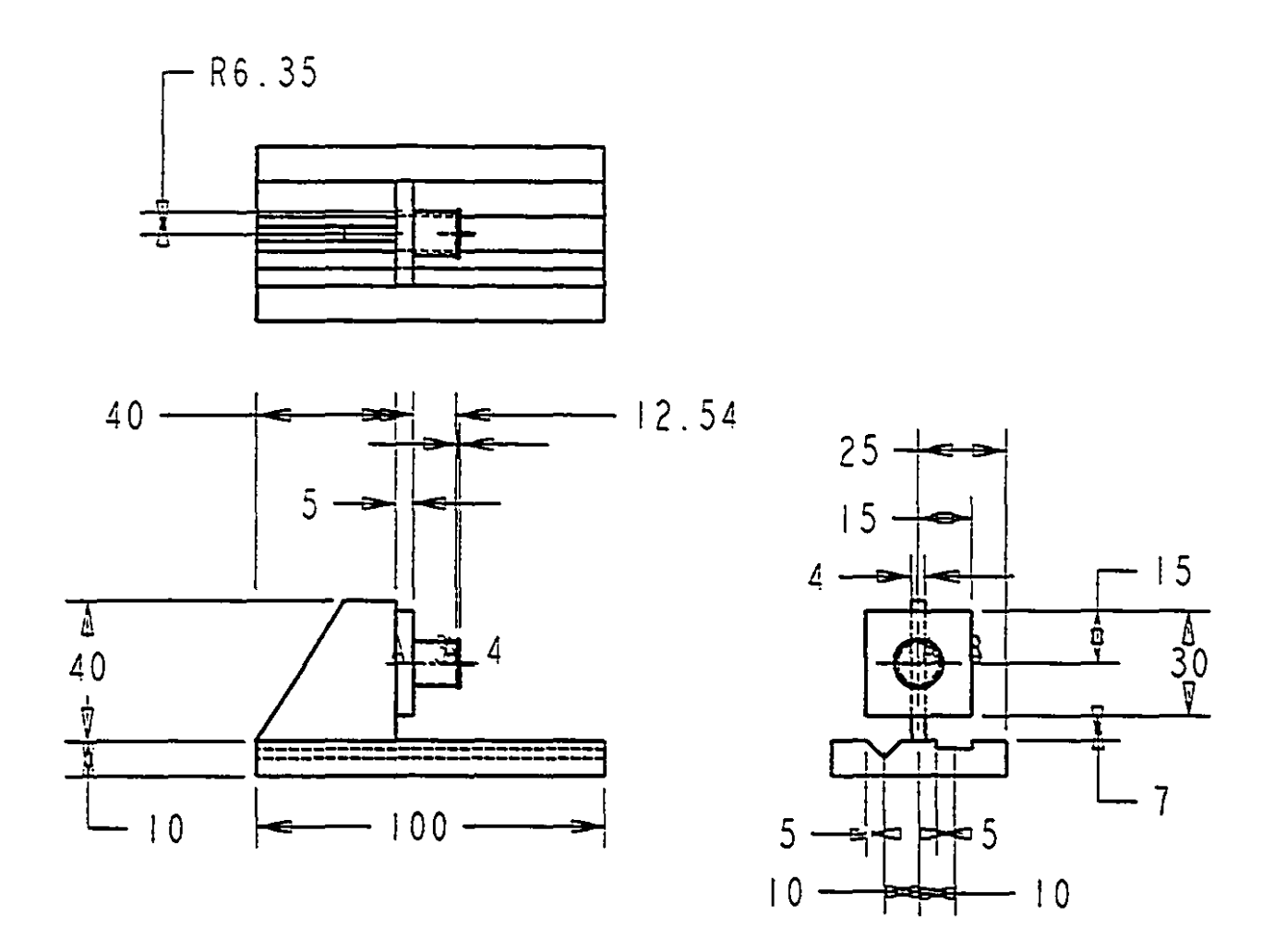
- Handbook of Chemistry and Physics, 73rd edition. London: CRC Press, Inc., 1992-93.
- Horowitz, P., Hill, W. The Art of Electronics. Cambridge: Cambridge University Press, 1980.
- Hues, S., Draper, C., Lee, K., Colton, R. Effect of PZT and PMN actuator hysteresis and creep on nanoindentation measurements using force microscopy. *Review of Scientific Instruments*, 1994, 65(5), 1561-1565.
- Ibe, J., Bey, P., Brandow, S., Brizzolara, R., Burnham, N., DiLella, D., Lee, K., Marrian, C., Colton, R. On the electrochemical etching of tips for scanning tunneling microscopy. *Journal of Vacuum Science and Technology A*, 1990, 8(4), 3570-75.
- Kuk, Y., Silverman, P.J. Scanning tunneling microscopy instrumentation. Review of Scientific Instruments, 1989, 60(2), 165-180.
- Jian, H., Wang, L., Chang, Y., Wang, G. Magnetically controlled coarse approach device for STM. Measurement Science and Technology, 1990, 1, 1116-8.
- Lyding, J.W., Skala, S., Hubacek, J., Brockenbrough, R., Gammie, G. Variable-temperature scanning tunneling microscope. *Review of Scientific Instruments*, 1988, 59(9), 1897-902.
- McCarley, R., Hendricks, S., Bard, A. Controlled Nanofabrication fo highly oriented pyrolytic graphite with the scanning tunneling microscope. *Journal of Physical Chemistry*, 1992, 96, 10089-10092.
- Meepagala, S., Real, F., Reyes, C., Novoselskaya, A. Compact scanning tunneling microscope with easy-to-construct X-Z intertial sample translation. *Journal of Vacuum Science and Technology A*, 1990, 8(4), 3555-7.
- Miller, R., Mizes, H., Samsavar, A. <u>Instructional Scanning Tunneling Microscope (tm)</u>
 Workbook. Fishers, NY: Burleigh Instruments, Inc., 1994.
- Muralt, P. Pohl, D., Denk, W. Wide-range, low-operating-voltage, bimorph STM: Application as a potentiometer. *IBM Journal of Research and Development.*, 1986, 30(5), 443-450.
- Nagahara, L., Thunday, T., Lindsay, S.. Preparation and characterization of STM tips for electrochemical studies. *Review of Scientific Instruments*, 1989, 60(10), 3128-30.
- Niedermann, P., Emch, R., Descouts, P. Simple peizoelectric translation device. *Review of Scientific Instruments*, 1988, 59, 368-69.
- Niksch, M., G. Binnig. Proposal for a novel gravitational-wave sensor. *Journal of Vacuum Science and Technology A*, 1988, 6(2), 470-71.

- Nunes, G., Freeman, M. Picosecond resolution in scanning tunneling microscopy. *Science*, 1993, 262.
- Ohanian, H. Physics. New York: W.W. Norton & Company, 1989.
- Ohtani, H., Wilson, R., Chiang, S., Mate, C. Scanning tunneling microscopy observations of benzene molecules on the Rh(11)-(3x3)(C₆H₆+2CO) surface. *Physics Review Letters*, 1988, 60 (23), 2398-2401.
- Okano, M., Kajimura, K., Wakiyama, S., Sakai, F., Mizutani, W., Ono, M. Vibrations isolation for scanning tunneling microscopy. *Journal of Vacuum Science and Technology A*, 1987, 5(6), 3313-20.
- Oppenheim, A., Schafer, R. <u>Discrete-time signal processing</u>. Englewoods Cliffs, NJ: Prentice Hall 1989.
- Park, S., Quate, C. Theories of the feedback and vibration isolation systems for the scanning tunneling microscope. *Review of Scientific Instruments*, 1987, 58(11), 2004-2009.
- Piner, R., Reifenberger, R. Computer control of the tunnel barrier width for the scanning tunneling microscope. Review of Scientific Instruments, 1989, 60(10), 3123-7.
- Pohl, D.W. Some design criteria in scanning tunneling microscopy. *IBM Journal of Research and Development.*, 1986, 3(4), 417-427.
- Pohl, D.W. Sawtooth nanometer slider: a versatile low voltage piezoelectric translation device. Surface Science, 1987, 181, 174-5.
- Pohl, D.W. Dynamic piezoelectric translation devices. Review of Scientific Instruments, 1987a, 58(1), 54-7.
- Renaud, P., and Alvarado, S. Nanometer scale resolution luminescence imaging of quantum wire structures with a scanning tunneling microscope, short abstract. *IEEE Trans. on Electron Dev.*, 1992, 39(11).
- Robinson, R., Widrig, C. Differential Conductance Tunneling Spectroscopy in Electrolytic Solution. *Langmuir*, 1992, 2311-2316.
- Schmid, M., Varga, P. Analysis of vibration-isolating systems for scanning tunneling microscopes. *Ultramicroscopy*, 1992, 42-44, 1610-15.
- Smith, D., Horber, H., Gerber, C., Binnig, G. Smectic Liquid Crystal Monolayers on Graphite Observed by Scanning Tunneling Microscopy. *Science*, 1989, 245, 43-45.

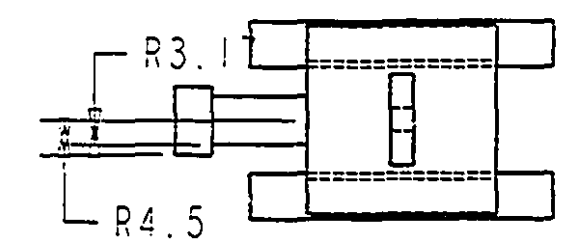
- Snow, E., Campbell, P.M. AFM Fabrication of Sub-10-Nanometer Metal-Oxide Devices with inSitu Control of Electrical Properties. *Science*, 1995, 270, 1639-1641.
- Stavely Sensors. EBL Piezoceramic Tubes for Ultraprecise Positioning Applications. (sales brochure), 91 Prestige Park Circle, East Hartford, CT, 1994.
- Steer, W., Hoffmann-Millack, B., Roberts, C. A versatile scanning tunneling microscope for use in air. *Measurement Science and Technology*, 1990, 1, 881-6.
- Stoll, E.. Correction of geometrical distortions in scanning tunneling and atomic force microscopes caused by piezo hysteresis and nonlinear feedback. *Review of Scientific Instruments*, 1994, 65 (9), 2864-9.
- Strozewski, K., McBride, S., Wetsel, G. High-frequency surface-displacement detection using an STM as a mixer-demodulator. *Ultramicroscopy*, 1992, 42-44, p. 388-92.
- Uchino, K. Photostrictive Actuator. 1990 Ultrasonics Symposium, IEEE, 1990, 721-723.
- Uehara, Y., Kimura, Y., Ushioda, S., Takeuchi, K. Theory of visible light emmision from scanning tunneling microscope. *Japanese Journal of Applied Physics*, 1992, 31(8), 2465-2469.
- Ushioda, S. STM light emission spectroscopy of Si surfaces. Solid State Communications, 1992, 84, 173-76.
- van Kempen, H., van de Walle, G.. Applications of a high-stability scanning tunneling microscope. *IBM Journal of Research and Development*, 1986, 30(5), 509-514.
- Vieira, S. The behaviour and calibration of some piezoelectric ceramics used in the STM. IBM Journal of Research and Development, 1986, 30(5), 553-556.
- Walls, M., Chaudri, M., Tang, T. STM profilometery of low-load Vickers indentations in a silicon crystal. *Journal of Physics D: Applied Physics*, 1992, 25, 500-507.

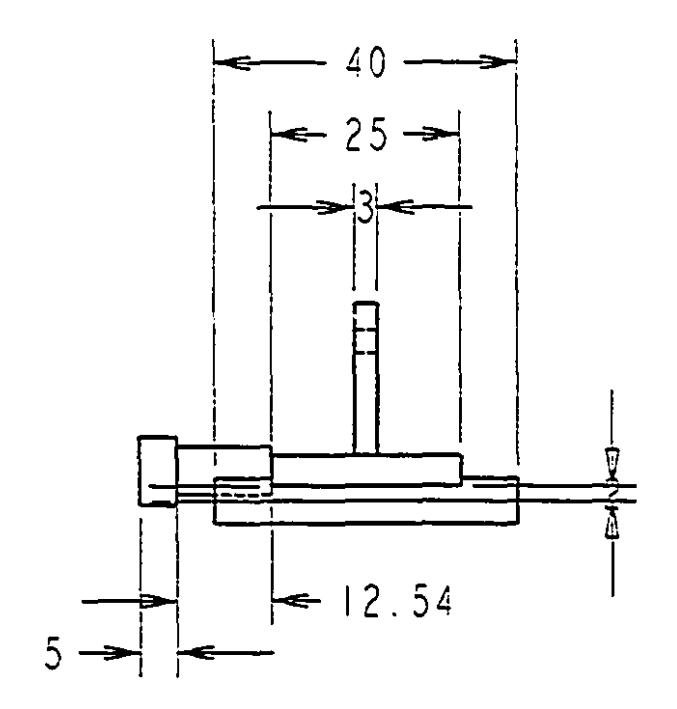
Appendix A: Construction Drawings for STM.

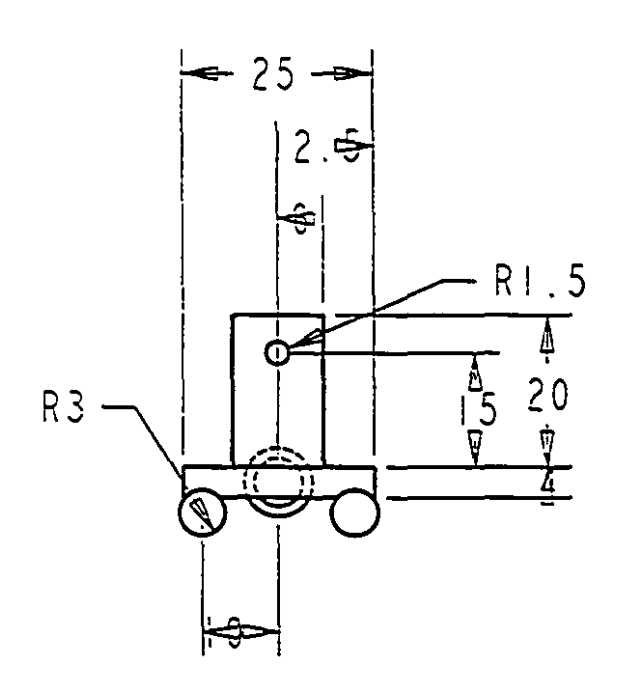
STM BASE (dimensions in millimeters)



STM NANOSLED (dimensions in millimeters)







Appendix B: C Code for Computer Control

Program Listings	page
stm3.c	122
fback2.c	126
nanosled.h	134
nanosled.c	135
table.c	138

stm3.c

```
..
          stmcontrol.c
..
                                            Peter Madden.
..
           April 10th, 1995
..
..
    Modified:
..
          May 11th, Peter Madden. Removed D term in feedback
                      to increase feedback rate. Also changed outputs so
..
••
                      that signals for X,Y, and Z are output and they
                      are then added using analog circuitry (instead of
..
**
                      digital addition followed by four (one for each channel)
..
                      DA outputs which was too slow.
.
      May 16th, P.M. Changed (b() a little bit to make it more general.
.
..
..
** Uses nanosledic and (back c to control the STM.
** nanosled routines are used for coarse approach in combination with]
** fbRamp from fback.c. (fbRamp moves the tip towards the sample until
** the selpoint current is reached or until the the max extension of the
** piezo is reached).
** Once the coarse approach nano-stepper has positioned the sample
** within the piezo tube range of motion, data is taken using the
** (b() routine.
** The PID constants are set by calling the fbSetupFB (also used to set
** the current setpoint and the sampling frequency used for the feedback
** foop).
** Scan parameters (number of x and y points, x and y size (in nanometers),
** scan rate, and pointer to the image array) are set using the fbSetupScan()
** subroutine.
..
•• VXI functions are from vxifcn.c (these are used to initialise the
** VXI, to close the VXI, and to write and read values).
** Finally, the interrupts can be turned off using interrupts_off()
** and restored with interrupts_on(). These come from the vxilib a file
** which must be included (use a make file to do this).
```

```
/* Rough outline:
1) Get P,I,D parameters, current setpoint, and feedback sampling rate.
2) Get scan parameters: number of x and y points, size of the scan,
           the scan rate (in pixels per second).
3) Call fbSetupFB and fbSetupScan to initialise these values.
4) Initialise the VXI.
5) Loop through until sample is within the range of the piezo tube:
           i) Ramp the piezo tube.
           ii) If not within range, jump the stepper toward the tip.
           (ii) repeat i)
6) Once peizo is within range, call the fb() routine. The first few
           seconds (on April 10, 30s stabilisation time) are used to
           settle the feedback loop, giving the integral term a chance
           to move towards the surface from the starting point which is well
           back. Then the image is recorded.
7) The tip is withdrawn.
8) The coarse positioner is stepper away at least a micron.
9) The tip position is returned to zero zero zero (x, y, z).
10) The VXI bus is close and the program ends.
*/
#include "/u/peterny/vxi/peter/vxifcn2.c"
#include "/u/peterm/vxl/peter/FBack/fback.c"
#include "/u/peterm/vxi/peter/NanoSted/nanosted.c"
#include "/u/peterm/vxi/peter/Matlab/matlabfcn.c"
#include <stdio.h>
/* O if interrupts are not turned off */
#define INTERRUPTS_OFF
void getfbparam();
void getscanparam(int *xpix, int *ypix.
                        float *xsize, float *ysize,
                        int *ReturnType);
void main() ( /* main routine */
```

•/

```
double stepsize, pulsetime; /* for Nanosled motion */
double t0, if; /* for timing purposes */
float *Pulse, *Image;
int xpix, ypix;
float xsize, ysize;
double dimage;
int ReturnType;
float apprate, temp;
int i.j;
short int Channel Gain[64];
float Vz, Vbias;
int Status;
MATFile *fmat;
           filename(50), string(10);
get(bparam();
getscanparam(&xpix, &ypix, &xsize, &ysize, &ReturnType);
printf("InPlease enter the tunneling bias voltage:");
scanf("%f", &Vbias);
printf("\n");
                           ************
l^{*} for (i = 0; i < 64; i++)
 ChannelGain[i] = 4:
/* +- 16V range for AD conversion. */
set_gains(ChannelGain);
initialise_vxi();
fbMoveAway();
printf("\nPlease enter the Nanosled step size (V):");
scanf("%f", &temp);
stepsize = (double)temp;
printf("InPlease enter the Nanosled pulse time (s):");
scanf("%f", &temp);
pulsetime = (double)temp;
```

```
printf("InPlease enter file name for stored vars;");
scanf("%s", filename);
nanosetchannel(100000.0,7); /* Channel for nanostepper signal. */
Pulse = nanomoveinit(stepsize, pulsetime, PLUSDIR);
printf("stepsize: %f pulsetime %f\n", stepsize, pulsetime);
printf("Please enter tunneling tip approach rate (V/s);");
scanf("%f", &apprate);
fbBiasOn(Vbias); /* turn on tunneling */
fbGotoXYstart(&Status); /* goto initial x,y voltages. */
if (Status != 0) (
 printf("Error in setting up: Vx or Vy is too large.\n");
 printf("Continuing anyway.");
i = 0:
Vz = fhRamp(apprate/50.0);
fbMovcAway();
print(("\nFirst approach, Vz = \%(\n^*, Vz);
printf("InPiezo voltage (at start of tunneling) is:\n");
Approach:
while (Vz == -10000.0) {
If (INTERRUPTS_OFF)
 interrupts_off();
nanomove();
i += 1;
t0 = second();
while (t0+0.075 > second()); /* wait 75 ms */
Vz = fbRamp(apprate);
fbMoveAway();
```

```
nanomove();
if (INTERRUPTS_OFF)
 interrupts_on();
fbZero(); /* set piezo voltages to zero */
fbBiasOff();
close_vxi();
printf("InSTM control program quitting.\n");
yold getscanparam(int *xpix, int *ypix,
                       float *xsize, float *ysize,
                       Int *ReturnType) {
/* Initialise (bSetupScan() */
int notok:
float scanrate;
int ScanType;
notok = 1;
while (notok) (
printf("Please enter the number of x pixels:");
scanf("%d", xpix);
printf("Please enter the number of y pixels:");
scanf("%d", ypix);
printf("Please enter the x size (nm):");
scanf("%f", xsize);
printf("Please enter the y size (nm):");
scanf("%f", ysize);
printf("Please enter the scan rate (pixels / second):");
scanf("%f", &scanrate);
printf("Please enter 0 for single point or 1 for averaging data:");
scanf("%d", &ScanType);
orint(("Please enter 0 for Pos, I for Error, or 2 for both saved:");
scanf("%d", ReturnType);
notok = fbSetupScan(*xpix, *ypix,
                         *xsize, *ysize,
                         ScanType, *ReturnType,
                         scanrate);
```

```
if (notok != 0)
  printf("Peror in Input values (getscanparam=%d)", notok);
 ); /* repeats if fbSetupScan does not return 0 */
void getfbparam() {
/* Initialise (bSetupi 73 */
float p.i.d. setpoint, samplefreq, settletime;
int notok;
notok = 1:
while (notok) {
 printf("Please enter P:");
 scanf("%f", &p);
 printf("Please enter I:");
 scanf("%f", &i);
 printf("Please enter D;");
 scanf("%f", &d);
 printf("Please enter the current set point:");
 scanf("%!", &setpoint);
 printf("Please enter the fb foop sample freq:");
 scanf("%f", &samplefreq);
 printf("Please enter the fb settle time (in seconds);");
 scanf("%f", & settletime);
 notok = fbSetupFB(p,i,d, setpoint, samplefreq, settletime);
 1: /* repeats until fbSetupFB returns 0 */
```

```
if (Vz != -10000.0) ( /* Confirm that sample is in range */
   Vz = fbRar.ip(apprate/20.0);
   fbMoveAway();
  if (INTERRUPTS_OFF)
   interrupts_on();
t0 = second();
while (10+0.1 > second()); /* wait 0.1 s */
Vz = fbRamp(apprate/20.0);
fbMoveAway();
printf(" Slow approach: %f\n", Vz);
if(Vz == \cdot 100000.0)
 goto Approach;
if (Vz < -3.0)
 Vz = -10000.0; /* Try for center of peizo range (less hysteresis) */
 goto Approach;
/* Now in good position: */
printf("\n\n"):
fbMoveAway(); /* move away and then start feedback: */
printf("\n%d steps to engage. Starting feedback!\n", i);
10 = second();
while ((0+0.100 > second()); /* pause to let stuff print on screen */
if (INTERRUPTS_OFF)
 interrupts_off();
(0 = second(); /* start timing */
Image = fb(&Status);
tf = second(): /* stop timing */
if (INTERRUPTS_OFF)
 interrupts_on();
if (Status != 0) [
 printf("\nERROR in fb(): %d\n", Status);
```

125

```
}
printf("\nAverage time per pixel: %.10e\n", (if-10)/(double)(xpix*ypix));
/* Need to convert Image to double to store for mailab: */
/* if ReturnType == RETBOTH, then matrix is twice as big!! */
dlmage =(double *)malloc(xpix*ypix*sizeof(double)*((ReturnType==RETBOTH)72:1));
for (i = 0; i < ((ReturnType==RBTBOTH)?2:1)*xpix*ypix; i++)
 dimage[i] = (double)image[i];
fmat = writeopen(filename);
temp = (double)xpix;
matrixwrite(fmat, "xpix",&temp, 1, 1);
temp = (double)ypix;
matrixwrite(fmat, "ypix", &temp, 1, 1);
temp = (double)xsize;
matrixwrite(fmal, "xsize", &temp, 1, 1);
temp = (double)ysize;
matrixwrite(fmat, "ysize", &temp, 1, 1);
matrixwrite(frnat, "Image", dlmage, ((ReturnType==RBTBOTII)?2:1)*xpix*ypix, 1);
matlabelose(fmat);
free(dlmage);
free(Image);
#if defined(DOTHIS)
printf("Enter number of seconds to wait:");
scanf("%f", &xsize); /* xsize not used anymore!!!! */
(0 = second();
printl("InWaiting %f seconds...\n", xsize);
10 += (double)xsize;
while (t0 > second());
#endil
fbMovcAway();
/* Back away 100 steps at maximum to make get way out of piezo range */
Pulse = nanomoveinit(stepsize, pulsetime, MINUSDIR);
If (INTERRUPTS_OFF)
interrupts_off();
for (i = 0; i < 100; i ++)
```

fback2.c

```
..
          fback2.c
..
          Peter Madden, April 7th, 1995
..
..
          Modified May 5th, 1995.
** fback.e contains routines to set up and run the STM.
** This includes both setting up the scan rate, resolution, etc. and
** setting the constants for the PID feedback loop.
*/
/* #define DEBUGFB */
/* Some includes: */
#include "/u/peterm/vxl/peter/vxifcn2.h"
#include <math.h>
#include "/u/peterm/vxi/peter/second.c" /* for realtime msmt's of time */
#include "/u/peterm/vxi/peter/Table/table.c" /* piecewise approx. to log(x) */
/* Some definitions: */
/* Constants for output */
#Jefine MAXVOLTAGE
                               120.0
#define OUTGAIN
                               15.0
/* next value is abs(MAXVOLTAGE/OUTGAIN) */
#define MAXVOLTDA
                               8.0
/* for scan setup */
                               1000
#define MAXXPTS
#define MAXYPTS 1000
/* Next value is in units of pixels/s (type int) */
#define MAXSCANRATE 100000.0
/* next two values are in units of nm (type float) */
/* MAXXSIZB is MAXVOLTAGE * 2 * DperVx == 1008 -> 1000nm */
/* MAXYSIZB is MAXVOLTAGE * 2 * DperVy == 1008 -> 1000nm */
/* NOTE: this is half the total scan range!!
#define MAXXSIZE 1000.0
```

```
#define MAXYSIZE 1000.0
/* next value in Hz */
#define MAXFBFREQ 100000.0
/* Piezo Tube constants. */
/* These are in nn/V */
#define DperVz 5.0
#define DperVx
#define DperVy 4.2
/* TASCO Channel Definitions */
#define XDAC
#define YDAC
#define ZDAC
                   2
#define VBIAS
                   4
/* for fb() ReturnType */
#define RETPOS 0
Mdefine RETERR 1
#define RBTBOTH 2
/* for fb() Sample Method */
#define SINGLE 0
#define AVERAGEPTS 1
/* Some structures that are used (GLOBAL VARIABLES) */
struct
          aScan
                   int
                             xpoints, ypoints; /* pixels */
                             xsize, ysize; /* nanometers */
                   float
                   int ScanType;
                                     /* SINGLE or AVERAGEPTS */
                   int ReturnType; /* RETPOS, RETERR, or RETBOTH */
                    float
                                                  /* pixels / second */
                             rate;
                             *Image;
                                                  /* pointer to image array */
                   float
                    Scan;
struct
          al Ti
                   float
                             P. I. D:
                   float
                             setpoint; /* nanoamps */
                             samplefreq; /* Hz */
                   float
                    float settletime; /*time of fb settle before data taken*/
              } FB;
```

```
int fbSetupScan(int xpts,
                       int ypts,
                       float xsize.
                       float ysize.
                       int ScanType,
                       int ReturnType.
                       float scanrate);
int fbSetupFB(float P, float I, float D,
               float setpoint.
               float freq.
               (loat settletime);
float fbRamp(float rate);
yold (bBiasOn(float bias);
                                 /* Turns on tunneling bias voltage (ch 4) */
yold fbBiasOff();
void fbZero();
void fbMoveAway();
void fbGoto(float Vx, float Vy, float Vz);
/* float *fb(int *Stat): */
int fbSetupScan(int xpts,
                      int ypts,
                      float xsize.
                      float ysize.
                      int ScanType,
                      int Return Type,
                      float scanrate)[
/* Initialises the Scan structure.
** Return values:
                   -1
                                 xpis not valid.
                                 -2
                                            ypts not valid.
••
                                            asize not valid.
                                 -3
                                 -4
                                           ysize not valid
..
                                 -5
                                            scanrate not valid
**
                                            memory for image storage not allocated
..
                     ScanType not valid
..
                    ReturnType not valid
** ScanType determines whether data stored is from a single point or is
** an average along the path followed by the tip. Either SINGLB or
```

```
•• ReturnType decides whether the fb routine returns the position information,
** the error information (error between desired setpoint and actual tunneling
** current, or both. (RETPOS, RETERR, or RETBOTH.
int returnval:
returnyai = 0:
if ((xpts >= 0) && (xpts <= MAXXPTS))
 Scan.xpoints = xpts;
else / Not a valid value for xpts */
 returnyal = -1;
if ((ypts >= 0) && (ypts <= MAXYPTS))
 Scan.ypoints = ypts;
else /* not a valid value for ypts */
 rcturnval = -2;
if ((xsize >= 0.0) && (xsize <= MAXXSIZE))
 Scan xsize = xsize;
else /* not a valid value for xsize */
 returnval = -3:
if ((ysize >= 0.0) && (ysize <= MAXYSIZE))
 Scan vsize = vsize:
else / not a valid value for vsize */
 returnval = -4:
if ((scanrate >= 0.0) && (scanrate <= MAXSCANRATE))
 Scan rate = scantate:
else /* not a valid value for xsize */
 returnval = -5:
if ((ScanType == SINGLE) # (ScanType ==: AVERAGEI*FS))
 Scan ScanType = ScanType;
clsc [
 Scan.ScanType = SINGLE; /* default is SINGLE */
 returnval = -7;
If (((ReturnType==RETPOS) # (ReturnType==RETERR)) # (ReturnType==RETBOTH))
 Scan ReturnType = ReturnType;
clsc f
 Scan.ReturnType = RETPOS;
```

** AVERAGEPTS.

```
do (
 Vz += Vzinc;
 writeda(ZDAC, Vz);
 readad0(&advalue);
 if (advalue >= 0.0)
  advalue = -0.00001; /* avoids taking the log of neg number */
 t += delt:
 while (t > second());
 ) while ((2*log(-advalue) < (FB.setpoint)) && (-Vz < abs(MAXVOLTAGE/OUTGAIN) -
 5*abs(Vzinc)) );
 if ((-Vz) > abs(MAXVOLTAGE/OUTGAIN) - 5*abs(Vzinc))
 return -10000.0:
 clse
 return Vz;
 void (bZero() (
 /* Moves tip to x_1y_1z = 0.0.0 */
 fbGoto(0.0,0.0,0.0);
void (bMoveAway() {
/* Withdraws the piezo tube as far as possible from the sample.
 •• and centers it at x = 0, y = 0
 •/
float Vx, Vy;
readdac0(&Vx); /* use current values of x and y */
readdacl(&Vy); /* just change the z value. */
fbGoto(Vx,Vy, MAXVOLTAGE/OUTGAIN);
```

```
void fbGoto(float Vx, float Vy, float Vz) (
/* Changes the output voltages to Vx, Vy, Vz */
/* Actual piezo voltage will be:
  OUTOAIN*(Vz + Vx)
  OUTGAIN*(Vz - Vx)
  OUTGAIN*(Vz + Vy)
  OUTGAIN*(Vz - Vy)
(voltages at DAC output's piezo voltage / OUTGAIN)
float
          (1,(2,(3)
float
          $1,$2,$3;
int
/* not time critical, do over 100 * (1/freq) time steps
  ble otherwise, would have a large current surge
readdac(XDAC, &f1); /* Read current output values. */
readdac(YDAC, &f2);
readdac(ZDAC, &f3);
s1 = \{1; s2 = \{2; s3 = \{3\}\}
for (i = 0; i < 100; i ++)
 $1 += (Vx - f1)/100.0; /* Change values by 1/100th of difference */
 $2 += (Vy - f2)/100.0;
 $3 += (Vz - f3)/100.0;
 if (abs(s1) > MAXVOLTDA) \{ s1 = s1/abs(s1) * MAXVOLTDA; \}
 if (abs(s2) > MAXVOLTDA) ( s2 = s2/abs(s2) *MAXVOLTDA; )
 if (abs(s3) > MAXVOLTDA) \{ s3 = s3/abs(s3) \cdot MAXVOLTDA; \}
 writeda(XDAC, $1);
 writeda(YDAC, $2);
 writeda(ZDAC, $3);
}/*------*/
/************ fbGotoXYstart *********/
void fbGotoXYstart(int *Stat) {
/* Status:
  returns 0 if everything is ok, 7 if Vx or Vy are out of range.
float Vx, Vy, Vz;
```

```
returnval = -8:
Scan.[mage = (float *)mailoc(xpts*ypts*sizeof(float)*((ReturnType==RETBOTfi)?2:f)); /*
allocate memory */
/* twice as much memory is needed if both POS and ERR values are returned */
if (Scan.Image == NULL)
 returnval = .6:
return returnyal;
1 /* end of fbSetupScan */
/*********** fbBlas Commands *********/
void fbBiasOn(float bias) { /* Turn on the tunneling bias voitage */
/* Use channel 4 for bias voltage. */
writeda(VBIAS, bias); /* set TASCO channel #VBIAS to bias volts */
} /* end of (bBiasOn() */
void fbBiasOff() { /* Turns of the tunneling bias voltage */
/* Channel 4 is used for bias voltage */
writeda(VBIAS, 0.0); /* set bias voltage to zero volts. */
} /* end of fbBiasOff() */
/******* (bSctupFB **********/
int fbSetupFB(float P, float I, float D,
              float setpoint,
              float freq.
              float settletime) (
/* Setup all the required constants for the computerized
** PiD control of the STM tunneling.
** Returns -1 if freq is not in correct range (0-100000 Hz)
int return val:
returnval = 0:
/* setup piecewise Linear approx. to log10 */
table_create(MAX_PIECB_NUM); /* use max. number of pieces allowed */
```

```
FBP=P:
FB.1 = 1:
FB.D = D:
FB.setpoint = log(setpoint); /* log converts from current to position */
if ((freq >= 0) && (freq <= MAXFBFREQ))
 FB.samplefreo = freo:
else
 returnval = -1:
if (settletime >= 0.0)
 I'B.settletime = settletime;
else
 returnval = -1;
return returnyal;
float fbRamp(float rate) [
/* fbRamp starts at furthest point and moves towards the surface.
** If the setpoint current is reached, then fbRamp returns the
** peizo voltage at which the setpoint was reached.
** Otherwise, fbRamp returns -10000.
** rate determines (in volts / second) the approach speed of the tip
** (where the volts specifies volts across the piezo tube).
** Approach starts at whatever x,y,z values are current!
float Vz;
float Vzinc:
float advalue;
double t. delt;
readdac2(&Vz); /* read current z voltage */
Vzinc = -OUTGAIN/abs(OUTGAIN) * rate / FB.samplefreq;
delt = (double)(1.0/FB.samplefreq);
t = second()+ 0.00001; /* wait ten microseconds for piezo to settle */
```

while (t > second());

```
Vyinc = - Vyinc;
setpt = FB.setpoint;
/* Define fb constants: (ref. Baselt et al. Rev.Sci.Instr. 64(7) p1872-1882
  July 1993.
a = FB.P + FB.I;
b = -FB.P + FB.I;
#ifdef DEBUGFB
printf("\na = %f
                      b = %f NO DERIVATIVE TERM",a,b);
printf("\nStarting fb: set point = %f", FB.setpoint);
/* number of th points per image point */
fbpersample = (int)(FB.samplefreq/Scan.rate);
oversbpersample = 1.0/((loat))bpersample;
Pos = 0.0; Err = 0.0; /* used for averaging data */
xpoints = Scan xpoints; /* to save the time needed to dereference. */
ypoints = Scan.ypoints;
SType = Scan.ScanType;
RType = Scan.ReturnType;
e0 = 0.0; e1 = 0.0; /* define initial errors */
fm[0] = 0.0; /* define these now so they are loaded into proc. cache mem. */
i = 0;
j = 0;
k = 0:
10 = 0.0:
t = second();
If = t + FB.settletime; /* SBTTLE TIME FOR PID CONTROLLER */
do { /* Settle the feeback foop. No data taken in this do { } */
t += delt; while (t > second());
 readad0(&advalue); /* I is proportional to negative of current */
 e0 = table_lookup(-advalue) - setpt;
```

```
Vz += a^*c0 + b^*c1;
 c1 = c0:
 Im[0] = 0.0; /* put here b/c I suspect that otherwise there are timing problems*/
        /* with the second loop */ ...
 if (abs(Vz) < MAXVOLTDA) ( writeda2(Vz); )
 clse (
  Vz = (Vz > 0.0) ? MAXVOLTDA: -MAXVOLTDA; /* antiwindup terms */
  writeda2( Vz );
) while (t < tf);
/ NOTE: image points are stored in the order they are taken */
/* to view matrix, every second line must be reordered */
t0 = t; /* time the equisition */
for (i = 0; i < ypoints; i++) {/*****Y LOOP*****/
for (i = 0; i < xpoints; i++) (/*****X LOOP ******/
 if (SType == SINGLE) {
   switch (RType) {
    case RETPOS: Im[i + j*xpoints] = Vz; /* save a data point */
    case RETERR: Im[i + j*xpoints] = e0; /* save error */
      break:
    case RBTBOTH: Im[2^{\circ}(i+j^{\circ}xpoints)] = Vz; /^{\circ} position ^{\circ}/
             Im[2^{\circ}(i + j^{\circ}xpoints) + 1] = c0; /^{\circ}error^{\circ}/
 for (k = 0; k < fbpersample; k++) (/*****FB LOOP ****/
  t += delt; while (t > second());
   readad0(&advalue);
   c0 = table_lookup(-advalue) - setpt;
   Vz += a*c0 + b*c1;
  e1 = e0;
  If (abs(Vz) < MAXVOLTDA) { writeda2(Vz); }
  else [ /* Vz is out of range */
   Vz = (Vz > 0.0) ? MAXVOLTDA: -MAXVOLTDA; /* antiwindup */
```

```
writeda2( Vz );
    *Stat I= 0x0008:
  Vx += Vxinc;
  If (abs(Vx) < MAXVOLTDA) \{ writedaO(Vx); \}
  else (
   Vx = (Vx > 0.0) 7 MAXVOLTDA: • MAXVOLTDA;
   writeda0( Vx );
    *Stat != 0x0002;
  /* No need to update Y because it has not changed. */
  Fos += Vz;
  Err += e0;
  1 /**** END OF FB LOOP******/
 /* Save averaged or not averaged points */
 if (SType == AVERAGEPTS) (
  switch (RType) (
   case RBTPOS: Im[i + j*xpoints] = Pos*over[bpersample;
      break; /* save average position */
   case RETERR: Im[i+j*xpoints] = Err*overfbpersample;
      break; /* save error */
   case RBTBOTH: Im[2*(i+j*xpoints)] = Pos*overfbpersample;
           Im[2*(i + j*xpoints)+1] = Err*overfbpersample;
 Pos = 0.0;
 Err = 0.0;
 } /* end of x loop */
/* Now move one y line */
for (k = 0; k < \text{fbpersample}; k ++) \{ /* \text{ 2nd FBLOOP } */ \}
 t += delt; while (t > second());
 readad0(&advalue);
 c0 = table_lookup(-advalue) - setpt;
 Vz += a*c0 + b*c1;
 e1 = e0;
 if (abs(Vz) < MAXVOLTDA) ( writeda2(Vz); )
  Vz = (Vz > 0.0) ? MAXVOLTDA: ·MAXVOLTDA; /* antiwindup */
```

```
writeda2( Vz );
  *Stat J= 0x0008;
 Vy += Vyinc;
 if (abs(Vy) < MAXVOLTDA) ( writedal(Vy); }
  Vy = (Vy > 0.0)? MAXVOLTDA: ·MAXVOLTDA;
  writedal(Vy);
  *Stat I= 0x0004;
 } /* end of 2nd FBLOOP */
/* Move back along x to align with last point taken */
Vxinc = -Vxinc; /* Change direction of motion */
for (k = 0; k < \text{fbpersample}; k++) ( /* 3rd FBLOOP */
t += delt; while (t > second());
readad0(&advalue):
c0 = table_lookup(-advalue) - setpt;
Vz += a*c0 + b*c1:
cl = c0;
if (abs(Vz) < MAXVOLTDA) { writeda2(Vz); }
  Vz = (Vz > 0.0) 7 MAXVOLTDA: -MAXVOLTDA; /* antiwindup */
  writeda2( Vz );
Vx += Vxinc:
if (abs(Vx) < MAXVOLTDA) { writeda0(Vx); }
  Vx = (Vx > 0.0)? MAXVOLTDA: -MAXVOLTDA;
  writeda0(Vx):
  *Stat I= 0x0002:
/* no need to update y b/c y does not change */
Pos += Vz:
Err += e0;
1/* end of 3rd FBLOOP */
if ((SType==AVERAGEPTS)&&(!!=xpoints-1)&&(j!=ypoints-1)) {
 switch (RType) (
```

```
case RETPOS: fm[l + j*xpoints] = Pos*overfbpersample;
break; /* save a data point */
case RETERR: fm[i + j*xpoints] = Err*overfbpersample;
break; /* save error */
case RETBOTH: Im[2*(i + j*xpoints)] = Pos*overfbpersample;
[m[2*(i + j*xpoints)] = Err*overfbpersample;
}
Pos = 0.0;
Err = 0.0;
Err = 0.0;
If = second();
return Im;
} /* end of void fb() */
```

nanosled.h

```
#if !defined(NANOSLEDINCLUDED)
#Jefine NANOSLEDINCLUDED
..
           nanosied h
..
..
           Peter Madden, April 4th, 1994
..
           nanosled.h has all the function definitions for operation
** of the nanosled.
•/
/* These two defines are used to determine the direction of
** the nanosled. PLUSDIR uses positive voltage pulses while
** MINUSDIR uses negative voltage pulses.
•• returns -1 if direction is not PLUSDIR (=1) or
** MINUSDIR (=-1)
#define PLUSDIR -1
#define MINUSDIR 1
/* Maximum output rate = 1000001fz. */
#define MAXRATE 100000
int nanosetchannel(double state, int channelnum);
/* Initialises tasco channel to use and the rate at which the outcut
** will be sent.
** Valid channels are from 0 to 7
** Valid rates are from 0 to 100000 Hz
** Returns 0 if ok, -1 if the rate is not valid, and -2 if the channel is not
** valid.
•/
```

float *nanomovelnit(double stepVsize, double steptime, Int direction);

```
/* Initialises the nanomove routine. Once this is called, all
** that needs to be done is call nanomove()
•• NOTE: the actual step size is determined by both pulse voltage
** (increasing pulse voltage increases step size) and by the steptime
** (shorter step times will increase the step size - this is because the
** pulse is shorter and so the maximum momentum of the counterweight will
** be higher; thus there is a larger momentum transfer to the sled).
** returns a pointer to an array that holds the pulse output via the
** TASCO. The pointer must be passed to nanomove.
•/
void nanomove();
1º Moves the nanosled one step. Direction, pulse voltage, and step
** time are all determined by nanomoveinit.
** NOTE: the actual step size is determined by both pulse voltage
** (increasing pulse voltage increases step size) and by the steptime
** (shorter step times will increase the step size - this is because the
** nulse is shorter and so the maximum momentum of the counterweight will
•• be higher; thus there is a larger momentum transfer to the sled).
#endif
```

nanosled.c

```
/•
 ..
            nanosled.c
            Peter Madden, April 4th, 1994
            nanosledic implements the functions for operation
 ** of the nanosled.
 #include "/u/peterm/vxi/peter/NanoSled/nanosled.h"
 Winclude "/u/peterm/vxi/peter/vxi/cn2.h"
 #include <stdio.h>
/* Global variables (not seen outside this module) */
/* initialised values will give zero output to force */
/* the user to initialise properly */
double Vsize;
double Pulsetime:
double Rate:
double Dir;
           Channel:
long int Numoutput;
           Pulse[50000];
#define MAXVOLTAGE 120.0
#define GAIN 15.0
#include "/u/peterm/vxi/peter/second.c"
int nanosetchannel(double srate, int channelnum) {
/* Initialises tasco channel to use and the rate at which the output
** will be sent.
..
** Valid channels are from 0 to 7
** Valid rates are from 0 to 100000 Hz
```

```
** Returns 0 if ok, -1 if the rate is not valid, and -2 if the channel is not
  ** valid.
  int returnyal = 0:
  Channel = -1;
  if ((state >= 0) && (state <= MAXRATE)) {
   Rate = srate;
  clse {
    Rate = MAXRATE; /* Don't want this undefined so set to MAXRATE */
   returnval = -1;
  if ((channelnum \geq= 0) && (channelnum \leq= 7)) (
   Channel = channelnum:
  clse (
   Channel = -1:
   returnval = 2;
  return returnyal;
float *nanomoveinit(double stepVsize, double steptime, int direction) [
/* Initialises the nanomove routine. Once this is called, all
** that needs to be done is call nanomove()
** returns a pointer to a Pulse. This pointer must be passed to
** nanomove().
    nanomoveinit sets the values of three global variables:
           Vsize
••
           Pulsetime
..
           Dir
           Numoutput
int returnval;
long int i;
double 1, 12, 14, 16, delt;
```

```
/* Pulse is a least squares fit to cardiod. (at^2+bt^4+ct^6) */
double a = 6.389757782204:
double b = -21.084111130178:
double c = 106.018155393218;
double Pulsefreg:
returnval = 0;
if ((stenVsize >= 0.0) && (stenVsize <= MAXVOLTAGE)) (
  Vsize = stepVsize / GAIN: /* max voltage output by DA //
clsc
  Vsize = 0.0:
Pulsetime = steptime;
if ((direction == PLUSDIR) II (direction == MINUSDIR)) {
  Dir = (double)direction;
else (
  Dir = 0.0; /* To gaurantee that output stays at zero */
              /* even if nanomove is called */
  returnyal = -1:
/* generate pulse shape: */
/* Pulse shape is stored in memory and output when a step is made */
Numoutput = (long int)(Pulsetime*Rate);
Pulsefreq = 1.0/Pulsetime;
delt = 1.0/Rate;
for (i = 0; i < Numoutput/2 - 1; i ++) [
 12 = ((double)(i*i))*delt*delt*Pulsefreq*Pulsefreq;
 14 = 12*12:
 16 = 14 12:
 Pulse[i] = (float)(Vsize^{a}Dir^{a}(a^{a}+2+b^{a}+4+c^{a}+6-1.0));
 Pulse[Numoutput - 2 - i] = Pulse[i]; /* Don't quite want mirror image */
                                                     /* reflect around max */
```

```
12 = ((double)((Numoutput/2-1)*(Numoutput/2-1)))*delt*delt*Pulsefreq*Pulsefreq;
  14 = 12*12:
 16 = 14 12:
 Pulse[Numoutput/2-1] = (float)(Vsize^{a}Dir^{a}(a^{a}+b^{a}+c^{a}+6-1.0));
  Pulse[Numoutput - 1] = Pulse[0];
 if (returnval == 0)
   return Pulse;
 else (
   return NULL:
void nanomove() [
/* Moves the nanosled one step. Direction, pulse voltage, and step
** time are all determined by nanomoveinit.
** NOTE: the actual step size is determined by both pulse voltage
** (increasing pulse voltage increases step size) and by the steptime
** (shorter step times will increase the step size - this is because the
** pulse is shorter and so the maximum momentum of the counterweight will
** be higher; thus there is a larger momentum transfer to the sled).
/* N.B. if you want interrupts off: turn them off before calling
** this routine. With the interrupts off, the step sizes will be
** more uniform!
•/
 double delt, t;
 int i:
 delt = 1.0/Rate;
  t= second();
  for (i = 0; i < Numoutput; i++)
   writeda(Channel, Pulse[i]);
   t += delt;
```

while (t > second()); }

table.c

```
/**********
          table.c
          Peter Madden, May 5th, 1995.
          Creates a lookup table that is a linear piècewise
          approximation of a the log function over the range
          -16V to 16V.
          For negative values and values less than NOISE_LBVEL,
          the table returns LOG_NOISB_LBVEL where noise level
          is chosen to be around or less than the noise level
          in the AD for the scanning tunneling microscopy
          system. (see function 'table_log()').
*************/
/*#define PRINTDEBUG 1*/
#include <math.h>
#define NOISB_LEVEL
                              (0.0001)
#define LOG_NOISB_LBVEL
                              (-4.0)
                              (16384)
#define MAX_PIECB_NUM
static float Slope[MAX_PIECB_NUM];
                    Intercept[MAX_PIECE_NUM];
static float
static float Number_of_pieces;
static float Num_pieces_div_16;
float
          table_log(float x);
          table_create(int Num_pieces);
int
float
          table_lookup(float x);
```

```
/**********
          float table_log(float x)
          Input: x
                               - value for which to calculate function
          output:
                               - log(x)
NOTE: for x < NOISE_LEVEL, table_log() returns LOG_NOISE_LEVEL. It
          is assumed that any x < NOISE_LEVEL is noise and corresponds
          to a very small signal.
*************/
float
          table_log(float x) {
float temp;
if (x > NOISE_LEVEL) (
 temp = (float)log(x);
 return temp;
return LOG_NOISE_LEVEL;
/***********
          int table_create(int Num_pieces)
                    Num_pieces
                                         - number of piecewise segments to use
                                         - Maximum is 1024.
          output: returns 0 if successul, 1 otherwise.
************
          table_create(int Num_pieces) [
int
int
float
          y1.y2;
if (Num_pieces > MAX_PIECE_NUM)
 return 1; /* Too many pieces specified */
Number_of_pieces = (float)Num_pieces;
Num_pieces_div_16 = Number_of_pieces/16.0;
for (i = 1; i \le Number_of_pieces; i++) {
 y2 = table_log((float)i * 16.0 / (float)Number_of_pieces);
 y1 = table_log((float)(i-1) * 16.0 / (float)Number_of_pieces);
```

```
Slope[i-1] = (y2 - y1) / (16.0/(float) \text{Number\_of\_pieces});
 Intercept[i-1] = - Slope[i-1] * (float)i * 16.0 / (float)Number_of_pieces
                               +yl;
 #if PRINTDEBUG
printf("%d %.4f
                     %.4f\n", i-1, Slope[i-1], Intercept[i-1]);
Hendif
 )
return 0;
/*********
          float table_lookup(float x)
          input: x - will calculate log(x)
output: returns the piece-wise linear approximation of log(x)
float table_lookup(float x) {
int i:
if (x < NOISB_LEVEL)
return LOG_NOISE_LEVEL;
i = (int)(x*Num_pleces_div_16);
return (Slope[i]*x + Intercept[i]);
```

Appendix C: Matlab Code for STM Simulation

stmsim2.m

```
% Simulation of STM with feedback.
% Peter Madden, June 5th, 1996.
% rev. June 7th
% June 5:
% This model is for the z direction only at the moment
% and won't initially incorporate the mechanical
% dynamics because the magnitude of the coupling is difficult
% to gauge (ie. how much does the actuator couple into the
% mechanism?).
% June 7: Added mechanical transfer function.
% There are five major components to the STM:
% 1) mechanical.
% 2) piezo tube
% 3) tunneling junction
% 4) current amplifier
% 5) computer feedback.
% 1) Mechanical dynamics:
wmech = 650*2*pi; % resonant frequency
etamech = 0.5:
                       % damping
NMech = 1;
DMech = [1/wmech^2 2*etamech/wmech 1]:
% 2) Piezo tube:
HVGain = 2:
NPiezo = HVGain * (5.3e-9); % gain in m / Volt from computer
DPiezo = [1/(2ºpiº4000) 1]; % limited by lateral resonance at ~4 kHz
                                   % (long. (z) res is at ~50 kHz but there is
                                   % cross coupling.)
% 3) tunneling junction (position to current. Note that
% the logarithm of the current is taken here before the current
% amplifier in order to make the analysis simpler. As a result,
% the model of the junction here has current depending linearly
% on the gap).
Kappa = 2.8e+9; % give ~ one order of magnitude change per angstrom
NTunnel = Kappa;
```

```
% 4) Current amplifier
% Note that since the logarithm is actually taken after the current
% amplifier, the gain of the current amplifier really only adds
% a DC term to the transfer function (log 10^8 = 8 log 10)
% so we can ignore this DC term ...
CAmpBW = 2000;
                               % Hertz
NCurrentAinp = 1; % Volts / Amp
DCurrentAmp = [1/(2*pi*CAmpBW) 1]; % low pass filter.
% 5) Computer feedback
% (b = l'e + 1/s le + s De
D = 0:
P = 0.01:
1 = 0.001 * 40000;
NFB = [D P I]; % num = s^2D + sP + I
DFB = [1 \ 0]; % den = 1/s
% Summary of Ti's:
% 1) Mechanical: NMech, DMech.
% 2) Piezo:
                               NPiezo, DPiezo
                               NTunnel, DTunnel
% 3) Tunnel Junction:
% 4) Current Amplifier:
                               NCurrentAmp, DCurrentAmp
                               NFB.DFB
% 5) Computer Peedback:
% Now do open loop from the input voltage at the piezo tube
% to the output voltage from the current amp.
NOL = conv(conv(NPiezo, NTunnel), conv(NMech, NCurrentAmp));
DOL = conv(conv(DPiezo, DTunnel), conv(DMech, DCurrentAmp));
%bode(NPiezo, DPiezo);subplot(211); title('Piezo Tube');
Higure(2);
%bode(NTunnel, DTunnel);subplot(211); title('Tunnel Junction');
%figure(3);
%bode(NCurrentAmp, DCurrentAmp);subplot(211); title('Current Amp');
%figurc(4);
bode(NFB, DFB); subplot(211); title('Feedback');
bode(NMech, DMech); subplot(211); title('Mechanical TF');
figure(6);
margin(NOL, DOL); subplot(211); title('Open Loop, no compensator');
```

DTunnel = 1;

NOLC = conv(NOL, NFB); DOLC = conv(DOL, DFB);

figure(7); margin(NOLC, DOLC); subploi(211); % title('open loop compensated');

(NCL, DCL) = cloop(NOLC, DOLC); figure(8); margin(NCL, DCL);